UNIVERSITY OF SOUTHAMPTON

The Low-Energy Phenomenology of a Supersymmetric extension of the Standard Model

by

Jonathan Keith Parry

A thesis submitted for the degree of

Doctor of Philosophy

Department of Physics and Astronomy

December 2003

UNIVERSITY OF SOUTHAMPTON

ABSTRACT

FACULTY OF SCIENCE

PHYSICS

Doctor of Philosophy

The Low-Energy Phenomenology of a Supersymmetric extension of the Standard Model

Jonathan Keith Parry

We attempt to explore the relationship between low-energy phenomenology and the pattern of Yukawa couplings at high-energies. A working supersymmetric Pati-Salam model which fits all phenomenological constraints is constructed. This model is typical of a broad class of models and its predictions are representative of all models of this type. A χ^2 analysis is used to determine points in parameter space where experimental measurements and bounds are most accurately reproduced. These best fit points are then used to make predictions for unmeasured quantities such as neutrino mixing angles and lepton flavour violating decays. For example we find that the branching ratio for $\tau \to \mu\gamma$ is very near its present experimental bound. In the context of this model we also study the degree of deviation from Yukawa unification observed by our best fit points. The effects of future experimental results upon the best fit regions of parameter space are also considered and we find that in some cases our allowed parameter space may be much reduced. We extend the study of our model's predictions by investigating Higgs-mediated contributions to rare flavour changing neutral current processes and discuss the possibility of them being among the very first indirect signals of supersymmetry. We also study rare lepton flavour violating decays mediated by Higgs bosons discovering that in this case the Higgs contribution is sub-dominant and doesn't hold such clear hopes for indirect discovery.

Contents

List of Figures

List of Tables

Preface

The work described in this thesis was carried out in collaboration with Prof. S.F. King and Dr. T. Blažek. The following list details our original work and gives the references for the material.

- Chapter 3: *Global analysis of a supersymmetric Pati-Salam model*, T. Blažek, S. F. King and J. K. Parry, J. High Energy Phys. JHEP 05 (2003) 016, arXiv:hep-ph/0303192.
- Chapter 4: *Implications of* $B_s \to \mu^+\mu^-$ *in SO(10)-like models*, T. Blažek, S. F. King and J. K. Parry, arXiv:hep-ph/0308068, to be published in Phys. Lett. B
- Chapter 5: contains work to be published

No claim to originality is made for the content of Chapters 1 and 2 which were compiled using a variety of other sources.

Acknowledgements

Firstly I would like very much to thank my two supervisors Prof. S.F. King and Dr. T. Blazek who have given me endless support. Their offices have always been open and they have been willing and patient in answering my questions. My collaboration with them has been a very rewarding experience.

Secondly I would like to thank Jenny and my family for putting up with me. I am particularly indebted to my parents, who continue to support me in every possible way, even though I don't stay in touch quite as much as I should.

I am also very grateful to PPARC for funding my research for the past 3 years and for enabling me to gain valuable experience at Summer Schools and visits to Manchester, St. Andrews, Trieste and CERN.

Last but not least I would like to thank the Department of Physics at Southampton University and in particular the SHEP group. Every member of the group from postgrads to postdocs and staff members have made the past 3 years a very enjoyable time. The group has always been very open and friendly. I am proud to have been a member of this group. Special thanks must go to those students and postdocs with whom I shared my early SHEP days: David Rayner, James Babington, James Hockings, Antonio Gatti, Stefano Arnone, David Lin, Martin Kurth, Sebastian Descotes-Genon, Vicente di Clemente, Martin Hirsch and David Crooks, who all made settling into life in the "capital of entertainment" so easy.

Chapter 1

Introduction

1.1 Preliminaries

1.1.1 Motivation

The work presented in this thesis is a detailed *top-down* study of the low-energy phenomenology of a Supersymmetric(SUSY) model with an extended gauge group. The general aims of the work are to:

- find an appropriate model to describe low-energy experimental data
- discover regions of parameter space where the model predictions best match the present experimental bounds and measurements,
- make predictions for unknown observable parameters such as the neutrino mixing angle θ_{13},
- probe the high-energy theory via Yukawa Unification,
- investigate the impact of new measurements on the model's predictions,

- study rare decays, their correlations and prospects as SUSY signals at the TeVatron and LHC.

1.1.2 Thesis Structure

This thesis is organised as follows: in the remaining sections of chapter 1 we review the Standard Model(SM) of particle physics and discuss the prospects for the discovery of the Higgs boson. In chapter 2 we motivate the extension of this model through both theoretical and experimental concerns. Out of all the possible extensions of the standard model we focus on supersymmetry and the Minimal Supersymmetric Standard Model(MSSM). Details of recent experimental inconsistencies of the SM are presented in the form of neutrino mass and oscillation. This is then used to motivate the introduction of extra super-heavy neutrino states which can account for such observations.

Chapter 3 is devoted to the construction of a working supersymmetric Pati-Salam model. We employ a χ^2 analysis to determine the regions of parameter space which best fit the present low-energy experimental measurements. These fits are then used to make predictions for the unmeasured neutrino mixing angle, θ_{13} and the lepton flavour violating decay $\tau \to \mu\gamma$. The extent to which Yukawa unification is violated by our best fit points is also explored.

In Chapter 4 we investigate the promising signal for supersymmetry that is the flavour changing neutral current process $B_s \to \mu\mu$. We find that the predictions of our model are right at the present experimental limit. It is shown that in the class of models we are studying it is quite plausible that a signal for this process and therefore supersymmetry will be found in the near future.

Chapter 5 extends the work of chapter 4 to include lepton flavour violating Higgs couplings. We study the branching ratios for the Higgs-mediated contributions to

the rare processes $B_s \to \tau\mu$, $\tau \to 3\mu$ and their correlation to the related processes $\tau \to \mu\gamma$ and $B_s \to \mu\mu$.

Chapter 6 contains an overview and conclusion to the whole thesis. At the end of the thesis there are a number of appendices and a bibliography.

The contributions to the original work found in chapters 3, 4 and 5 undertaken by the author are as follows. The construction of the Pati-Salam model of chapter 3, in particular the choice of non-renormalisable operators and U(1) family charges, was undertaken in collaboration with Prof. S. F. King and Dr. T. Blazek. The numerical χ^2 global analysis had been previously developed by Dr. T. Blazek. Together we incorporated a complete analysis of the neutrino sector into the numerical procedure. It was then the authors responsibility to determine the model's best fit points as presented in chapter 3. The calculation of the branching ratio for $B_s \to \mu^+\mu^-$, $\tau \to 3\mu$ and $B_s \to \tau^+\mu^-$ were undertaken by the author and integrated within the numerical code. Studies of the impact of future experimental measurements and correlations of physical observables were also undertaken by the author.

1.2 The Standard Model

In this section we shall assemble the ingredients of the Standard Model(SM) of particle physics [1]. This model was proposed in the late 1960's and early 1970's and has since been successfully verified by numerous accelerator experiments. The model encompasses Quantum Chromo Dynamics(QCD) and the unified Electroweak theory of Glashow, Weinberg and Salam. After defining the SM we shall continue to briefly explore some of its phenomenology and discuss the prospects for the discovery of its final pieces.

[1] There are many excellent reviews of the Standard Model, see [1].

1.2.1 Definition of the Standard Model

To completely define a gauge theory it suffices to specify just three things, the gauge group, the particle representations and the symmetry breaking mechanism. Hence for the Standard model we have:

- **Gauge Group of the Standard Model**

  The Quark model of Strong interactions developed by Gell-Mann and Zweig in 1964 required the existence of colour: a new charge obeying an unbroken $SU(3)$ symmetry. The observed Electroweak interactions demand the existence of two massive vector bosons and a massless photon. These conditions are most simply satisfied by the spontaneous braking of a local gauge group

  $$SU(2)_L \otimes U(1)_Y \rightarrow U(1)_{\text{em}}$$

  Hence the combined gauge group of the SM is

  $$G_{SM} = SU(3)_c \otimes SU(2)_L \otimes U(1)_Y$$

- **Particle Representations: Matter content**

  The SM contains 3 families of Quarks and Leptons with quantum numbers assigned as written in table 1.1. The left handed components transform as $SU(2)$ doublets and right handed components as $SU(2)$ singlets. This ensures that only the left handed quarks and leptons couple to the gauge bosons $W^{\pm}$.

  As the right and left handed fields transform in different $SU(2)_L$ representations a Dirac mass of the form,

  $$m_D \left(\bar{\psi}_R \psi_L + \bar{\psi}_L \psi_R\right), \tag{1.1}$$

  would break gauge invariance. Gauge invariance also requires the gauge bosons

Particles	Spin	$SU(3)_c$	$SU(2)_L$	$Y/2$
Left handed quarks, $Q_{iL} \equiv (u\,d)_{iL}$	1/2	3	2	1/6
Right handed up quarks, u_{iR}	1/2	3	1	2/3
Right handed down quarks, d_{iR}	1/2	3	1	−1/3
Left handed leptons, $L_{iL} \equiv (\nu\,e)_{iL}$	1/2	1	2	−1/2
Right handed electrons, e_{iR}	1/2	1	1	−1
Higgs bosons, $\phi \equiv (\phi^+, \phi^0)$	0	1	2	1/2
Gluons, $g^\alpha(\alpha = 1 \ldots 8)$	1	8	1	0
Weak bosons, $W^a(a = 1 \ldots 3)$	1	1	3	0
Hypercharge boson, B	1	1	1	0

Table 1.1: Matter content of the SM with associated G_{SM} gauge quantum numbers. A family index, $i = 1 \ldots 3$, has been included.

of unbroken symmetries to be massless. This is clearly a problem as we observe both massive fermions and gauge bosons. The solution to this is to introduce a scalar doublet which is used to spontaneously break the gauge symmetry and simultaneously generate masses for both fermions and gauge bosons. This is known as the Higgs mechanism.

- **Spontaneous Symmetry Breaking: The Higgs mechanism**

  If we consider a Lagrangian with a wrong sign mass term,

$$\mathcal{L} = |\mathrm{D}_\mu \phi|^2 - V(\phi) \tag{1.2}$$

$$\text{where} \qquad V(\phi) = -\mu^2 \phi^\dagger \phi + \lambda (\phi^\dagger \phi)^2. \tag{1.3}$$

  Here ϕ is an $SU(2)_L$ complex doublet with hypercharge $Y/2 = 1/2$ and D_μ is the covariant derivative, defined later in eq. (1.9). The scalar potential in eq. (1.3) has a minimum at,

$$(\phi^\dagger \phi) = \frac{\mu^2}{2\lambda}, \tag{1.4}$$

  rather than at $\phi = 0$ which is the case if the mass term is of the correct sign. This minimum is invariant under $SU(2)$ rotations. Making use of this symmetry

we can write the vacuum expectation value(VEV) of ϕ as,

$$< \phi >= \frac{1}{\sqrt{2}} \begin{pmatrix} 0 \\ v \end{pmatrix} \quad \text{with} \quad v = \sqrt{\frac{\mu^2}{\lambda}}, \tag{1.5}$$

By making a specific choice of vacuum the $SU(2)_L$ and $U(1)_Y$ symmetries have been spontaneously broken. But as ϕ is neutral the symmetry $U(1)_{\text{em}}$ is unbroken with generator $Q = \mathrm{T}^3 + Y/2$. Expanding about the vacuum eq. (1.5) we can write,

$$\phi = \frac{1}{\sqrt{2}} \begin{pmatrix} 0 \\ v + h(x) \end{pmatrix} \quad \text{where} \quad < h >= 0, \tag{1.6}$$

the real scalar field h is known as the physical Higgs boson. In eq. (1.6) we have chosen to work in the unitary gauge where the non-physical degrees of freedom are not explicitly present in ϕ. We shall revisit these non-physical degrees of freedom later in this chapter. Substituting eq. (1.6) into eq. (1.3) and using the expression for v in eq. (1.5) gives a Higgs potential,

$$V(h) = -\frac{\mu^2}{2}(v+h)^2 + \frac{\lambda}{4}(v+h)^4 \tag{1.7}$$

$$= \ldots + \mu^2 h^2. \tag{1.8}$$

Notice that the physical Higgs field now has a mass term of the correct sign, $m_h = \sqrt{2\mu^2} = v\sqrt{2\lambda}$.

1.2.2 Gauge Boson Masses and Higgs couplings

In order to determine the gauge boson masses and couplings we must take the same expansion, eq. (1.6), and apply it to the kinetic term in eq. (1.2). Doing so we find

that,

$$|\mathrm{D}_\mu\phi|^2 \equiv \left|\left(\partial_\mu - i\frac{g'}{2}Y\,B_\mu - ig\,W_\mu^a T^a\right)\phi\right|^2 \tag{1.9}$$

$$= \ldots + \frac{1}{8}\left|\begin{pmatrix} g'B_\mu + gW_\mu^3 & g\,(W_\mu^1 - iW_\mu^2) \\ g\,(W_\mu^1 + iW_\mu^2) & g'B_\mu - gW_\mu^3 \end{pmatrix}\begin{pmatrix} 0 \\ v+h \end{pmatrix}\right|^2 \tag{1.10}$$

$$= \ldots + \left[m_W^2\,W_\mu^+ W^{-\,\mu} + \frac{1}{2}m_Z^2 Z_\mu Z^\mu + 0\times A_\mu A^\mu\right].\left(1+\frac{h}{v}\right)^2. \tag{1.11}$$

Here $Y/2 = 1/2$ is the hypercharge of ϕ and T^a are related to the $SU(2)$ Pauli matrices as, $T^a = \frac{\sigma^a}{2}$. In eq. (1.11) the gauge fields W_μ^a, B_μ have been combined to form the mass eigenstates,

$$W_\mu^\pm = \left(W_\mu^1 \mp iW_\mu^2\right)/\sqrt{2}, \qquad m_W = \frac{1}{2}\,g\,v \tag{1.12}$$

$$Z_\mu = \cos\theta_w\,W_\mu^3 - \sin\theta_w\,B_\mu, \quad m_Z = \frac{1}{2}\,v\,\sqrt{g^2+g'^2} \tag{1.13}$$

$$A_\mu = \sin\theta_w\,W_\mu^3 + \cos\theta_w\,B_\mu, \quad m_A = 0. \tag{1.14}$$

Here we have defined the weak mixing angle θ_w as the mixing angle involved in the change of basis from the weak eigenstates, W^3, B to the mass eigenstates, Z, A, with

$$\cos\theta_w = \frac{g}{\sqrt{g^2+g'^2}}, \quad \sin\theta_w = \frac{g'}{\sqrt{g^2+g'^2}}. \tag{1.15}$$

This leads to the W, Z mass relation $m_W^2 = m_Z^2\cos^2\theta_W$. Hence it is the mixing between W_μ^3 and B_μ that is responsible for the inequality in the W and Z masses. As a complex doublet ϕ contains four real degrees of freedom, but we saw in eq. (1.6) that symmetry breaking leaves us with just one, h. As a consequence of symmetry breaking the other 3 degrees of freedom become Goldstone bosons and are "eaten" by the $W^\pm$, Z bosons as they become the longitudinal components of these now massive vector bosons. The first and second term of eq. (1.11) provide mass terms for the two gauge bosons, $W^\pm$ and Z, the final term shows that we are also left with one massless

neutral gauge boson, A_μ. The presence of one massless gauge boson means that the initial $SU(2)_L \otimes U(1)_Y$ symmetry has been spontaneously broken to $U(1)_{\rm em}$, with the massless A_μ identified as the photon. Eq. (1.11) also arms us with Higgs couplings to the gauge bosons, these couplings are summarised in Table 1.2.

We can now write the covariant derivative, D_μ, in terms of the mass eigenstates

$$\begin{aligned} \mathrm{D}_\mu = \partial_\mu - i\frac{g}{\sqrt{2}}\left(W_\mu^+ T^+ + W_\mu^- T^-\right) - i\frac{1}{\sqrt{g^2+g'^2}} Z_\mu \left(g^2 T^3 - g'^2 \frac{Y}{2}\right) \\ -i\frac{gg'}{\sqrt{g^2+g'^2}} A_\mu \left(T^3 + \frac{Y}{2}\right), \end{aligned} \tag{1.16}$$

where $T^\pm = T^1 \pm iT^2$. The application of eq. (1.16) to fermion kinetic terms, $\bar{\psi}(i\not{\partial})\psi$, will give us fermion couplings to the gauge bosons. By inspection of the photon coupling in eq. (1.16) we can identify the electric charge e as,

$$e = -\frac{gg'}{\sqrt{g^2+g'^2}}. \tag{1.17}$$

and the electric charge quantum number as, $Q = T^3 + \frac{Y}{2}$.

	WW	ZZ
h	$\frac{i2M_W^2}{v}$	$\frac{iM_Z^2}{v}$
hh	$\frac{iM_W^2}{v}$	$\frac{iM_Z^2}{2v}$

Table 1.2: 3-pt and 4-pt Standard Model Higgs couplings to the massive gauge bosons.

So we have found that through the Higgs mechanism the $\mathrm{SU(2)}_L \otimes \mathrm{U(1)}_Y$ symmetry is broken to the $\mathrm{U(1)}_{em}$ of electromagnetism. In doing so the gauge bosons have also acquired masses. But what about fermion masses?

1.2.3 Fermion masses and the CKM Matrix

Fermion masses can also be generated by the Higgs mechanism via a Yukawa coupling to the Higgs doublet ϕ written as,

$$\mathcal{L}_{\rm yuk} = -Y_d^{ij} Q_{iL}^\dagger \, \phi \, d_{jR} - Y_u^{ij} Q_{iL}^\dagger \, \phi^{\rm c} \, u_{jR} - Y_e^{ij} L_{iL}^\dagger \, \phi \, e_{jR} + \text{h.c.}. \tag{1.18}$$

Here we have defined the charge conjugate Higgs field $\phi^{\rm c}$ as

$$\phi = \begin{pmatrix} \phi^+ \\ \phi^0 \end{pmatrix} \, , \, \phi^{\rm c} = i\sigma_2 \phi^* = \begin{pmatrix} \phi^{0\,*} \\ -\phi^{+\,*} \end{pmatrix} . \tag{1.19}$$

Again expanding ϕ as in eq. (1.6) produces both mass terms and Higgs couplings,

$$\mathcal{L}_{yuk} = \left[-m_d^{ij} \, d_{iL}^\dagger \, d_{jR} - m_u^{ij} \, u_{iL}^\dagger \, u_{jR} - m_e^{ij} \, e_{iL}^\dagger \, e_{jR} + \text{h.c.} \right] . \left(1 + \frac{h}{v} \right) , \tag{1.20}$$

where $m_{u,d,e}^{ij} = Y_{u,d,e}^{ij} \frac{v}{\sqrt{2}}$. Note that eq. (1.18) contains no Yukawa term for the neutrinos, hence they remain massless in the SM.

In general the quark Yukawa couplings Y_q are non-diagonal, here $q = u, \, d$. Let us define the unitary matrices V_L and V_R as the matrices which diagonalise the hermitian combinations of the Yukawa couplings

$$Y_q Y_q^\dagger \; = \; V_L^q \, (Y_q^{\rm diag})^2 \, V_L^{q\,\dagger} \tag{1.21}$$

and

$$Y_q^\dagger Y_q \; = \; V_R^q \, (Y_q^{\rm diag})^2 \, V_R^{q\,\dagger} . \tag{1.22}$$

Here $Y_q^{diag} = \text{diag}(y_1^q, y_2^q, y_3^q)$, where, $m_i^q = y_i^q \frac{v}{\sqrt{2}}$, are the mass eigenstates. The matrices $V_{L,\,R}^q$ therefore diagonalise the Yukawa couplings, such that,

$$Y_q = V_L^q \, Y_q^{\rm diag} \, V_R^{q\,\dagger}, \tag{1.23}$$

and define the change of basis between the weak eigenstates and the mass eigenstates,

$$q'_{iL} \equiv V_L^{q\,\dagger ij}\, q_{jL}, \quad q'_{iR} \equiv V_R^{q\,\dagger ij}\, q_{jR} \tag{1.24}$$

$$\text{with} \quad q^\dagger_{iL}\, Y_q^{ij}\, q_{jR} = q'^\dagger_{iL}\, Y_{q\,ij}^{\text{diag}}\, q'_{jR}. \tag{1.25}$$

Eq. (1.25) shows that the mass terms and Higgs couplings are flavour diagonal in the basis $q'_{L,R}$. When changing basis the matrices $V_{L,R}^{u,d}$ will cancel out in all electroweak currents involving the gauge bosons A_μ and Z_μ. This is not true for those involving the $W^\pm$ gauge bosons which become,

$$J^{\mu +} = \frac{1}{\sqrt{2}} u^\dagger_{iL} \gamma^\mu d_{iL} = \frac{1}{\sqrt{2}} u'^\dagger_{iL} \gamma^\mu\, V_{CKM}^{ij}\, d'_{jL}, \tag{1.26}$$

here we have defined the Cabibbo-Kobayashi-Maskawa(CKM) [2] matrix as,

$$V_{CKM} = V_L^{u\,\dagger} V_L^d. \tag{1.27}$$

V_{CKM} is a 3×3 unitary matrix and so contains 9 parameters; 3 real mixing angles and 6 phases. It is very important to keep track of these complex phases and in particular to identify which are physical and which are not.

Inspecting eq. (1.21) and (1.22) more closely it is clear that there is a phase freedom in the definition of the matrices $V_{L,R}^q$. Therefore we can make the transformation,

$$V_{L,R}^q \;\rightarrow\; V_{L,R}^q\, P_{L,R}^q, \tag{1.28}$$

where

$$P_L^{q\,ij} = \mathrm{e}^{\mathrm{i}\theta_q^i}\, \delta_{ij} \quad \text{and} \quad P_R^{q\,ij} = \mathrm{e}^{\mathrm{i}\phi_q^i}\, \delta_{ij}, \tag{1.29}$$

with the guarantee that eq. (1.21) and (1.22) will still hold true. Ensuring that eq. (1.23) is still satisfied gives the constraint, $\phi_q^i = \theta_q^i$, and leaves us the freedom to pick the 6 phases, θ_u^i and θ_d^i, $i = \ldots, 3$. Applying the transformation in eq. (1.28) to

the CKM matrix, eq. (1.27), we find that

$$V_{CKM} \rightarrow P_L^{u\dagger} V_{CKM} P_L^d. \tag{1.30}$$

Hence it is possible to use the 6 phases $\theta_{u,d}^i$ of $P_L^{u,d}$ to eliminate 5 out of 6 phases in V_{CKM} leaving 3 real mixing angles and 1 physical phase. In the standard model the single phase, known as the Dirac phase, is the sole source of CP violation.

1.2.4 Lepton Flavour Violation

To carry out the same diagonalisation procedure for the leptons we start with the Yukawa coupling Y_e. As before this can be diagonalised as,

$$Y_e = V_L^e Y_e^{\text{diag}} V_R^{e\dagger}, \tag{1.31}$$

where $Y_e^{\text{diag}} = \text{diag}(y_1^e, y_2^e, y_3^e)$ with $m_i^e = y_i^e \frac{v}{\sqrt{2}}$ being the mass eigenvalues. As there is no neutrino Yukawa coupling Y_ν we can define the change of basis,

$$e_L'^i = V_L^{e\dagger ij} e_L^j, \qquad \nu_L'^i = V_L^{e\dagger ij} \nu_L^j \tag{1.32}$$

$$e_R'^i = V_R^{e\dagger ij} e_R^j \quad . \tag{1.33}$$

Again this will diagonalise the Yukawa coupling, Y_e, and therefore the tree level mass matrix for the charged leptons. Notice that this time each component of the lepton doublet receives the same rotation and so unlike eq. (1.26) the matrices $V_{L,R}^e$ cancel completely from the theory. Therefore the SM is flavour diagonal in the lepton sector and so the lepton number of each generation is conserved. The experimental evidence for this conserved quantity is very compelling with the non-observation of Lepton Flavour Violation(LFV) at the level of $\text{Br}(\mu \rightarrow e\gamma) < 1.2 \times 10^{-11}$ and $\text{Br}(\mu \rightarrow 3e) < 10^{-12}$ [3].

1.2.5 Higgs boson searches

The only Standard Model particle left undiscovered is the Higgs boson itself. This section reviews much of the past and future experimental effort being devoted to the discovery of the Higgs boson. The case for the existence of a light SM Higgs is presented and the prospects for its discovery in the near future are discussed.

The very fact that the Higgs couples to fermions and gauge bosons with a coupling strength proportional to the mass of that particle makes it a particularly elusive creature. It couples strongly to the heaviest quarks, which are highly unstable, but couples weakly to the readily available light quarks and leptons.

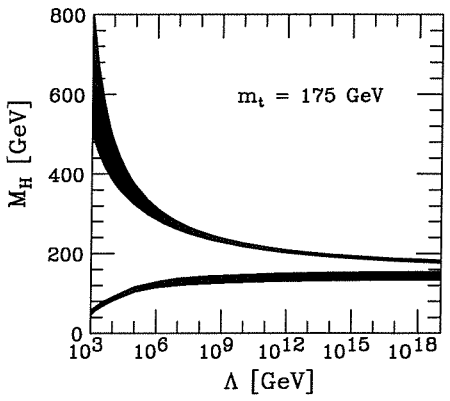

Figure 1.1: Upper and lower Higgs mass bounds as a function of the cutoff, Λ [4].

The experimental determination of the Fermi constant, G_F, fixes the value of the Higgs VEV as,

$$\frac{G_F}{\sqrt{2}} = \frac{g^2}{8m_W^2} = \frac{1}{2v^2}, \tag{1.34}$$

so that $v = 247\,\text{GeV}$. This also restricts the allowed values of the physical Higgs mass, $m_h = v\sqrt{2\lambda}$, to be a few hundred GeV. The self interaction coupling λ has a

Renormalisation Group Equation(RGE) of the form,

$$\frac{d\lambda}{d\ln(Q/M_W)} = \frac{3}{2\pi^2}\left(\lambda^2 + \lambda Y_t^2 - Y_t^4\right), \tag{1.35}$$

with Y_t being the top Yukawa coupling. Hence for large values of $\lambda(M_W)$ the coupling diverges as the energy scale increases. In order to avoid this problem we must define a cutoff for the theory. If we want this cutoff to be at a particularly high scale, say the Planck scale, then we must have a small value of $\lambda(M_W)$, corresponding to $m_h \lesssim 200$ GeV. Conversely for the theory to be valid up to the 1 TeV scale then we can have a larger $\lambda(M_W)$ corresponding to $m_h \lesssim 600$ GeV. Therefore for a given cutoff scale Λ there is a maximum $\lambda(M_W)$ for which $\lambda(\Lambda)$ is finite.

On the other hand, for small values of $\lambda(M_W)$, and therefore m_h, the negative contribution from the top Yukawa coupling will drive λ negative, resulting in an unstable minimum. Hence we are forced to define a cutoff at the point where λ changes sign. So for any given cutoff Λ there is also a minimum value for $\lambda(M_W)$ for which $\lambda(\Lambda) > 0$.

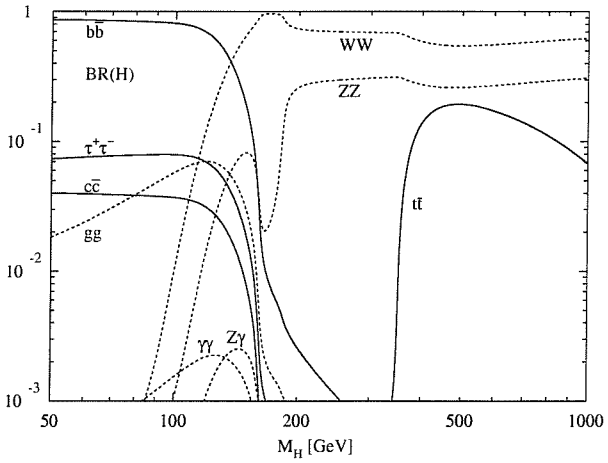

Figure 1.2: Branching ratios for the dominant Higgs decay channels as a function of the Higgs mass [4].

These conditions provide theoretical upper and lower bounds for $\lambda(M_W)$, and therefore m_h, as a function of the theory's cutoff(Λ) see fig. (1.1). We see that the larger the cutoff of the theory the more constrained the Higgs mass becomes, with $\Lambda \to M_{pl}$ implying a range $m_h = 130 - 180$ GeV, the so called desert scenario.

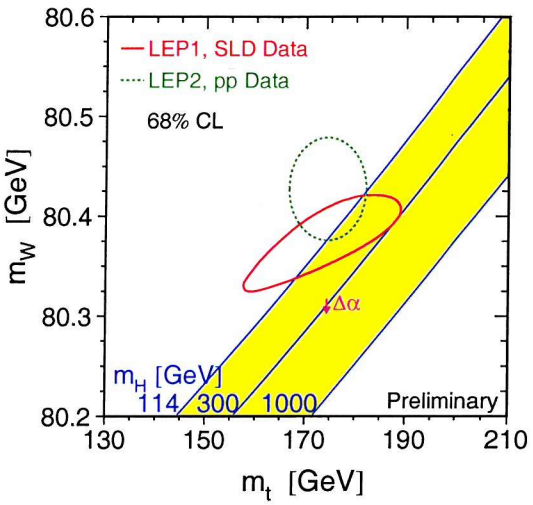

Figure 1.3: Direct(dashed line) and indirect(solid lines) measurements of M_W and m_t [5].

Direct Higgs searches at LEP were based primarily on the Bjorken process,

$$e^+e^- \to Z \to Z + h, \tag{1.36}$$

with the Higgs decaying dominantly into $b\bar{b}$ for $m_h < 2M_W$ and into WW for $m_h > 2M_W$, as shown in fig. (1.2). Unsuccessful Higgs searches at LEP have resulted in the limit $m_h > 114.1$ GeV.

It is also possible to find clues for the mass of the SM Higgs through indirect observations. Quantum corrections to the Z and W boson mass relation, $M_W^2 = M_Z^2 \cos^2\theta_W$,

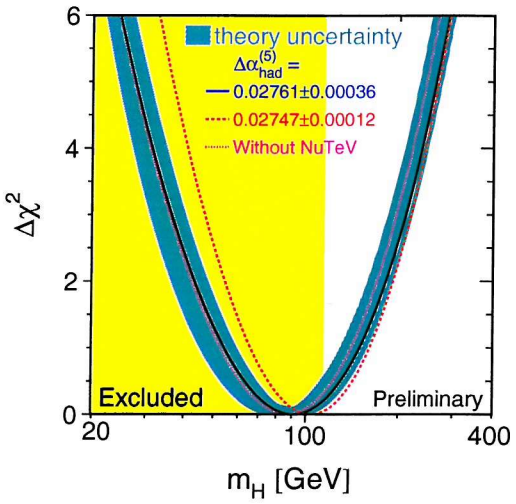

Figure 1.4: Plot of $\Delta\chi^2$ from a global fit to precision data against the Higgs boson mass. The solid curve shows the results of the fit with estimated theoretical errors shown as the shaded band. The vertical band represents the 95% C.L. exclusion limit on m_h from direct searches and the dashed curve represents the sensitivity to a change in $\alpha(M_Z^2)$ [5].

give

$$M_W^2 = M_Z^2 \cos^2\theta_W \left[1 + \delta_{\text{top}} + \delta_{\text{Higgs}}\right]. \tag{1.37}$$

The top quark correction, δ_{top}, is quadratically dependent on the top mass, whereas the Higgs correction, δ_{Higgs}, is only logarithmically dependent on the Higgs mass. Therefore eq. (1.37) is particularly sensitive to the top mass. At LEP I, before the discovery of the top quark, the top mass could be inferred from eq. (1.37) using measurements of M_W and M_Z. The discovery of the top quark and the accurate measurement of its mass at the TeVatron means that the Higgs corrections in eq. (1.37) can now be probed. The Z boson mass is particularly well known and so it is possible to examine the dependence of M_W upon m_t and m_h, see fig. (1.3). Both the direct and indirect 1σ regions shown in fig. (1.3) agree that a light SM Higgs boson is preferable.

The m_h dependence of the LEP Electroweak working group's SM global fit is shown in fig. (1.4), they deduce a 95% C.L. bound of $m_h \lesssim 170$ GeV. Combined with the lower bound from direct searches this hints that the SM Higgs should be just around the corner.

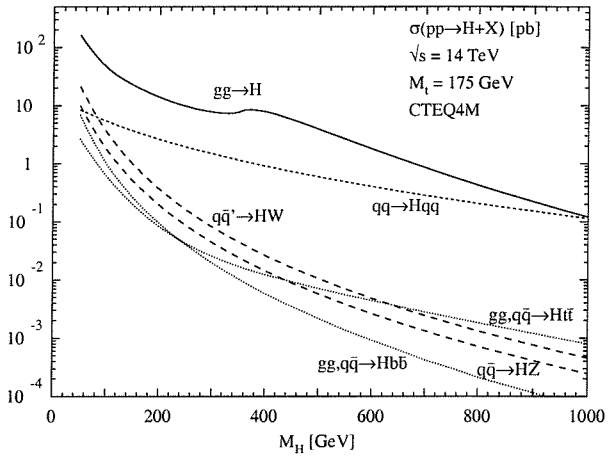

Figure 1.5: Higgs production cross-sections at the LHC [4].

The present expectation is that the Higgs boson will be found at either the TeVatron or LHC. At these hadronic machines Higgs production is dominated by gluon-gluon fusion through a top loop. The other main production processes and their cross-sections are summarised in fig. (1.5). In the region $m_h < 2M_W$, $h \to \gamma\gamma$ is the cleanest decay channel but it suffers from a small branching ratio, see fig. (1.2). For $m_h > 2M_W$ the channel $h \to ZZ \to l^+l^-l^+l^-$ becomes important. The planned searches at the LHC could discover a SM Higgs with mass up to 1 TeV.

1.3 Conclusion

In this section we have introduced the basic components of the Standard Model. The Higgs boson plays a major role in this model, it allows the gauge bosons and fermions in the theory to acquire masses through the breaking of the local gauge symmetry. Yet this most important particle is the only piece of the SM which has eluded experimental discovery. This situation is set change in the near future as the next generation of hadron colliders begin to record data.

Chapter 2

Extensions of the Standard Model

The Standard Model is a very successful theory which has been found to be in wonderful agreement with experimental measurements. It is clearly incomplete though as it doesn't incorporate gravity. Neglecting this, there are a few theoretical and experimental hints that the introduction of some new physics is desirable. The following sections will explore some of the problems of the Standard Model and their proposed solutions. Firstly we examine supersymmetry as a cure for the "Hierarchy Problem". We shall also see that supersymmetric theories are well motivated through the ideas of gauge coupling unification and radiative electroweak symmetry breaking. We then go on to discuss the minimal supersymmetric extension of the SM known as the MSSM. At present the only concrete evidence for physics beyond the standard model comes from the recently confirmed phenomenon of neutrino oscillation. Such oscillations require the neutrino to have mass, but this mass must be no larger than 0.23 eV[1], 2000 times smaller than the electron mass. An explanation for the neutrino's tiny mass is then presented in the form of right-handed neutrinos and the "see-saw mechanism".

[1]This limit comes from the 2dF Galaxy Redshift Survey [6] and the resent WMAP results [7].

2.1 Supersymmetry(SUSY)

Supersymmetry(SUSY)[2] is an extremely elegant theory which unites fermions and bosons. For every Standard Model fermion supersymmetry introduces an associated boson, known as a sfermion, with identical gauge quantum numbers. Supersymmetry extends the 4 bosonic dimensions of space-time with the addition of 4 fermionic dimensions. These Grassmann coordinates allow the Coleman-Mandula no-go theorem to be evaded and the space-time Poincaré group to be extended to include supersymmetry. Local SUSY also offers the inclusion of gravity and indeed it is a vital ingredient in Superstring theory, although low-energy SUSY is not a necessary consequence of such a theory.

2.1.1 The Motivation for low-energy supersymmetry

A brief discussion of the main motivational points for the introduction of weak scale supersymmetry is now given:

- **The Hierarchy Problem**

  In the Standard Model the mass of the photon is protected from radiative corrections by the exact $U(1)$ gauge invariance of QED. The broken chiral symmetry protects the electron mass by ensuring that any radiative correction is proportional to the mass of the electron. Unfortunately the SM does not possess a similar symmetry to protect the physical Higgs mass from radiative corrections. Therefore the contribution to the Higgs self energy from a fermion loop, as shown in fig. (2.1), will produce a quadratic divergence.

  Consider a fermion-Higgs coupling, $-\lambda_f \phi \bar{f} f$. Then evaluating the diagram

[2]The literature contains many fine reviews of supersymmetry some of which are listed in [8, 9].

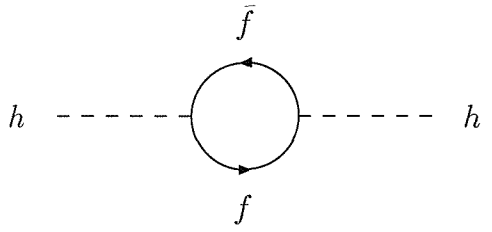

Figure 2.1: A fermion anti-fermion contribution to the Higgs self energy in the Standard Model.

shown in fig. (2.1) at zero external momentum gives,

$$\pi^f_{hh}(0) = -2N(f)\lambda_f^2 \int d^4k \left[\frac{1}{k^2 - m_f^2} + \frac{2m_f^2}{(k^2 - m_f^2)^2}\right]. \tag{2.1}$$

Here the electroweak symmetry breaking identity, $\phi = (v + h)/\sqrt{2}$, has been used and $N(f)$ is a multiplicity factor, e.g. for quarks $N(f) = 3$ due to colour. The first term of eq. (2.1) is clearly quadratically divergent. Completing the integration by introducing a momentum space cutoff Λ shows this explicitly, see eq. (2.2).

$$\delta m_h \simeq \frac{N(f)\lambda_f^2}{16\pi^2}\left[-2\Lambda^2 + 12m_f^2 \ln\left(\frac{\Lambda}{m_f}\right) + \ldots\right]. \tag{2.2}$$

The problem here is that if we want the cutoff of the theory to be at the level of M_{GUT} or M_{pl}, then the correction in eq. (2.2) will be 30 orders of magnitude larger than the physical Higgs mass. In order to preserve $m_h < 1\,\text{TeV}$, as we saw in section 1.2.5 that it must be, requires fine tuning at the level of 1 part in 10^{15} at all orders of perturbation theory. This is known as the "hierarchy problem" . Essentially the problem is that there is no explanation in the SM for the ratio M_{pl}/M_W.

One possibility is to introduce a pair of complex scalars, $\tilde{f}_{L,R}$ with couplings to

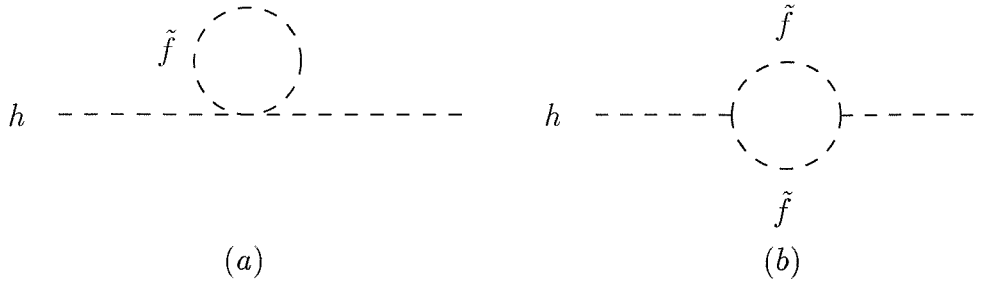

Figure 2.2: Sfermion contribution to the Higgs self energy with $\tilde{f} = \tilde{f}_{L,R}$.

the Higgs boson as follows,

$$\mathcal{L}_{\phi\tilde{f}} = \tilde{\lambda}_f \, \phi^2 \left(|\tilde{f}_L|^2 + |\tilde{f}_R|^2 \right) + \left(\lambda_f A_f \, \phi \tilde{f}_L \tilde{f}_R^* + \text{h.c.} \right). \tag{2.3}$$

The Lagrangian in eq. (2.3) leads to Higgs self energy contributions as shown in fig. (2.2). Again evaluating these contributions at zero external momentum we find,

$$\begin{aligned} \pi_{hh}^{\tilde{f}}(0) = & -\tilde{\lambda}_f N(\tilde{f}) \int \bar{d}^4 k \left[\frac{1}{k^2 - m_{\tilde{f}_L}^2} + \frac{1}{k^2 - m_{\tilde{f}_R}^2} \right] \\ & + \left(\tilde{\lambda}_f v \right)^2 N(\tilde{f}) \int \bar{d}^4 k \left[\frac{1}{\left(k^2 - m_{\tilde{f}_L}^2 \right)^2} + \frac{1}{\left(k^2 - m_{\tilde{f}_R}^2 \right)^2} \right] \\ & + |\lambda_f A_f|^2 N(\tilde{f}) \int \bar{d}^4 k \, \frac{1}{\left(k^2 - m_{\tilde{f}_L}^2 \right) \left(k^2 - m_{\tilde{f}_R}^2 \right)}. \end{aligned} \tag{2.4}$$

The first line of eq. (2.4) comes from the evaluation of diagram (a) in fig. (2.2), once again we find that it contains a quadratic divergence. The second and third lines represent the evaluation of diagram (b) in fig. (2.2). Comparing the first line of eq. (2.4) with eq. (2.1) we see that the quadratic divergencies can

be arranged to cancel if,

$$N(f) = N(\tilde{f}_L) = N(\tilde{f}_R) \tag{2.5}$$

$$\tilde{\lambda}_f = -\lambda_f^2. \tag{2.6}$$

The total Higgs mass corrections, eq. (2.1) and (2.4), can be made to cancel completely by requiring the additional conditions,

$$A_f = 0, \quad m_{\tilde{f}_L} = m_{\tilde{f}_R} = m_f. \tag{2.7}$$

This result hints that there is an additional symmetry, *Supersymmetry*, which protects the Higgs mass against radiative corrections. The condition eq. (2.6) shows the efficiency of supersymmetry with vertices for both the fermions and bosons being defined with the single coupling λ_f.

A particularly nice feature of SUSY is that if the condition of equal masses in eq. (2.7) is violated by some small amount, $\delta = m_{\tilde{f}} - m_f$, then we find that the radiative corrections will be proportional to δ. Therefore, provided that δ is small, the Higgs mass will remain stabilised against radiative corrections. The same cannot be said for the dimensionless couplings with, $\epsilon = \lambda_S - |\lambda_f|^2$, leading to a quadratic divergence.

- **Gauge Coupling Unification**

It is a common theoretical belief that the gauge group of the Standard Model should be embedded at high energy in the gauge group of a Grand Unified Theory(GUT). Examples of the possible GUT group are $SU(5)$, E_6, and $SO(10)$. In such a theory the three gauge couplings of the SM are unified into a single gauge coupling. The scaling of the SM couplings with energy scale μ is described by renormalisation group equations, eq. (2.8), which allow the extrapolation of the

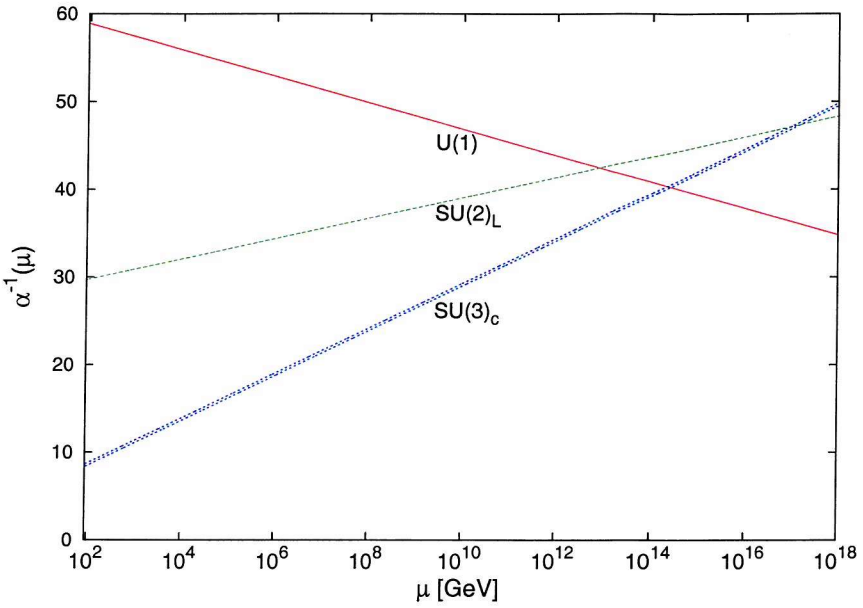

Figure 2.3: Gauge coupling evolution in the SM derived from solving the 1-loop beta functions, $\mu\frac{d\alpha_a}{d\mu} = -\frac{b_a}{(4\pi)^2}\alpha_a^2$. Here $\alpha_a = g_a^2/4\pi$, the index a refers to the three groups U(1), $SU(2)_L$ and $SU(3)_c$. In the standard model the coefficients b_a are, $b_a^{SM} = \left(\frac{41}{10}, -\frac{19}{6}, -7\right)$.

high energy couplings from the measured weak scale values, see fig. (2.3).

$$\mu\frac{\partial g_i}{\partial \mu} = \beta_i. \tag{2.8}$$

In eq. (2.8), g_i, with $i = 1, 2, 3$, represent the three standard model gauge couplings and the functions β_i come from quantum corrections to these couplings. Fig. (2.3) clearly shows that there is no single point at which the three SM couplings converge. On the other hand the additional particle content of a supersymmetric extension of the Standard Model results in the modification of the β-functions of eq. (2.8). Examining the minimal extension, the Minimal Supersymmetric Standard Model(MSSM) (see section 2.2), we find that the couplings do in fact approximately unify, see fig. (2.4), at a GUT scale of 10^{16} GeV. Hence

there is a real possibility of embedding the SM within a supersymmetric grand unified theory.

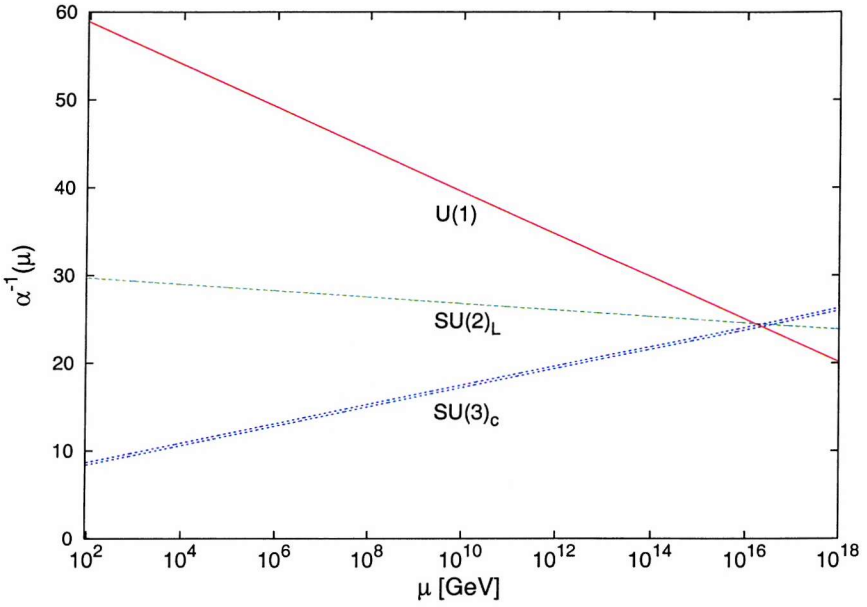

Figure 2.4: Gauge coupling evolution in the MSSM. As in fig. (2.3) this is derived from the solution of the 1-loop beta function with the coefficients, $b_a^{\mathrm{MSSM}} = \left(\frac{33}{5}, 1, -3\right)$. For simplicity the SUSY β functions have been assumed to be active down to the weak scale.

- **Radiative Electroweak Symmetry Breaking**

  An additional advantage of supersymmetric theories is that they can provide a theoretical explanation for the negative Higgs mass which initiates electroweak symmetry breaking via the Higgs mechanism. Radiative corrections to the Higgs mass, $m_{H_u}^2$, are dominated by top and stop loops. Corrections from RGE evolution from the GUT scale down to the weak scale drive $m_{H_u}^2$ negative and thus kick start the Higgs mechanism.

2.1.2 SUSY Algebra

We have seen in section 2.1.1 that the Higgs 2-pt function $\pi_{hh}(0)$ can be made to vanish exactly due to the addition of new bosonic fields. We claimed that this hinted at an additional symmetry. We would like to explore this new symmetry, in particular its Algebra, generators and the space in which it lives. Eq. (2.5) and (2.7) tell us that this symmetry must connect equal numbers of bosonic and fermionic degrees of freedom of equal mass. Also eq. (2.6) suggests that there should be a connection between boson and fermion Lagrangian interaction terms. Hence the generators, Q, of this symmetry connect fermions and bosons, see eq. (2.9) and therefore must be spin-$\frac{1}{2}$.

$$\begin{aligned} Q|\text{Fermion}>&=|\text{Boson}> \\ Q|\text{Boson}>&=|\text{Fermion}>\,. \end{aligned} \tag{2.9}$$

The simplest choice of generators are 2-component Weyl spinors Q and $\bar{Q}$ obeying the anti-commutation relations:

$$\{Q_\alpha,\, Q_\beta\} = \{\bar{Q}_{\dot{\alpha}},\, \bar{Q}_{\dot{\beta}}\} = 0 \tag{2.10}$$

$$\{Q_\alpha,\, \bar{Q}_{\dot{\beta}}\} = 2\sigma^\mu_{\alpha\dot{\beta}} P_\mu \quad \text{and} \quad [Q_\alpha,\, P_\mu] = \left[\bar{Q}_{\dot{\alpha}},\, P_\mu\right] = 0. \tag{2.11}$$

Here the indices α, β and $\dot{\alpha}$, $\dot{\beta}$ take the values 1 or 2, $\sigma^\mu = (1, \sigma_i)$ with σ_i being the Pauli matrices, and P_μ is the translation generator. The dot above the $\bar{Q}$ indices is a reminder that Q and $\bar{Q}$ transform under different representations of the Lorentz group. See appendix B for a review of the 2-component Weyl spinor notation. The anti-commutators and commutators in eq. (2.10) and (2.11) imply the extension of space-time and the Poincaré group with supersymmetry to become superspace and the super Poincaré group.

It is convenient to work with the superspace coordinates, $\{x^\mu,\, \theta,\, \bar{\theta}\}$, where θ, $\bar{\theta}$ are 2-

component anti-commuting Grassmann coordinates, i.e. $\{\theta, \theta\} = \{\theta, \bar{\theta}\} = \{\bar{\theta}, \bar{\theta}\} = 0$. A general superspace translation can therefore be written as

$$G_S(y, \epsilon, \bar{\epsilon}) = \mathrm{e}^{i\left(-y^\mu P_\mu + \epsilon Q + \bar{\epsilon}\bar{Q}\right)}. \tag{2.12}$$

Here, ϵ, $(\bar{\epsilon})$ parameterises an infinitesimal SUSY translation due to $Q\,(\bar{Q})$ in the same way that y parameterises the infinitesimal space-time translations due to P_μ. This SUSY transformation acts on *superfields* which are functions in superspace, $\Phi(x, \theta, \bar{\theta})$. Consider the effect of left multiplication by a supertranslation generator, $G_S(\epsilon, \bar{\epsilon})$, on an arbitrary superspace element $\Omega(x, \theta, \bar{\theta}) = \exp i\left[-x^\mu P_\mu + \theta Q + \bar{\theta}\bar{Q}\right]$

$$\begin{aligned} G_S(\epsilon, \bar{\epsilon})\Omega(x, \theta, \bar{\theta}) &= \exp i\left[\epsilon Q + \bar{\epsilon}\bar{Q}\right] \exp i\left[-x^\mu P_\mu + \theta Q + \bar{\theta}\bar{Q}\right] \\ &= \Omega\left(x^\mu - i\epsilon\sigma^\mu\bar{\theta} + i\theta\sigma^\mu\bar{\epsilon},\, \theta + \epsilon,\, \bar{\theta} + \bar{\epsilon}\right). \end{aligned} \tag{2.13}$$

In reaching the final line we have used Hausdorff's formula, $\mathrm{e}^A\mathrm{e}^B = \mathrm{e}^{A+B+\frac{1}{2}[A,B]+\cdots}$, and the anti-commutation relations in eq. (2.11). Therefore the action of the supertranslation $G_S(\epsilon, \bar{\epsilon})$ results in the coordinate variation,

$$\begin{aligned} \delta x &= i\left(\theta\sigma^\mu\bar{\epsilon} - \epsilon\sigma^\mu\bar{\theta}\right) \\ \delta\theta &= \epsilon, \qquad \delta\bar{\theta} = \bar{\epsilon}. \end{aligned} \tag{2.14}$$

From the coordinate variations we can deduce that the SUSY generators take the form,

$$Q_\alpha = -i\frac{\partial}{\partial\theta^\alpha} - (\sigma^\mu\bar{\theta})_\alpha\partial_\mu \quad \bar{Q}_{\dot{\alpha}} = i\frac{\partial}{\partial\bar{\theta}^{\dot{\alpha}}} + (\theta\sigma^\mu)_{\dot{\alpha}}\partial_\mu. \tag{2.15}$$

It is now convenient to define a SUSY covariant derivative which anti-commutes with the SUSY generators,

$$D_\alpha = \frac{\partial}{\partial\theta^\alpha} + i(\sigma^\mu\bar{\theta})_\alpha\partial_\mu \quad \bar{D}_{\dot{\alpha}} = \frac{\partial}{\partial\bar{\theta}^{\dot{\alpha}}} + i(\theta\sigma^\mu)_{\dot{\alpha}}\partial_\mu. \tag{2.16}$$

Hence the SUSY covariant derivatives obey the anti-commutation relations,

$$\{D_\alpha,\, D_\beta\} = \{\bar{D}_{\dot{\alpha}},\, \bar{D}_{\dot{\beta}}\} = 0 \tag{2.17}$$

$$\{D_\alpha,\, \bar{D}_{\dot{\beta}}\} = 2\sigma^\mu_{\alpha\dot{\beta}} P_\mu \tag{2.18}$$

$$\{D_\alpha,\, Q_{\dot{\beta}}\} = \{\bar{D}_{\dot{\alpha}},\, Q_\beta\} = \{D_\alpha,\, \bar{Q}_{\dot{\beta}}\} = \{\bar{D}_{\dot{\alpha}},\, \bar{D}_{\dot{\beta}}\} = 0. \tag{2.19}$$

Notice that both $(Q_\alpha)^\dagger = \bar{Q}_{\dot{\alpha}}$ and $(D_\alpha)^\dagger = \bar{D}_{\dot{\alpha}}$.[3] Therefore SUSY covariant derivatives commute with superspace translations; $G_S(\epsilon,\, \bar{\epsilon})\,(D_\alpha \Phi) = D_\alpha\,(G_S(\epsilon,\, \bar{\epsilon})\Phi)$, and $G_S(\epsilon,\, \bar{\epsilon})\,(\bar{D}_{\dot{\alpha}}\Phi) = \bar{D}_{\dot{\alpha}}\,(G_S(\epsilon,\, \bar{\epsilon})\Phi)$. Therefore a condition such as, $D_\alpha \bar{\Phi} = 0$ or $\bar{D}_{\dot{\alpha}}\Phi = 0$ is SUSY invariant.

A general scalar superfield, $\Phi(x,\, \theta,\, \bar{\theta})$, is a scalar function in superspace. Owing to the Grassmann nature of θ and $\bar{\theta}$, a Taylor series expansion in these coordinates will have a finite number of terms as shown in eq. (2.20).

$$\begin{aligned}\Phi(x,\, \theta,\, \bar{\theta}) = {} & f(x) + \theta\phi(x) + \bar{\theta}\bar{\chi}(x) + \theta\theta m(x) + \bar{\theta}\bar{\theta} n(x) \\ & + \theta\sigma^\mu\bar{\theta} v_\mu(x) + (\theta\theta)\,\bar{\theta}\bar{\lambda}(x) + \left(\bar{\theta}\bar{\theta}\right)\theta\psi(x) + \theta^2\bar{\theta}^2 d(x).\end{aligned} \tag{2.20}$$

Clearly, $\phi(x)$, $\chi(x)$, $\lambda(x)$, $\psi(x)$ are all fermionic fields, $f(x)$, $m(x)$, $n(x)$, $d(x)$ are complex scalars and $v_\mu(x)$ is a complex vector field. We now proceed to describe two irreducible superfield representations; Chiral and Vector superfields.

The Chiral Superfield

Enforcing the SUSY invariant condition,

$$\bar{D}_{\dot{\alpha}}\Phi(x,\, \theta,\, \bar{\theta}) = 0, \tag{2.21}$$

[3] Recall that $(\partial_\mu)^\dagger = -\partial_\mu$.

onto this general scalar superfield defines a chiral superfield, and likewise the condition

$$D_\alpha \bar{\Phi}(x,\, \theta,\, \bar{\theta}) = 0, \tag{2.22}$$

defines an anti-chiral superfield. We notice that

$$\begin{aligned} &D_\alpha \bar{\theta} = \bar{D}_{\dot{\alpha}} \theta = D_\alpha \bar{y}^\mu = \bar{D}_{\dot{\alpha}} y^\mu = 0 \\ &D_\alpha \theta^\beta = \delta_\alpha^\beta, \qquad\qquad \bar{D}_{\dot{\alpha}} \bar{\theta}^{\dot{\beta}} = \delta_{\dot{\alpha}}^{\dot{\beta}}, \\ &\qquad\qquad \text{and} \\ &D_\alpha y^\mu = 2i(\sigma^\mu \bar{\theta})_\alpha, \qquad \bar{D}_{\dot{\alpha}} \bar{y}^\mu = 2i(\theta \sigma^\mu)_{\dot{\alpha}}, \end{aligned} \tag{2.23}$$

and so it will be convenient to change variables to, $y^\mu = x^\mu + i\theta\sigma^\mu\bar{\theta}$ and $\bar{y}^\mu = x^\mu - i\theta\sigma^\mu\bar{\theta}$. Eq. (2.23) implies that $\Phi = \Phi(y,\, \theta)$ is independent of $\bar{\theta}$ and $\bar{\Phi} = \bar{\Phi}(\bar{y},\, \bar{\theta})$ is independent of θ. Therefore the component expansion of the chiral superfield Φ and the anti-chiral superfield $\bar{\Phi}$ now become particularly simple,

$$\Phi(y,\, \theta) = \phi(y) + \sqrt{2}\theta\psi(y) + \theta\theta F(y) \tag{2.24}$$

$$\bar{\Phi}(\bar{y},\, \bar{\theta}) = \phi^*(\bar{y}) + \sqrt{2}\bar{\theta}\bar{\psi}(\bar{y}) + \bar{\theta}\bar{\theta} F^*(\bar{y}), \tag{2.25}$$

or written as a Taylor series expansion in terms of x, θ and $\bar{\theta}$,

$$\begin{aligned} \Phi(y,\, \theta) &= \left[\phi(x) + i(\theta\sigma^\mu\bar{\theta})\partial_\mu\phi(x) - \tfrac{1}{2}(\theta\sigma^\mu\bar{\theta})(\theta\sigma^\nu\bar{\theta})\partial_\mu\partial_\nu\phi(x)\right] \\ &+ \left[\sqrt{2}\theta\psi(x) + \sqrt{2}i(\theta\sigma^\mu\bar{\theta})\partial_\mu(\theta\psi(x))\right] + \theta\theta F(x) \\ \Phi^\dagger(\bar{y},\, \bar{\theta}) &= \left[\phi^*(x) - i(\theta\sigma^\mu\bar{\theta})\partial_\mu\phi^*(x) - \tfrac{1}{2}(\theta\sigma^\mu\bar{\theta})(\theta\sigma^\nu\bar{\theta})\partial_\mu\partial_\nu\phi^*(x)\right] \\ &+ \left[\sqrt{2}\bar{\theta}\bar{\psi}(x) - \sqrt{2}i(\theta\sigma^\mu\bar{\theta})\partial_\mu(\bar{\theta}\bar{\psi}(x))\right] + \bar{\theta}\bar{\theta}F^*(x). \end{aligned} \tag{2.26}$$

Physically these fields describe a complex scalar ϕ, a Weyl fermion ψ and an auxiliary complex scalar field F used to ensure that the number of fermionic and bosonic degrees of freedom match on and off-shell. Therefore chiral superfields can be used to describe the 3 generations of fermions and the Higgs boson of the standard model.

It is clear from eq. (2.14) that the spinor θ has mass dimension $-\frac{1}{2}$. Assuming that the scalar field ϕ has mass dimension $+1$, then ψ must have mass dimension $+\frac{3}{2}$ and F has $+2$.

Applying the SUSY generators Q, $\bar{Q}$ to the chiral superfield Φ it can be easily shown that the components of Φ must transform as,

$$\begin{aligned} \delta_S\phi &= \sqrt{2}\,\epsilon\,\psi && \text{(boson} \rightarrow \text{fermion)} \\ \delta_S\psi &= \sqrt{2}\,\epsilon\,F + i\sqrt{2}\,\sigma^\mu\bar{\epsilon}\,\partial_\mu\phi && \text{(fermion} \rightarrow \text{boson)} \\ \delta_S F &= -i\sqrt{2}\,\partial_\mu\psi\,\sigma^\mu\bar{\epsilon} && (F \rightarrow \text{total derivative}). \end{aligned} \tag{2.27}$$

Notice that the component field F, which is accompanied by the maximum allowed number of θ's in the superfield expansion, transforms as a total derivative.

The Vector Superfield

To describe the spin-1 gauge bosons of the standard model we must introduce vector superfields. A vector superfield V is constrained to be self conjugate,

$$V(x,\,\theta,\,\bar{\theta}) \equiv V^\dagger(x,\,\theta,\,\bar{\theta}). \tag{2.28}$$

This leads us to the representation,

$$\begin{aligned} V = &\left(1 + \frac{1}{4}\theta\theta\bar{\theta}\bar{\theta}\partial_\mu\partial^\mu\right)C + \left(i\theta + \frac{1}{2}\theta\theta\sigma^\mu\bar{\theta}\partial_\mu\right)\chi + \frac{i}{2}\theta\theta\,[M + iN] \\ &+ \left(-i\bar{\theta} + \frac{1}{2}\bar{\theta}\bar{\theta}\sigma^\mu\theta\partial_\mu\right)\bar{\chi} - \frac{i}{2}\bar{\theta}\bar{\theta}\,[M - iN] \\ &- \theta\sigma_\mu\bar{\theta}A^\mu + i\theta\theta\bar{\theta}\bar{\lambda} - i\bar{\theta}\bar{\theta}\theta\lambda + \frac{1}{2}\theta\theta\bar{\theta}\bar{\theta}D. \end{aligned} \tag{2.29}$$

Here, $C(x)$, $M(x)$, $N(x)$ and $D(x)$ are real scalars, $\chi(x)$, $\lambda(x)$ are Weyl spinors, and $A^\mu(x)$ is a vector field. We would like A^μ to describe a gauge boson and so V, and therefore each component of V, must transform in the adjoint representation of the gauge group.

We can write the supersymmetric version of a non-abelian gauge transformation of a vector superfield V as,

$$e^{gV} \to e^{-ig\Lambda^\dagger} e^{gV} e^{ig\Lambda}, \tag{2.30}$$

where, $\Lambda(x, \theta, \bar{\theta})$, is a chiral superfield and g is the gauge coupling. The chiral superfield Λ contains 4 bosonic and fermionic degrees of freedom. This means that it is possible to choose a gauge, called the Wess-Zumino gauge, in which the scalars C, M, N and the spinor χ are eliminated from eq. (2.29). This leaves us with only the last line of eq. (2.29) and so V_{WZ} contains a vector field A^μ, an adjoint spinor λ and a real scalar D, see eq. (2.31). In this gauge we are still left with one bosonic degree of freedom which corresponds to the usual gauge freedom.

$$V_{WZ} = -\theta\sigma_\mu\bar{\theta}A^\mu + i\theta\theta\bar{\theta}\bar{\lambda} - i\bar{\theta}\bar{\theta}\theta\lambda + \frac{1}{2}\theta\theta\bar{\theta}\bar{\theta}D. \tag{2.31}$$

If we assume that the field A^μ has mass dimension $+1$ this implies that the fermion λ has mass dimension $+\frac{3}{2}$ and the field D has mass dimension $+2$.

In the Wess-Zumino gauge every term of the vector superfield contains at least one factor of θ or $\bar{\theta}$, therefore the only non-vanishing power of V_{WZ} is,

$$V_{WZ}^2 = \frac{1}{2}\theta\theta\bar{\theta}\bar{\theta}A_\mu A^\mu, \quad V_{WZ}^n = 0, \quad \text{for } n \geq 2. \tag{2.32}$$

It is useful to notice that the auxiliary field D transforms as a total derivative,

$$\delta_S D = -\epsilon\sigma^\mu\partial_\mu\bar{\lambda} + \bar{\epsilon}\sigma^\mu\partial_\mu\lambda. \tag{2.33}$$

Having introduced the concept of chiral and vector superfields Φ and V we would now like to construct an action out of them which is invariant under SUSY transformations.

2.1.3 Constructing a SUSY invariant Action

In this section we would like to construct a Lagrangian which leads to an action that is invariant under SUSY transformations, i.e.

$$\delta_S \int d^4x\, \mathcal{L}(x) = 0. \tag{2.34}$$

For eq. (2.34) to be satisfied it is enough that the Lagrangian $\mathcal{L}$ transforms as a total derivative. It is very useful to notice that the superfield components with the largest number of θ and $\bar{\theta}$ factors do indeed transform as total derivatives, see eq. (2.27) and (2.33). Therefore we can write an action,

$$S = \int d^4x \left(\int d^2\theta \mathcal{L}_F + \int d^2\theta d^2\bar{\theta} \mathcal{L}_D \right), \tag{2.35}$$

where the procedure of integration over Grassmann variables is identical to the action of differentiation, see appendix A. In eq. (2.35) we have used $\mathcal{L}_F$ and $\mathcal{L}_D$ respectively to denote general chiral and vector superfields. The subscript reminds us that the Grassmann integration will leave only the auxiliary field components F and D. We would now like to find all Lagrangian contributions to $\mathcal{L}_F$ and $\mathcal{L}_D$.

Products of (anti)chiral superfields are themselves (anti)chiral superfields, hence $\mathcal{L}_F$ can contain a product of chiral superfields. From eq. (2.24) it is straightforward to deduce that the product of two chiral superfields will provide fermion mass terms and the product of three chiral superfields will have Yukawa type interactions as the highest order components. Explicitly we can write the "F-terms" of these products as,

$$\Phi_1|_{\theta\theta} = F_1 \tag{2.36}$$

$$\Phi_1\Phi_2|_{\theta\theta} = \phi_1 F_2 + \phi_2 F_1 - \psi_1\psi_2 \tag{2.37}$$

$$\Phi_1\Phi_2\Phi_3|_{\theta\theta} = \phi_1\phi_2 F_3 + \phi_2\phi_3 F_1 + \phi_3\phi_1 F_2 - \phi_1\psi_2\psi_3 - \phi_2\psi_3\psi_1 - \phi_3\psi_1\psi_2. \tag{2.38}$$

The hermitian conjugate of a chiral superfield is an anti-chiral superfield $\Phi^\dagger \equiv \bar{\Phi}$. As in eq. (2.26) we can write this anti-chiral superfield as an expansion in x, θ, $\bar{\theta}$. This means that a contribution to $\mathcal{L}_D$ coming from the product of a chiral superfield with its hermitian conjugate will yield,

$$\int d^2\theta\, d^2\bar{\theta}\, \Phi\, \Phi^\dagger = \partial_\mu\phi\, \partial^\mu\phi^* + FF^* - i\psi\, \sigma^\mu\, \partial_\mu\bar{\psi} + (\text{total derivatives}). \tag{2.39}$$

Clearly eq. (2.39) contains kinetic energy terms for the scalar component ϕ and the fermionic component ψ, but not for F. Therefore the field F does not contain propagating degrees of freedom and so this auxiliary field can be eliminated by its equation of motion. An on-shell chiral superfield Φ then has two physical bosonic and fermionic degrees of freedom and so F ensures that this number is balanced both on and off-shell. This can be made explicit by examining the following *superpotential*,

$$W(\Phi_i) = k_i\Phi_i + \frac{1}{2}m_{ij}\Phi_i\Phi_j + \frac{1}{3}g_{ijk}\Phi_i\Phi_j\Phi_k. \tag{2.40}$$

A term like $\Phi^\dagger\Phi$ is not allowed to enter the superpotential as it is self-conjugate and is therefore a vector superfield. Therefore W mustn't contain any anti-chiral superfields and only chiral superfields, in other words the superpotential is an analytic function. Here Φ_i are chiral superfields and k_i, m_{ij}, g_{ijk}, are constants with mass dimension, 2, 1, 0 respectively. An implicit sum over repeated superfield indices is also assumed. A product of superfields is itself a superfield, hence W is a chiral superfield and so its $\theta\theta$ term will transform as a total derivative. Therefore W may constitute a Lagrangian term of a SUSY invariant action.

With the aid of the superpotential we can summarise the Lagrangian terms of eq. (2.36)-(2.39) in the compact form,

$$\mathcal{L} = \int d^2\theta d^2\bar{\theta}\ \Phi_i\Phi_i^\dagger + \left[\int d^2\theta\ W(\Phi_i) + h.c.\right]. \tag{2.41}$$

The superpotential $W(\Phi_i)$ is a function of superfields, $\Phi_i = \phi_i + \sqrt{2}\theta\psi_i + \theta\theta F_i$. It will be useful to Taylor expand W about the scalar field ϕ_i, eq. (2.42).

$$W(\Phi_i) = W(\phi_i) + \sqrt{2}\,\frac{\partial W}{\partial \phi_i}\theta\psi_i + \theta\theta\left(\frac{\partial W}{\partial \phi_i}F_i - \frac{1}{2}\frac{\partial^2 W}{\partial\phi_i\partial\phi_j}\,\psi_i\psi_j\right). \tag{2.42}$$

The partial derivatives of the superpotential, $\frac{\partial W}{\partial \phi_i} \equiv \frac{\partial W}{\partial \phi_i}\Big|_\phi$ and $\frac{\partial^2 W}{\partial\phi_i\partial\phi_j} \equiv \frac{\partial^2 W}{\partial\phi_i\partial\phi_j}\Big|_\phi$, are evaluated at the point about which the expansion is taken, namely the scalar field ϕ.

The Taylor expansion in eq. (2.42) now becomes very useful in simplifying the Lagrangian of eq. (2.41). The integration over $d^2\theta$ will pick out only the final line in the Taylor expansion. We may also make use of eq. (2.39) to write,

$$\mathcal{L} = \left(F_i F_i^* + |\partial_\mu\phi|^2 - i\psi_i\sigma^\mu\partial_\mu\bar{\psi}_i\right) + \left[\frac{\partial W}{\partial\phi_i}F_i - \frac{1}{2}\frac{\partial^2 W}{\partial\phi_i\partial\phi_j}\,\psi_i\psi_j + h.c.\right]. \tag{2.43}$$

Again an implicit sum over repeated indices is assumed. As the fields F_i have no kinetic term in eq. (2.43) they have a particularly simple equation of motion,

$$\frac{\partial\mathcal{L}}{\partial F_i^*} = 0 \quad \Rightarrow \quad F_i = -\left(\frac{\partial W}{\partial\phi_i}\right)^*, \tag{2.44}$$

which can be used to eliminate these auxiliary fields from the Lagrangian. This then leads us to the SUSY invariant action,

$$S = \int d^4x\left[\mathcal{L}_{kin} - \left(\frac{1}{2}\frac{\partial^2 W}{\partial\phi_i\partial\phi_j}\,\psi_i\psi_j + h.c.\right) - \left|\frac{\partial W}{\partial\phi_i}\right|^2\right]. \tag{2.45}$$

Here, $\mathcal{L}_{kin} = |\partial_\mu\phi|^2 - i\psi_i\sigma^\mu\partial_\mu\bar{\psi}_i$, contains the kinetic terms for the scalar ϕ and fermion ψ. Recall that the partial derivatives of the superpotential are evaluated at the scalar fields ϕ_i. This leads us to the observation that the scalar potential is

determined by,

$$V_F = \left| \frac{\partial W}{\partial \phi_i} \right|^2 . \tag{2.46}$$

So far the only "D-terms", i.e. terms with a $(\theta\theta)\bar{\theta}\bar{\theta}$ factor, we have explored are $\Phi\Phi^\dagger$. This is the simplest choice of Kähler potential, $K(\Phi_i^\dagger, \Phi_j)$, where K is real. We shall not consider any more complicated Kähler potentials here. Gauge-matter interactions can be accomplished by a SUSY version of the familiar "minimal coupling",

$$\begin{aligned} \int d^2\theta\, d^2\bar{\theta}\; \Phi^\dagger \mathrm{e}^{2gV} \Phi &= \int d^2\theta\, d^2\bar{\theta}\; \Phi^\dagger \left(1 + 2g\, V_{WZ} + 2g^2\, V_{WZ}^2\right) \Phi \\ &= |\mathrm{D}_\mu \phi|^2 - i\bar{\psi}\sigma^\mu \mathrm{D}_\mu \psi + g\phi^* D\phi \\ &\quad + ig\sqrt{2}\left(\phi^* \lambda\psi - \bar{\lambda}\bar{\psi}\phi\right) + |F|^2 . \end{aligned} \tag{2.47}$$

In the first line of eq. (2.47) we have expanded the exponential in powers of the vector superfield V_{WZ} in the Wess-Zumino gauge, which has only two terms, see eq. (2.32). To arrive at the final line we have made use of the Taylor expansion of Φ and $\Phi^\dagger$ shown in eq. (2.26) and the identities found in appendix B. We have also introduced the gauge-covariant derivative, $\mathrm{D}_\mu = \partial_\mu + igA_\mu$, where g is the gauge coupling. We write the gauge field as $A_\mu = A_\mu^a \mathrm{T}_a$, and in the same fashion $\lambda = \lambda^a \mathrm{T}_a$ and $D = D^a \mathrm{T}_a$, where T_a are the gauge generators. The Lagrangian terms in eq. (2.47) therefore not only introduces interactions of matter fields with gauge fields, but also gauge strength Yukawa-like interactions between fermions-sfermions-gauginos. These additional interactions include things like *top-stop-Wino* and *higgsino-higgs-Bino* interactions.

Finally we would like to include a kinetic energy term for the gauge fields. This can be done be introducing the superfield,

$$W_\alpha = \left(\bar{D}^{\dot{\beta}} \bar{D}_{\dot{\beta}}\right) \mathrm{e}^{-gV} D_\alpha \mathrm{e}^{gV}, \tag{2.48}$$

D_α and $\bar{D}_{\dot{\beta}}$ again being the SUSY-covariant derivatives. Here W_α is a chiral superfield as $\bar{D}_{\dot{\alpha}} W_\alpha = 0$. Hence the $\theta\theta$ component of the product $W^\alpha W_\alpha$ may contribute to a SUSY invariant action.

$$\frac{1}{32g^2} W^\alpha W_\alpha \Big|_{\theta\theta} = -\frac{1}{4} F^a_{\mu\nu} F_a^{\mu\nu} + \frac{1}{2} D_a D^a + \left(-\frac{i}{2} \lambda^a \sigma_\mu \partial^\mu \bar{\lambda}_a + \frac{1}{2} g f^{abc} \lambda_a \sigma_\mu A^\mu_a \bar{\lambda}_c + h.c. \right). \tag{2.49}$$

Here, $F_{\mu\nu} = \partial_\mu A_\nu - \partial_\nu A_\mu + i\,[A_\mu,\, A_\nu]$, are usual field strength tensor for the gauge fields, A_μ. Notice that in addition to the usual kinetic term for the gauge fields, $F^a_{\mu\nu} F_a^{\mu\nu}$, we also get a kinetic term for the gauginos λ_a and a coupling of the gauginos to the gauge fields. Note that eq. (2.49) does not contain a kinetic energy term for the field D and so we are again able to eliminate this field from the Lagrangian. The equation of motion for this field can easily be determined from eq. (2.47) and (2.49) to be,

$$\frac{\partial \mathcal{L}}{\partial D_a} = 0 \quad \Rightarrow \quad D_a = -g \left(\phi_i^* \mathrm{T}_a^{ij} \phi_j \right). \tag{2.50}$$

Using this equation of motion we can now substitute eq. (2.50) into the second term of eq. (2.49) and the third term of eq. (2.47). These terms now give a contribution to the scalar potential,

$$V_D = \frac{1}{2} \left| g\, \phi_i^* \mathrm{T}_a^{ij} \phi_j \right|^2, \tag{2.51}$$

here there is an implicit sum over the indices i, j and a. So far we have dealt only with the supersymmetry conserving lagrangian terms. As it is clear that supersymmetry is broken we must also look at possible SUSY breaking contributions.

2.1.4 Soft SUSY Breaking Lagrangian

In previous sections we found that in supersymmetric theories the masses of fermions and their super-partner bosons are identical. Clearly nature doesn't reflect this as no superpartner has ever been discovered. Hence supersymmetry must be a broken symmetry. Therefore any realistic model must have a Lagrangian which is invariant under supersymmetry, but a vacuum which is not. It is very interesting to notice that the SUSY algebra eq. (2.11) acting on a momentum eigenstate $|p\rangle$ can be written as,

$$\left\{Q_\alpha, \bar{Q}_{\dot{\beta}}\right\}|p\rangle = 2\begin{pmatrix} p_0 + p_3 & p_1 - ip_2 \\ p_1 + ip_2 & p_0 - p_3 \end{pmatrix}_{\alpha\dot{\beta}} |p\rangle. \tag{2.52}$$

The energy of the state $|p\rangle$ is given by p_0 and so,

$$p_0|p\rangle = \frac{1}{4}\left[\left\{Q_1, Q_1^\dagger\right\} + \left\{Q_2, Q_2^\dagger\right\}\right]|p\rangle. \tag{2.53}$$

We can then interpret this as the Hamiltonian, and take the expectation value of a state $|\psi\rangle$ which is given by a sum of squares,

$$\langle\psi|H|\psi\rangle = \frac{1}{4}\left(||Q_1|\psi\rangle||^2 + ||Q_1^\dagger|\psi\rangle||^2 + ||Q_2|\psi\rangle||^2 + ||Q_2^\dagger|\psi\rangle||^2\right) \geq 0. \tag{2.54}$$

If the vacuum state $|0\rangle$ is supersymmetric then the vacuum has zero energy as it is annihilated by the supercharges. But if the vacuum state is not annihilated by at least one SUSY generator then we have a positive vacuum energy and so supersymmetry is spontaneously broken if the vacuum energy is positive.

Let us assume that supersymmetry is broken by the VEV of some scalar particle. The scalar potential contains two pieces, as mentioned in eq. (2.46) and (2.50), so we

have,

$$V_F + V_D = \left|\frac{\partial W}{\partial \phi_i}\right|^2 + \frac{g_l^2}{2}\left|\phi_i^* \mathrm{T}_{l,a}^{ij} \phi_j\right|^2, \tag{2.55}$$

where l labels the gauge group. Again we see that $V \geq 0$ and so supersymmetry is broken by either $\langle F_i \rangle \sim \langle \frac{\partial W}{\partial \phi_i} \rangle \neq 0$ ("F-term" breaking) or $\langle D_{l,a} \rangle \sim \langle \phi_i^* \mathrm{T}_{l,a}^{ij} \phi_j \rangle \neq 0$ ("D-term" breaking).

There is a problem in the spontaneous breaking of supersymmetry by F-terms and D-terms. There exists a sum rule for the tree-level squared masses of the scalars and fermions,

$$\mathrm{Tr}\, M_S^2 = 2\,\mathrm{Tr}\, M_f^2. \tag{2.56}$$

Where M_S are the masses of the scalars and M_f are the masses of the fermions. If supersymmetry is unbroken then eq. (2.56) follows naturally from the mass degeneracy of complex scalars and their Weyl fermion superpartners. This relation still holds at tree-level even when supersymmetry is broken by F or D-terms. This sum rule is incompatible with phenomenology because it suggests that the sfermion partners of the standard model fermions should be lighter than the known fermions. The favoured solution to this problem is to have SUSY breaking occur indirectly through the breaking of SUSY in some "hidden sector". The term hidden means that its particles share no(or very small) direct interaction with those of our own "visible sector". Supersymmetry breaking is communicated from this "hidden sector" to the "visible sector" through some shared interactions, e.g. gravity. In this scenario the sum rule of eq. (2.56) no longer holds and so a realistic model can be constructed.

The exact mechanism of supersymmetry breaking is as yet unknown. However it is very useful to pass over this complication and simply introduce extra terms which break supersymmetry explicitly. As we saw in section 2.1.1 these extra terms should

only contain couplings of positive mass dimension and must "softly" break supersymmetry in order to maintain the solution to the hierarchy problem. It has been shown [10] that the most general soft SUSY breaking Lagrangian may include,

- scalar squared masses: $-m_\phi^2|\phi_i|^2$
- trilinear scalar interactions: $-A_{ijk}\phi_i\phi_j\phi_k$
- gaugino masses: $-\frac{1}{2}m_l\bar{\lambda}_l\lambda_l$
- bilinear terms: $-B_{ij}\phi_i\phi_j + h.c.$
- gauge singlet linear terms: $-C_i\phi_i$

This completes our discussion of the construction of a SUSY invariant Lagrangian. We are now ready to construct a realistic example.

2.2 The Minimal Supersymmetric Standard Model

We would now like to study a realistic supersymmetric theory, that is a model with broken SUSY which also satisfies all phenomenological constraints. The Minimal Supersymmetric Standard Model(MSSM)[4] represents the simplest realistic SUSY model. This model is a straightforward supersymmetrisation of the standard model. The gauge group is not extended beyond the $SU(3)_c \otimes SU(2)_L \otimes U(1)_Y$ of the standard model. Also the minimal number of superfields have been introduced. As the fermions and gauge bosons of the standard model reside in different representations of the gauge group they cannot be contained within the same superfield, e.g. the component field λ within V_{WZ} of eq. (2.31) cannot be identified with a quark or lepton field. This means that we require 5 superfields for each generation, see table 2.1. In addition

[4]See reference [9] for other reviews of the MSSM.

Particles		Spin 0	Spin 1/2	$SU(3)_c$	$SU(2)_L$	$Y/2$
squarks, quarks	$\hat{Q}_i$	$\tilde{Q}_{iL} = \begin{pmatrix} \tilde{u}_{iL} \\ \tilde{d}_{iL} \end{pmatrix}$	$Q_{iL} = \begin{pmatrix} u_{iL} \\ d_{iL} \end{pmatrix}$	**3**	**2**	1/6
	$\hat{U}_i^c$	$\tilde{u}_i^c = \tilde{u}_{iR}^*$	$u_i^c = -i\sigma^2 u_{iR}^*$	$\bar{\mathbf{3}}$	**1**	−2/3
	$\hat{D}_i^c$	$\tilde{d}_i^c = \tilde{d}_{iR}^*$	$d_i^c = -i\sigma^2 d_{iR}^*$	$\bar{\mathbf{3}}$	**1**	1/3
slepton, lepton	$\hat{L}_i$	$\tilde{L}_{iL} = \begin{pmatrix} \tilde{\nu}_{iL} \\ \tilde{e}_{iL} \end{pmatrix}$	$L_{iL} = \begin{pmatrix} \nu_{iL} \\ e_{iL} \end{pmatrix}$	**1**	**2**	−1/2
	$\hat{E}_i^c$	$\tilde{e}_i^c = \tilde{e}_{iR}^*$	$e_i^c = -i\sigma^2 e_{iR}^*$	**1**	**1**	1
Higgs, Higgsino	$\hat{H}_u$	$H_u = \begin{pmatrix} H_u^+ \\ H_u^0 \end{pmatrix}$	$\tilde{H}_u = \begin{pmatrix} \tilde{H}_u^+ \\ \tilde{H}_u^0 \end{pmatrix}$	**1**	**2**	1/2
	$\hat{H}_d$	$H_d = \begin{pmatrix} H_d^0 \\ H_d^- \end{pmatrix}$	$\tilde{H}_d = \begin{pmatrix} \tilde{H}_d^0 \\ \tilde{H}_d^- \end{pmatrix}$	**1**	**2**	−1/2

Table 2.1: Quarks, leptons and superpartner squarks and sleptons of the MSSM with associated G_{SM} gauge quantum numbers. A family index, $i = 1 \ldots 3$, has been included. The notation here is that $\tilde{f} = \tilde{f}_L$ is the scalar superpartner of the left-handed fermion f_L and $\tilde{f}^c = \tilde{f}_R^*$ is the scalar partner of the right-handed fermion f_R.

vector superfields are required for the eight $SU(3)_c$ gluons, three $SU(2)_L$ W bosons and the single $U(1)_Y$ B gauge field. These superfields are listed in table 2.2 which also lists their fermionic superpartners; eight gluinos $\tilde{g}$, three Winos $\tilde{W}$ and a Bino $\tilde{B}$.

Particles	Spin 1/2	Spin 1	$SU(3)_c$	$SU(2)_L$	$Y/2$
gluino, gluon	$\tilde{g}^\alpha$	g^α	**8**	**1**	0
Winos, W bosons	$\tilde{W}^a$	W^a	**1**	**3**	0
Bino, B boson	$\tilde{B}$	B	**1**	**1**	0

Table 2.2: Gauge bosons and superpartner gauginos of the MSSM with associated G_{SM} gauge quantum numbers. With indices, $\alpha = 1 \ldots 8$, $a = 1 \ldots 3$.

Table 2.1 highlights the doubling of the Higgs sector as a significant extension of the SM Higgs sector. We would like to break the gauge group with an $SU(2)_L$ scalar

doublet with $|Y| = 1$. If we had a single Higgs doublet, as in the standard model, then there would be problems with triangle anomalies. In the standard model the trace over the $U(1)_Y$ quantum numbers of a complete fermion generation vanishes. In the MSSM we must also worry about higgsino contributions to such an anomaly and so we are required to have two Higgs doublets,

$$H_u = \begin{pmatrix} H_u^+ \\ H_u^0 \end{pmatrix} \quad \text{with} \quad Y/2 = +1/2 \tag{2.57}$$

$$H_d = \begin{pmatrix} H_d^0 \\ H_d^- \end{pmatrix} \quad \text{with} \quad Y/2 = -1/2. \tag{2.58}$$

Two Higgs doublets are also required due to the superpotential being analytic and so we cannot use the conjugate of a single Higgs doublet to generate up quarks masses as we do in the standard model, see eq. (1.18).

We would now like to determine the interactions present in the MSSM. As we saw in the previous section the interaction terms of the SM fermions and their scalar partners are determined by the superpotential. The superpotential of the MSSM is,

$$W_{\text{MSSM}} = -\hat{H}_u \hat{Q} Y_u \hat{U}^c + \hat{H}_d \hat{Q} Y_d \hat{D}^c + \hat{H}_d \hat{L} Y_e \hat{E}^c + \mu \hat{H}_u \hat{H}_d. \tag{2.59}$$

Here the multiplication of doublets, $H_u Q = \epsilon_{ab} H_u^a Q^b = H_u^+ d_L - H_u^0 u_L$, is defined by the tensor $\epsilon_{12} = -\epsilon_{21} = +1$, with $a, b = 1, 2$. The matrices $Y_{u,d,e}^{ij}$ are Yukawa couplings with the generation indices $i, j = 1 \ldots 3$. Importantly the superpotential in eq. (2.59) respects the lepton and baryon number symmetry. Unfortunately these symmetries are not necessarily obeyed as they must be in the standard model and only emerge here due to the choice of superpotential.

With this superpotential, eq. (2.59), we can derive interaction terms for the sfermions from F and D-term Lagrangian contributions as written in eq. (2.55). The F-term,

$\left|\frac{\partial W}{\partial \phi_i}\right|^2_\phi$, generates 3 and 4-pt scalar interactions. For example the Higgs μ-term and the Yukawa couplings combine to yield 3-pt interactions of the form, $\mu^* \tilde{e}^*_R y_e \tilde{e}_L H^{0*}_u$, $\mu^* \tilde{u}^*_R y_u \tilde{u}_L H^{0*}_d$ and $\mu^* \tilde{d}^*_R y_d \tilde{d}_L H^{0*}_u$. The D-term, eq. (2.51), contribution can be written as,

$$V_D = \frac{1}{2} D^a_l D^a_l = \frac{1}{2}\left[D_Y D_Y + D^x_2 D^x_2 + D^\alpha_3 D^\alpha_3\right], \qquad (2.60)$$
$$\text{with} \qquad D^a_l =, g_l(\phi^* \mathrm{T}^a_l \phi)$$

where the index a labels the generators of the group l, with an implicit sum over both. It is straightforward to determine that,

$$D_Y = g'\left(-\frac{1}{2}|\tilde{L}|^2 + \frac{1}{6}|\tilde{Q}|^2 + |\tilde{e}_R|^2 - \frac{2}{3}|\tilde{u}_R|^2 + \frac{1}{3}|\tilde{d}_R|^2 + \frac{1}{2}|H_u|^2 - \frac{1}{2}|H_d|^2\right) \qquad (2.61)$$

$$D^x_2 = g\left(\tilde{L}^\dagger t^x \tilde{L} + \tilde{Q}^\dagger t^x \tilde{Q} + H^\dagger_u t^x H_u + H^\dagger_d t^x H_d\right) \qquad (2.62)$$

$$D^\alpha_3 = g_3\left(\tilde{Q}^\dagger \mathrm{T}^\alpha \tilde{Q} - \tilde{u}_R \mathrm{T}^{\alpha *} \tilde{u}^*_R - \tilde{d}_R \mathrm{T}^{\alpha *} \tilde{d}^*_R\right). \qquad (2.63)$$

Here t^x and T^α represent the generators of $SU(2)$ and $SU(3)$ respectively. It is clear from eq. (2.60-2.63) that, in the event of H_u, H_d acquiring their VEVs, D_Y and D^3_2 will contribute mass terms for the sfermions.

The superpotential also provides interaction terms for fermions via the Lagrangian contribution,

$$\Delta\mathcal{L} = -\frac{1}{2}\frac{\partial^2 W}{\partial\phi_i \partial\phi_j}\psi_i \psi_j + h.c., \qquad (2.64)$$

as in eq. (2.45). Here ψ_i are the fermionic superpartners of ϕ_i. These interactions importantly include the usual Yukawa couplings of the fermions to the respective Higgs fields and therefore generate masses via spontaneous symmetry breaking, e.g. $m^{ij}_u = v_u Y^{*ij}_u$, $m^{ij}_d = v_d Y^{*ij}_d$ and $m^{ij}_e = v_d Y^{*ij}_e$. In addition interactions of the form, higgsino-fermion-sfermion, are also generated with a coupling strength determined by

the Yukawa couplings.

As we saw in eq. (2.47) there will also be gaugino-fermion-sfermion interactions,

$$\Delta\mathcal{L} = g'\sqrt{2}\phi^*\tilde{B}\frac{Y}{2}\psi + g\sqrt{2}\phi^*\tilde{W}^x t^x\psi + g_3\sqrt{2}\phi^*\tilde{g}^\alpha \mathrm{T}^\alpha\psi. \tag{2.65}$$

It turns out that the MSSM Lagrangian contains terms which have an even number of superpartners. This leads to "R-parity" conservation which means that any sparticle decay must contain an odd number of sparticles. Hence the Lightest SUSY Particle(LSP) must be stable. This provides a standard signature of sparticle production at colliders that can be distinguished from SM events. Another consequence of a stable LSP, owing to the stringent big-bang relic density constraints, is that the LSP must be neutral. Therefore a characteristic signal of LSP events at colliders will be missing energy.

Finally, the MSSM must be a model with softly broken supersymmetry. Therefore the general soft SUSY breaking Lagrangian for the MSSM is,

$$\begin{aligned}
-\mathcal{L}_{\text{soft}} &= m_{\tilde{Q}}^2|\tilde{Q}|^2 + m_{\tilde{L}}^2|\tilde{L}|^2 + m_{\tilde{u}}^2|\tilde{u}_R|^2 + m_{\tilde{d}}^2|\tilde{d}_R|^2 + m_{\tilde{e}}^2|\tilde{e}_R|^2 \\
&+ \left(A_e H_d \tilde{L}\tilde{e}_R^* + A_d H_d \tilde{Q}\tilde{d}_R^* + A_u H_u \tilde{Q}\tilde{u}_R^* + B\mu H_d H_u + h.c.\right) \\
&+ m_{H_d}^2|H_d|^2 + m_{H_u}^2|H_u|^2 + \frac{1}{2}M_1\tilde{B}\tilde{B} + \frac{1}{2}M_2\tilde{W}\tilde{W} + \frac{1}{2}M_3\tilde{g}\tilde{g}.
\end{aligned} \tag{2.66}$$

Here, the soft scalar masses, $m_{\tilde{Q}}^2$, $m_{\tilde{L}}^2$, $m_{\tilde{u}}^2$, $m_{\tilde{d}}^2$, $m_{\tilde{e}}^2$, are 3×3 hermitian matrices, and A_e, A_d, A_u are general 3×3 matrices. The masses $M_{1,2,3}$ are soft gaugino masses and $m_{H_{u,d}}^2$ are soft higgs mass terms.

The soft SUSY breaking Lagrangian of eq. (2.66) adds over 100 unknown parameters to the MSSM and many of these can be involved in flavour mixing and CP violation. Fortunately this means that these parameters can be constrained by experimental measurements. For example if either one of $m_{\tilde{e}}^2$ or $m_{\tilde{L}}^2$ is non-diagonal in the lepton

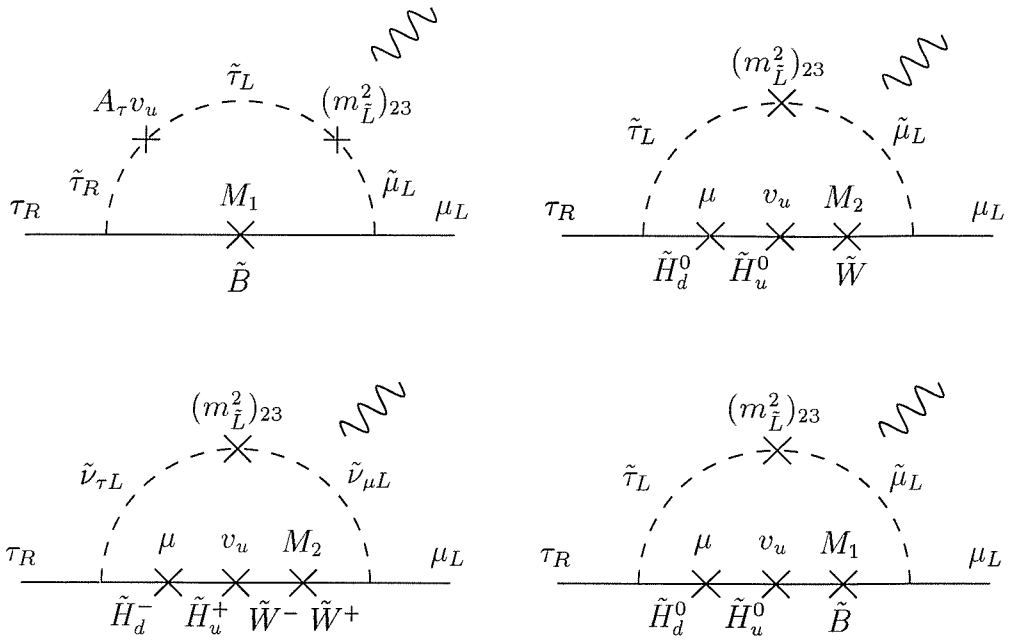

Figure 2.5: Diagrams that contribute to $\tau \to \mu\gamma$ in the MSSM. Notice that the diagrams shown here have $\tan\beta$ enhancement.

mass eigenstate basis then there will be flavour mixing amongst sleptons. This mixing can enter into the leptons radiatively through virtual slepton loops, see fig. (2.5) for example contributions to $\tau \to \mu\gamma$. Therefore experimental limits on lepton flavour violation, e.g. $\mu \to e\gamma$, provides strong constraints on such non-diagonal elements of the slepton mass squared matrix. Similar constraints for the squark soft mass squared matrices, $m^2_{\tilde{Q}}$, $m^2_{\tilde{u}}$, $m^2_{\tilde{d}}$, are provided by $K^0 \leftrightarrow \bar{K}^0$ mixing and $b \to s\gamma$, see fig. (2.6) for example diagrams. These constraints also apply to $A_{u,d,e}$ as after the Higgs fields acquire their VEVs they contribute non-diagonal terms to the squark and slepton mass squared matrices, see fig. (2.5) and (2.6) for examples. The CP violating phases are further constrained by limits on the electric dipole moment of the neutron and electron.

All such flavour changing and CP violating effects arising from the soft parameters

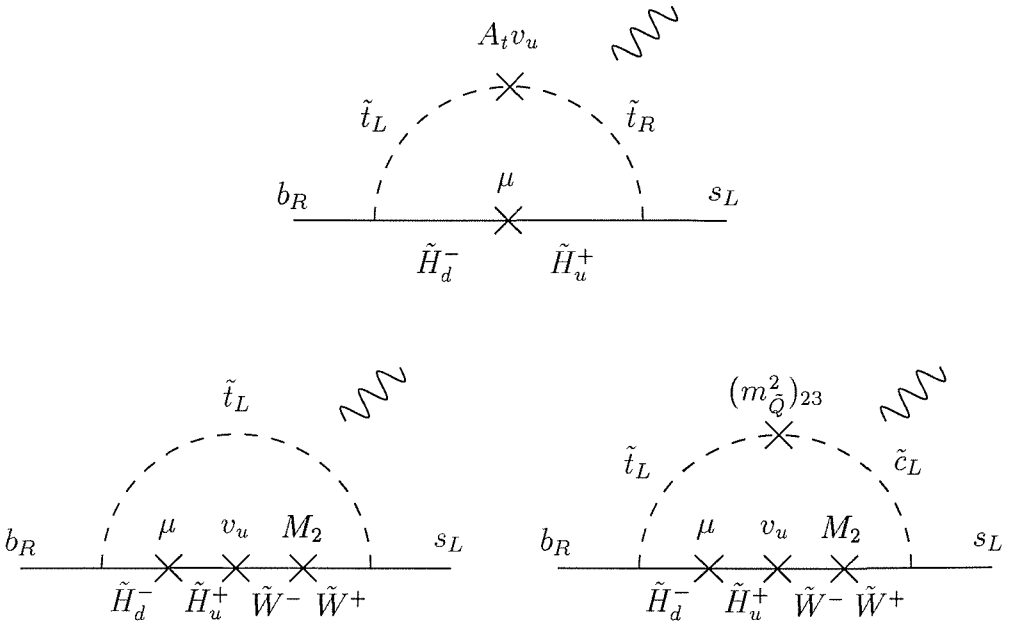

Figure 2.6: Chargino contributions to $b \to s\gamma$ in the MSSM. The three diagram shown here are enhanced by large $\tan\beta$.

can be evaded if we assume universality,

$$\begin{aligned} \mathbf{m}^2_{\tilde{Q},\tilde{u},\tilde{d}} &= m^2_{\tilde{Q},\tilde{u},\tilde{d}}\mathbf{1} \\ \mathbf{m}^2_{\tilde{L},\tilde{e}} &= m^2_{\tilde{L},\tilde{e}}\mathbf{1} \\ \mathbf{A}_{u,d,e} &= A^0_{u,d,e}\mathbf{Y}_{u,d,e} \\ \text{with} \quad & \mu,\ B\mu,\ m^2_{H_u,H_d},\ m^2_{\tilde{Q},\tilde{u},\tilde{d}},\ m^2_{\tilde{L},\tilde{e}},\ A^0_{u,d,e} \quad \text{all real.} \end{aligned} \tag{2.67}$$

The above universality condition means that the only CP-violating phase is that of the CKM matrix. This kind of scenario is quite plausible, for instance if the mediating interactions between the "hidden" and "visible" sectors are flavour blind then universality is automatic. One such example comes from gravity mediation in which case we have, $m_0^2 = m^2_{\tilde{Q},\,\tilde{u},\,\tilde{d},\,\tilde{L},\,\tilde{e}}$ and $A_0 = A^0_{u,\,d,\,e}$. In addition it is natural in

Grand Unified Theories to define all three gaugino masses to be equal , $M_{1/2} = M_1 = M_2 = M_3$, at the GUT scale.

This completes the definition of the MSSM Lagrangian. Let us now investigate the mechanism of symmetry breaking and the resulting Higgs sector of the MSSM.

2.2.1 The Higgs mechanism in the MSSM

We would like spontaneous breaking of the gauge symmetry, hence the scalar potential is required to have a minimum away from the origin. The Higgs scalar potential has three contributions from; the superpotential F-term of eq (2.46), the D-terms of eq. (2.60) and the soft Higgs masses in eq. (2.66). The complete potential then takes the form,

$$\begin{aligned} V_{\rm H} &= m_1^2|H_d|^2 + m_2^2|H_u|^2 + \left(m_3^2 H_d H_u + h.c.\right) \\ &+ \frac{g'^2+g^2}{8}\left(|H_u|^2 - |H_d|^2\right)^2 + \frac{g^2}{2}\left|H_u H_d^*\right|^2 \qquad (2.68) \\ &\text{with,} \qquad m_1^2 = m_{H_d}^2 + |\mu|^2 \\ &\qquad\qquad m_2^2 = m_{H_u}^2 + |\mu|^2 \\ &\qquad\qquad m_3^2 = B\mu. \end{aligned}$$

The first three terms come from a combination of soft SUSY breaking Higgs masses m_{H_u,H_d}^2 and the F-term Higgs mass μ. The last two terms come from the D-term contributions of eq. (2.60) [5]. It is worth noting that the strength of the quartic interaction is determined by the gauge couplings rather than being a free parameter as in the standard model, we will see later the consequences of this.

[5]The $SU(2)$ identity, $\sigma_{ij}^a \sigma_{kl}^a = 2\delta_{il}\delta_{jk} - \delta_{ij}\delta_{kl}$, is used to simplify the D-term contributions

As with the standard model we are free to use $SU(2)$ invariance to choose the vacuum,

$$< H_u >= \begin{pmatrix} 0 \\ v_u \end{pmatrix} \qquad < H_d >= \begin{pmatrix} v_d \\ 0 \end{pmatrix}, \tag{2.69}$$

where v_u and v_d are real. We will see later that the two Higgs VEVs can be related to the SM Higgs VEV v of eq. (1.5) as,

$$\frac{1}{2}v^2 = v_u^2 + v_d^2. \tag{2.70}$$

Therefore we can write the Z boson mass, as in eq. (1.13), in terms of the Higgs VEVs,

$$M_Z^2 = \frac{1}{2}(v_u^2 + v_d^2)\left(g'^2 + g^2\right). \tag{2.71}$$

It is useful to write these two VEVs in terms of a single parameter, $\tan\beta$,

$$\tan\beta \equiv \frac{v_u}{v_d} \quad \text{with} \quad v_u = \frac{v}{\sqrt{2}}\sin\beta, \quad v_d = \frac{v}{\sqrt{2}}\cos\beta. \tag{2.72}$$

Using the above definitions the minimization conditions for the Higgs potential in eq. (2.68), $\frac{\partial V_{\rm H}}{\partial H_u^0} = \frac{\partial V_{\rm H}}{\partial H_d^0} = 0$, can be written as,

$$\begin{aligned} m_1^2 &= -m_3^2\tan\beta - \tfrac{1}{2}M_Z^2\cos 2\beta \\ m_2^2 &= -m_3^2\cot\beta + \tfrac{1}{2}M_Z^2\cos 2\beta. \end{aligned} \tag{2.73}$$

The presence of M_Z here is a direct consequence of the fact that the quartic coupling is determined by the gauge couplings as mentioned earlier. These conditions can be used to derive expressions for $B\mu$ and μ in terms of $\tan\beta$, $m_{H_u}^2$ and $m_{H_d}^2$,

$$B\mu = \frac{1}{2}\left[(m_{H_d}^2 - m_{H_u}^2)\tan 2\beta + m_Z^2\sin 2\beta\right] \tag{2.74}$$

$$\mu^2 = \frac{1}{\cos 2\beta}\left(m_{H_d}^2 \sin^2\beta - m_{H_u}^2 \cos^2\beta\right) - \frac{1}{2}M_Z^2. \tag{2.75}$$

We shall later use the fact that eq. (2.74) allows us to eliminate $B\mu$ in favour of $\tan\beta$. We can also determine $\mu(M_{GUT})$ from $\mu(M_Z)$, leaving the condition eq. (2.75) to be determined by the two parameters, m_{H_u}, m_{H_u} in order for the correct minimization of the Higgs potential.

The Higgs doublets, H_d, H_u, contain eight degrees of freedom, three of which are eaten by the $W^{\pm}$, Z gauge bosons as in the standard model. This leaves five physical degrees of freedom, which are arranged into 2 CP-even neutral Higgs, h^0, H^0, 1 neutral pseudoscalar A^0 and a charged Higgs H^+. Compare this with the single physical Higgs boson of the standard model.

The Higgs mass squared matrices and mass eigenstates can easily be determined from the matrix of second derivatives evaluated at the minimum of the potential, eq. (2.69). For the imaginary degrees of freedom we have,

$$\mathcal{M}_I^2 = \begin{pmatrix} -m_3^2\cot\beta & -m_3^2 \\ -m_3^2 & -m_3^2\tan\beta \end{pmatrix} \qquad \text{in the basis} \quad \left\{\Im H_u^0/\sqrt{2},\, \Im H_d^0/\sqrt{2}\right\}. \tag{2.76}$$

Notice that, $\det \mathcal{M}_I^2 = 0$, so there is a massless neutral Goldstone mode and a massive pseudoscalar A^0. For the real degrees of freedom,

$$\mathcal{M}_R^2 = \begin{pmatrix} -m_3^2\cot\beta + M_Z^2\sin^2\beta & m_3^2 - \frac{1}{2}M_Z^2\sin 2\beta \\ m_3^2 - \frac{1}{2}M_Z^2\sin 2\beta & -m_3^2\tan\beta + M_Z^2\cos^2\beta \end{pmatrix} \qquad \text{in the basis} \quad \left\{\Re H_u^0/\sqrt{2},\, \Re H_d^0/\sqrt{2}\right\}. \tag{2.77}$$

Here we have two massive CP-even Higgs states, h^0 and H^0, with $m_{h^0} < m_{H^0}$. In

terms of the original gauge eigenstate fields we can write the mass eigenstates as,

$$\begin{pmatrix} G^0 \\ A^0 \end{pmatrix} = \frac{1}{\sqrt{2}} \begin{pmatrix} \sin\beta & -\cos\beta \\ \cos\beta & \sin\beta \end{pmatrix} \begin{pmatrix} \Im H_u^0 \\ \Im H_d^0 \end{pmatrix} \tag{2.78}$$

$$m_{A^0}^2 = \mathrm{Tr}\left(\mathcal{M}_I^2\right) = -\frac{2m_3^2}{\sin 2\beta}, \qquad m_{G^0}^2 = 0$$

$$\begin{pmatrix} h^0 \\ H^0 \end{pmatrix} = \frac{1}{\sqrt{2}} \begin{pmatrix} \cos\alpha & -\sin\alpha \\ \sin\alpha & \cos\alpha \end{pmatrix} \begin{pmatrix} \Re H_u^0 \\ \Re H_d^0 \end{pmatrix} \tag{2.79}$$

$$m_{h^0,H^0}^2 = \frac{1}{2}\left(m_{A^0}^2 + M_Z^2 \mp \sqrt{(m_{A^0}^2 + M_Z^2)^2 - 4M_Z^2 m_{A^0}^2 \cos^2 2\beta}\right).$$

Here the CP-even mixing angle α is written as,

$$\frac{\sin 2\alpha}{\sin 2\beta} = -\frac{m_{A^0}^2 + M_Z^2}{m_{H^0}^2 - m_{h^0}^2}, \quad \frac{\cos 2\alpha}{\cos 2\beta} = -\frac{m_{A^0}^2 - M_Z^2}{m_{H^0}^2 - m_{h^0}^2}. \tag{2.80}$$

The mass squared matrix for charged Higgs states is written as,

$$\mathcal{M}_\pm^2 = \begin{pmatrix} -m_3^2\cot\beta + M_W^2\cos^2\beta & m_3^2 - \frac{1}{2}M_W^2\sin^2\beta \\ m_3^2 - \frac{1}{2}M_W^2\sin^2\beta & -m_3^2\tan\beta + M_W^2\sin^2\beta \end{pmatrix} \tag{2.81}$$

$$\text{in the basis} \quad \left\{H_u^+,\, H_d^{-*}\right\}.$$

Again we have, $\det \mathcal{M}_\pm^2 = 0$, and we have a second Goldstone mode G^+ and a massive charged Higgs boson H^+. Written in terms of the original gauge fields we have,

$$\begin{pmatrix} G^+ \\ H^+ \end{pmatrix} = \begin{pmatrix} \sin\beta & -\cos\beta \\ \cos\beta & \sin\beta \end{pmatrix} \begin{pmatrix} H_u^+ \\ H_d^{-*} \end{pmatrix} \tag{2.82}$$

$$\text{with,} \qquad m_{H^\pm}^2 = m_{A^0}^2 + M_W^2, \qquad m_{G^+}^2 = 0,$$

with $G^- = G^{+*}$ and $H^- = H^{+*}$.

Eq. (2.78), (2.79), (2.82), give us important information about the relative tree-level

masses of the Higgs bosons,

$$\begin{aligned} m_{H^\pm} &> M_W \\ m_{H^0} &> M_Z \\ m_{h^0} &< m_{A^0} \\ m_{h^0} &< M_Z |\cos\beta|. \end{aligned} \tag{2.83}$$

The final identity of eq. (2.83) implies that the tree-level mass of the lightest Higgs m_{h^0} should be lighter than the mass of the Z boson. This particularly restricting bound is the final result of the Higgs quartic coupling in eq. (2.69) being determined by the gauge couplings rather than being a free parameter as it is in the standard model eq. (1.3). Fortunately top-stop loop corrections give a large logarithmic correction, $\sim \ln\left(\frac{m_{\tilde{t}}}{m_t}\right)$, to this limit. Including all such corrections and assuming all sparticle masses are below 1 TeV this limit can be extended to,

$$m_{h^0} \lesssim 150\,\text{GeV}. \tag{2.84}$$

One interesting situation to look at is, $m_{A^0} \gg M_Z$, with m_{A^0}, m_{H^0}, $m_{H^\pm}$, being much heavier than, $m_{h^0} \approx M_Z|\cos\beta|$, and almost degenerate. In this limit eq. (2.80) implies that the mixing angle $\alpha \sim \beta - \pi/2$ which, see table 2.3, means that h^0 has the same couplings to quarks, leptons and gauge bosons as the Higgs of the non-supersymmetric standard model. So h^0 would be the only detectable MSSM Higgs boson at future colliders, yet it would be very difficult to distinguish from the usual SM Higgs. Despite this the discovery of a Higgs mass below 150 GeV would imply new physics must appear at a relatively low scale, as indicated in fig. (1.1). The search for the Higgs is therefore a key tool in the search for physics beyond the standard model and particularly the MSSM.

A discussion of the mixings involved in the SUSY partners of the Higgs and gauge bosons can be found in appendix C. Also in this appendix can be found details of

the squark and slepton mass squared matrices.

2.2.2 Higgs couplings

In section 1.2.2 we derived the Standard Model Higgs couplings to the gauge bosons. We can execute exactly the same procedure for the MSSM through the examination of the covariant derivative. The only real difference to the results in eq. (1.11) is that we now have two Higgs doublets with $Y = \pm 1$. So it is straight forward to write the MSSM Higgs-gauge boson couplings as,

$$\begin{aligned}\mathcal{L}_{Higgs-gauge} = & \frac{g^2}{2}\left[v_u^2\left|1+\frac{H_u^0}{v_u}\right|^2 + v_d^2\left|1+\frac{H_d^0}{v_d}\right|^2\right] W_\mu^+ W^{-\mu} \\ & + \frac{(g^2+g'^2)}{4}\left[v_u^2\left|1+\frac{H_u^0}{v_u}\right|^2 + v_d^2\left|1+\frac{H_d^0}{v_d}\right|^2\right] Z_\mu Z^\mu. \end{aligned} \tag{2.85}$$

As was mentioned earlier eq. (2.85) defines the gauge boson masses in terms of the two Higgs VEVs as,

$$M_Z^2 = \frac{1}{2}\left(v_u^2+v_d^2\right)\left(g^2+g'^2\right), \quad M_W^2 = \frac{g^2}{2}\left(v_u^2+v_d^2\right), \tag{2.86}$$

and comparing these results with the Z boson mass in the SM, eq. (2.13), we can relate the MSSM and SM VEVs as in eq. (2.71).

As in section 1.2.2 we can also extract the couplings of the Higgs to the gauge bosons. Table 2.3 contains the vertex factors for the 3-point MSSM Higgs gauge boson interactions. Notice that all the couplings of Higgs bosons to gauge bosons are suppressed by, $\sin(\beta-\alpha)$ or $\cos(\beta-\alpha)$, relative to the SM couplings. As we mentioned earlier, in the limit $m_A^0 \to \infty$, the CP-even mixing angle is approximately $\alpha = \beta - \pi/2$. Hence in this limit, $s_{\beta-\alpha} \to 1$, $c_{\beta-\alpha} \to 0$. Therefore in the large m_{A^0} limit h^0 is indistinguishable from the SM Higgs and H^0 decouples from the gauge bosons.

	WW	ZZ
h^0	$ig\, M_W\, s_{\beta-\alpha}$	$\frac{iM_Z}{v} s_{\beta-\alpha}$
H^0	$ig\, M_W\, c_{\beta-\alpha}$	$\frac{iM_Z}{v} c_{\beta-\alpha}$
A^0	0	0

Table 2.3: MSSM Higgs couplings to gauge bosons. [a]

[a] A complete list of Higgs couplings can be found in [11].

2.2.3 MSSM Higgs searches

The production of MSSM Higgs bosons proceeds via similar mechanisms to those in the SM, discussed in section 1.2.5. The main differences are that production through vector bosons and Higgs-strahlung is only possible for the CP-even Higgs states and is suppressed by factors of $s_{\beta-\alpha}$ or $c_{\beta-\alpha}$. This can be understood by inspecting the couplings for the CP-odd Higgs in table 2.3. The dominant production process will again be gluon-gluon fusion via a top-quark loop. A bottom-quark loop will contribute equally in the large $\tan\beta$ region, as $y_b/y_t = m_b/m_t \tan\beta$.

Fig. (2.7) shows the expected discovery potential for MSSM Higgs bosons at the ATLAS experiment at the LHC. Very similar figures are also produced for the CMS experiment. The lightest Higgs state h^0 produced in association with $t\bar{t}$ may be seen in the $b\bar{b}$ decay channel for $m_{A^0} \gtrsim 110\,\text{GeV}$ and in the mass range, $m_{A^0} \gtrsim 200$ GeV, h^0 may be found through the $\gamma\gamma$ channel. For $m_{A^0} \gtrsim 100$ GeV and moderate to large $\tan\beta$ the heavy states H^0, A^0 can be seen in the $\tau\tau$ channel. The coupling of Higgs bosons to charged leptons will grow with large $\tan\beta$ in the same way as for the bottom-quark, therefore the $\mu\mu$ channel will also open for large $\tan\beta$. It is also possible to see the charged Higgs in the channel $t \to bH^+$ in the region $m_{A^0} \lesssim 140$ GeV. It is therefore possible to find a signal for an extended Higgs sector over a large region of the m_{A^0}, $\tan\beta$ parameter space.

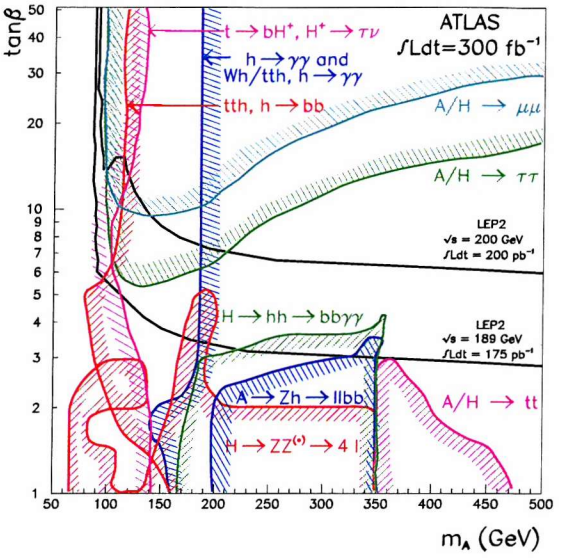

Figure 2.7: Expected discovery contours for the MSSM Higgs bosons at ATLAS with 300 fb^{-1} integrated luminosity. The limits on m_{h^0} set by direct searches at LEP II are also shown [12].

2.3 Massive Neutrinos

The previous sections introduced the concept of supersymmetry purely on the grounds of theoretical prejudice. Neutrino physics[6] on the other hand represents the first piece of experimental evidence for physics beyond the standard model. In recent years the solar neutrino problem and the atmospheric anomaly have been explained by the discovery of neutrino oscillations. Such oscillations require neutrinos to have masses, but these masses are constrained by galaxy observations to be very small. We shall see that these tiny masses can be explained very naturally by the "see-saw mechanism". This mechanism requires the introduction of right-handed neutrinos which are also a necessary ingredient of many Grand Unified Theories. The large atmospheric neutrino mixing can be constructed in such a mechanism with the aid of "single right-handed neutrino dominance".

[6] A list of excellent reviews of Neutrino Physics can be found in [13].

The present section will present an outline of the experimental work which has led to the discovery of neutrino masses. Following this will be a discussion of the above mentioned theoretical scenarios which explain these experimental observations.

2.3.1 Motivation

In the standard model the neutrino must remain massless due to the accidental lepton number symmetry. Also the neutrinos of the standard model are left handed only in accordance with electroweak observations. Conversely recent neutrino oscillation experiments have shown that the neutrino must indeed have mass, albeit an extremely small mass. The challenge for theorists is now to explain the origin of these masses and mixings. The mixings observed among neutrinos are far larger than those in the quark sector and this only adds to the puzzle.

The study of neutrino physics has focused on neutrinos from a variety of different sources; the sun, the upper atmosphere, nuclear reactors, particle accelerators and supernovae. Here we shall concentrate on just atmospheric and solar neutrino experiments.

Atmospheric neutrinos are produced when cosmic rays collide with the upper atmosphere to produce pions. The subsequent decay of the pion leads to the production of both electron and muon type neutrinos with a relative ratio of approximately $1:2$. Hence it is useful to study the ratio, $R = \frac{(N_\mu/N_e)_{\text{exp}}}{(N_\mu/N_e)_{\text{theory}}}$, where $N_{\mu,e}$ denotes the number of observed neutrinos of flavour μ, e, and its zenith angle variation. The experimental results, primarily from the water Cherenkov detectors Kamiokande [14] and Super-Kamiokande [15], show that the double ratio is $R = 0.54 \pm 0.05 \pm 0.01$ [16] rather than the non-oscillation prediction of $R = 1$. This startling observation can be explained by either the disappearance of muon neutrinos or the appearance of electron neutrinos or both. The study of the zenith angle variation of R has shown that this

suppression is in fact due to the disappearance of muon neutrinos. It was also noticed that the suppression was greater for muon neutrinos travelling from the other side of the earth, through its core and into the detector than for those travelling the short distance from the upper atmosphere directly above the detector. The result is that this can be very well explained by a simple two-state mixing $\nu_\mu \leftrightarrow \nu_\tau$ with a mixing matrix,

$$\begin{pmatrix} \nu_\mu \\ \nu_\tau \end{pmatrix} = \begin{pmatrix} \cos\theta_{23} & \sin\theta_{23} \\ -\sin\theta_{23} & \cos\theta_{23} \end{pmatrix} \begin{pmatrix} \nu_2 \\ \nu_3 \end{pmatrix}. \tag{2.87}$$

Here $\nu_{\mu,\tau}$ are the flavour eigenstates associated with the corresponding charged leptons μ, τ and $\nu_{2,3}$ are the neutrino mass eigenstates. The oscillation probability is written,

$$P(\nu_\mu \to \nu_\tau) = \sin^2 2\theta_{23} \sin^2\left(1.27\,\Delta m^2_{32}\frac{L}{E}\right). \tag{2.88}$$

Where L is in km, E in GeV, $\Delta m^2_{ij} = m^2_i - m^2_j$ is in eV^2 and the numerical factor of 1.27 comes from the conversion of units. The best fit analysis gives,

$$\begin{gathered} 1.3 \times 10^{-3}\, eV^2 < |\Delta m^2_{32}| < 3.0 \times 10^{-3}\, eV^2 \\ \sin^2 2\theta_{23} > 0.92, \quad \text{at } 90\%\ C.L.. \end{gathered} \tag{2.89}$$

Therefore the experimental results indicate maximal $\nu_\mu - \nu_\tau$ mixing. Eq. (2.88) shows that the existence of neutrino mass is vital to the oscillation phenomenon and the solution to the atmospheric anomaly.

The story is very similar for the solar neutrinos produced by the nuclear reactions within the sun. For many years experimentalists and theorists where puzzled by the "solar neutrino problem": there was an apparent mismatch between the number of electron neutrinos reaching earth from the sun and the number expected from studies of the nuclear reactions within the sun. It was recently shown by the

heavy water detector at the Sudbury Neutrino Observatory(SNO) [17] that the solution must be the oscillation of electron neutrinos into a combination of muon and tau neutrinos, $\nu_e \rightarrow \nu_{\mu,\tau}$. Pre-SNO there had been a number of different oscillation scenarios; VAC(vacuum oscillations), LOW(large mixing angle, small Δm^2), SMA(small mixing angle), the matter enhanced LMA(large mixing angle) and oscillations into singlet(sterile) neutrinos. Combining the data from SNO and the reactor experiment KamLAND [18] tells us that the only remaining solution is the MSW[7] LMA solution with, $\tan^2\theta_{12} \simeq 0.4$ and has a relatively small mass squared splitting $|\Delta m^2_{21}| \simeq 1 \times 10^{-5}\, eV^2$.

This leads us to a 3 generation mixing described by,

$$\begin{pmatrix} \nu_e \\ \nu_\mu \\ \nu_\tau \end{pmatrix} = \begin{pmatrix} U_{e1} & U_{e2} & U_{e3} \\ U_{\mu 1} & U_{\mu 2} & U_{\mu 3} \\ U_{\tau 1} & U_{\tau 2} & U_{\tau 3} \end{pmatrix} \begin{pmatrix} \nu_1 \\ \nu_2 \\ \nu_3 \end{pmatrix}. \tag{2.90}$$

Here U_{li} is a 3×3 unitary matrix known as the Maki-Nakagawa-Sakata(MNS) [19] matrix. Unlike the CKM matrix, discussed in section 1.2.3, the lepton equivalent contains 3 mixing angles and 3 phases. This is due to the Majorana nature of the neutrino. A significant difference is that the mixing in the neutrino sector is unusually large compared to the quark sector.

The final mixing angle θ_{13} remains unmeasured, but the reactor experiment CHOOZ [20] is able to provide the bound, $\sin^2 2\theta_{13} < 0.1 - 0.3$, due to the non-observation of $\bar{\nu}_e$ disappearance[8]. Also unknown are the signs of the mass squared differences, Δm^2_{32}, Δm^2_{21} and it will be very important for these unknown quantities to be determined at future neutrino experiments in order to determine the neutrino mass matrix,

[7]MSW stands for Mikheyev, Smirnov and Wolfenstein who are credited with proposing the solution in which neutrino oscillations are enhanced by matter effects within the sun.

[8]For this reason the neutrino mixing angle θ_{13} is often referred to as the CHOOZ angle.

2.3.2 See-Saw mechanism

Having found that neutrinos indeed have mass we are then confronted with the conundrum of how such a tiny mass comes about. One very popular explanation is given by the introduction of right-handed neutrino states, ν_R. These extra neutrinos are gauge singlets and so can have arbitrarily large masses. We shall see that through the see-saw mechanism it is these large masses which suppress the mass scale of the neutrino states found in the electroweak interactions.

The familiar Dirac mass term involving a fermion and its conjugate takes the form,

$$\mathcal{L}_D = -m\bar{\psi}\psi = -m\left(\bar{\psi}_L\psi_R + \bar{\psi}_R\psi_L\right). \tag{2.91}$$

The mass term of eq. (2.91) obeys the conservation of fermion number and the conservation of charge. This is the only possible mass term for fermions which carry a $U(1)_{\text{em}}$ charge.

As neutrinos carry no such charge it is possible for them to have other types of mass terms containing 2 neutrinos or 2 anti-neutrinos. These additional terms violate lepton number but are otherwise allowed. Such Majorana mass terms are discussed in more detail in appendix. B.2

Therefore there are three possible mass terms for the neutrino. They can be written as,

$$\begin{aligned}\mathcal{L}^{\nu}_{\text{mass}} &= \frac{1}{2}\left[\bar{\nu}_L m_D \nu_R + \bar{\nu}^c_R m_D^{\mathrm{T}} \nu^c_L + h.c.\right] \\ &\quad - \frac{1}{2}\left[\bar{\nu}^c_R\, m_S\, \nu_R + h.c.\right] - \frac{1}{2}\left[\bar{\nu}_L\, m_T\, \nu^c_L + h.c.\right].\end{aligned} \tag{2.92}$$

In the first term of eq. (2.92) we have rewritten the Dirac mass in terms of charge conjugate fields, $\psi^c = \hat{C}\bar{\psi}^{\mathrm{T}}$ as defined in appendix B. This is done so that we can

construct the mass matrix,

$$\mathcal{L}^{\nu}_{mass} = -\frac{1}{2}\,(\bar{\nu}_L,\, \bar{\nu}^c_R) \begin{pmatrix} m_T & m_D \\ m_D^{\mathrm{T}} & m_S \end{pmatrix} \begin{pmatrix} \nu^c_L \\ \nu_R \end{pmatrix} + h.c.. \tag{2.93}$$

Here m_D is the Dirac mass, m_S is the Majorana mass for the gauge singlet fields ν_R and m_T is the Majorana mass for the left neutrino fields, ν_L. If we have 3 generations of both right and left handed neutrinos then the mass matrix in eq. (2.93) will be 6×6. Diagonalising this mass matrix with unitary matrices, U_L and U_R such that,

$$U_L^{\dagger}\, M\, U_R = M_{\mathrm{diag}}, \tag{2.94}$$

where M is the mass matrix of eq. (2.93), defines the change of basis from the original neutrino fields,

$$\psi_L = \begin{pmatrix} \nu_L \\ \nu^c_R \end{pmatrix}, \psi_R = \begin{pmatrix} \nu^c_L \\ \nu_R \end{pmatrix}, \tag{2.95}$$

into the mass eigenstates,

$$\eta_L = U_L^{\dagger}\psi_L, \qquad \eta_R = U_R^{\dagger}\psi_R. \tag{2.96}$$

If we consider the case of a single generation with $m_T = 0$ and $m_S \gg m_D$, then the mass matrix will have eigenvalues equal to m_S and $-m_D^2/m_S$. The neutrino Dirac mass m_D is expected to be of the same order of magnitude as the associated charged lepton mass. There is no such expectation for the Majorana mass, m_S, and so if we allow it to have a GUT scale mass then the lighter mass eigenstate will be greatly suppressed. This is the see-saw mechanism in which the tiny neutrino masses $m_\nu \sim m_D^2/m_S$ are generated through the introduction of heavy right-handed neutrinos with Majorana masses m_S.

In this simple case the mass matrix is diagonalised by the orthogonal matrix,

$$U = \begin{pmatrix} 1 & m_D/m_S \\ -m_D/m_S & 0 \end{pmatrix}. \tag{2.97}$$

Eq. (2.96) then leads us to the mass eigenstates,

$$\begin{aligned} \eta_1 &= \eta_{1L} + \eta_{1R} = (\nu_L + \nu_L^c) - \tfrac{m_D}{m_S}(\nu_R^c + \nu_R) \\ \eta_2 &= \eta_{2L} + \eta_{2R} = (\nu_R^c + \nu_R) + \tfrac{m_D}{m_S}(\nu_L + \nu_L^c). \end{aligned} \tag{2.98}$$

Then it is clear that, $\nu_L = \eta_{1L} + \frac{m_D}{m_S}\eta_{2L}$, with mass $\sim m_D^2/m_S$ can be associated with the neutrino of the electroweak interactions. On the other hand, $\nu_R = \eta_{2R} - \frac{m_D}{m_S}\eta_{1R}$, with mass $\sim m_S$ is a heavy right-handed neutrino state.

This one generation case can be generalised by taking m_D and m_S to be $n \times n$ matrices. Provided the eigenvalues of m_S are much larger than those of m_D then again we will have a spectrum of very light and very heavy neutrino states. In this general case the see-saw formula for the light neutrino mass matrix is,

$$m_{LL} = m_D m_S^{-1} m_D^{\mathrm{T}}, \tag{2.99}$$

with the Lagrangian term, $m_{LL}\bar{\nu}_L \nu_L^c$. The see-saw mechanism can be incorporated within the MSSM by the simple addition of two extra terms into the superpotential of eq. (2.59). The two terms to be added will be a Yukawa coupling Y_ν, and a large Majorana mass term for the right-handed neutrinos. These two terms will reproduce m_D and m_S above. The new superpotential can be written as,

$$\begin{aligned} W_{MSSM+\nu^c} &= W_{MSSM} + W_{\nu^c} \\ \text{with} \qquad W_{\nu^c} &= -\hat{H}_u \hat{L}\, Y_\nu\, \hat{\nu}^c + \frac{1}{2}\hat{\nu}^c\, M_{RR}\, \hat{\nu}^c. \end{aligned} \tag{2.100}$$

Here M_{RR} is the Majorana mass for the right-handed neutrino states ν^c. Integrating

out the heavy fields we find that,

$$\frac{\partial W_{\nu^c}}{\partial \hat{\nu}^c} = 0 \quad \Rightarrow \quad W_{\nu^c} = -\frac{1}{2}(\hat{H}_u \hat{L})\; Y_\nu M_{RR}^{-1} Y_\nu^{\mathrm{T}}\; (\hat{H}_u \hat{L})^{\mathrm{T}}. \tag{2.101}$$

Therefore after the up type Higgs acquires its VEV a Majorana mass, similar to eq. (2.99) will be generated for the doublet neutrinos,

$$m_{LL}^* = v_u^2\, Y_\nu M_{RR}^{-1} Y_\nu^{\mathrm{T}}, \tag{2.102}$$

with the Lagrangian term, $\nu_L^T m_{LL}^* \nu_L$. Diagonalisation of m_{LL} with the unitary matrix V_L^ν is achieved as,

$$m_{LL} = V_L^\nu\, m_{LL}^{\mathrm{diag}}\, V_L^{\nu\mathrm{T}}, \quad \text{or} \quad m_{LL}^* = V_L^{\nu *}\, m_{LL}^{*\,\mathrm{diag}}\, V_L^{\nu\dagger}, \tag{2.103}$$

which defines the change of basis, $\nu_L' = V_L^{\nu\,\dagger}\nu_L$, where ν_L' are the neutrino mass eigenstates. If we assume that the charged lepton Yukawa coupling is diagonalised via,

$$Y^e = V_L^e\, Y_{\mathrm{diag}}^e\, V_R^{e\dagger}, \tag{2.104}$$

so that, $e_L' = V_L^{e\,\dagger}\, e_L$ and $e_R' = V_R^{e\,\dagger}\, e_R$, define the rotation into the mass eigenstates, $e_{L,R}'$. As in the quark sector the charged current interaction leads to the definition of a CKM like matrix,

$$V^{MNS} = V_L^{e\,\dagger}\, V_L^\nu, \tag{2.105}$$

defined so that,

$$J^{\mu -} = \frac{1}{\sqrt{2}}\, e_{iL}'^{\dagger}\, \gamma^\mu\, V_{MNS}^{ij}\, \nu_{jL}'. \tag{2.106}$$

It is clear from eq. (2.103) and (2.104) that unlike the quark sector we only have the

freedom to choose three phases in V_L^e, i.e. there is no phase freedom in the definition of V_L^ν. Therefore the physical degrees of freedom within V_{MNS} are the three mixing angles and three phases.

2.3.3 Single Right-Handed Neutrino Dominance

The see-saw mechanism is an extremely attractive method to explain neutrino masses many orders of magnitude lighter than the masses of their associated charged lepton. It is also necessary for theorists to account for the observed large mixings in the neutrino sector. One very natural scheme in which the maximal atmospheric mixing is reproduced is Single Right-Handed Neutrino Dominance(SRHND) [22].

If we assume that the right-handed Majorana mass matrix, M_{RR}, is approximately diagonal, then we can parameterise the Yukawa and Majorana matrices as,

$$M_{RR} = \begin{pmatrix} X' & 0 & 0 \\ 0 & X & 0 \\ 0 & 0 & Y \end{pmatrix}, \quad Y_\nu = \begin{pmatrix} a' & a & d \\ b' & b & e \\ c' & c & f \end{pmatrix}. \tag{2.107}$$

SRHND assumes that the contribution to the light neutrino mass matrix is dominated by one of X', X, Y, with the others contributing sub-dominantly. Here we shall assume that $Y \gg X \gg X'$ and that it is Y which is dominant. Using the parameterization in eq. (2.107), the see-saw mechanism of eq. (2.102) yields,

$$m_{LL} = \begin{pmatrix} \frac{a'^2}{X'} + \frac{a^2}{X} + \frac{d^2}{Y} & \frac{a'b'}{X'} + \frac{ab}{X} + \frac{de}{Y} & \frac{a'c'}{X'} + \frac{ac}{X} + \frac{df}{Y} \\ . & \frac{b'^2}{X'} + \frac{b^2}{X} + \frac{e^2}{Y} & \frac{b'c'}{X'} + \frac{bc}{X} + \frac{ef}{Y} \\ . & . & \frac{c'^2}{X'} + \frac{c^2}{X} + \frac{f^2}{Y} \end{pmatrix}. \tag{2.108}$$

If the heaviest right-handed neutrino dominates in the lower 23 block of m_{LL}, with

the second heaviest contributing sub-dominantly, then

$$\frac{|e^2|, |f^2|, |ef|}{Y} \gg \frac{|xy|}{X} \gg \frac{|x'y'|}{X'} \quad \text{with} \quad \begin{matrix} x = b,\, c \\ x' = b',\, c'. \end{matrix} \tag{2.109}$$

As, $Y \gg X,\, X'$, the Yukawa couplings $e,\, f$ must be large such that the heaviest right-handed neutrino dominates. Without the subdominant contributions the 23 determinant is zero, hence there would be a massless eigenstate. The effect of the subdominant contributions will be to give this eigenstate a very small mass and a relatively large mass splitting to the second eigenstate. In such a scenario with, $e \sim f \sim 1$, there is also large 23 mixing in the neutrino mass matrix. The combination of a large mass splitting and large mixing in the 23 sector reproduces the atmospheric oscillation parameters very well. In this kind of SRHND model the pattern of neutrino masses and mixings are created in a very natural way without the need for fine tuning.

The situation we will be studying in the remaining chapters of this thesis has, $d \ll e \approx f \sim 1$ and can be written approximately as,

$$Y_\nu \sim \begin{pmatrix} 0 & 0 & 0 \\ 0 & 0 & 1 \\ 0 & 0 & 1 \end{pmatrix}. \tag{2.110}$$

We can approximate the MNS mixings under such conditions to be,

$$\tan\theta_{12} \approx \frac{a}{(c_{23}b - s_{23}c)}, \quad \tan\theta_{23} \approx \frac{e}{f}, \quad \theta_{13} \approx \frac{a(s_{23}b + c_{23}c)}{X\, m_3}, \tag{2.111}$$

where m_3 is the heaviest eigenstate of m_{LL}. Therefore the subdominant Yukawa couplings $a,\, b,\, c$ can be chosen to arrange for the a large 12 and small 13 mixing.

2.4 Conclusion

We have seen that the elegant theory of supersymmetry represents an attractive solution to the quadratic divergences of the hierarchy problem. In addition it has been found that such theories lead to gauge coupling unification and the possibility of Grand Unification. Therefore the minimal supersymmetric extension of the standard model, the MSSM, is an attractive model to study. Owing to anomaly cancellation this model must contain two Higgs doublets and so it is possible for the Higgs sector to be quite different from that of the standard model. Unfortunately there is also the possibility that the Higgs sector of the MSSM may behave in a similar way to the standard model Higgs. So the discovery of supersymmetry through the detection of an extended Higgs sector is a possibility but not a certainty at the next generation of collider experiments. Neutrino Physics is one of the major success stories of recent years. Neutrino oscillations have been proved to be the answer to both the atmospheric and solar neutrino problems. A very appealing mechanism for the generation of the tiny neutrino masses is the see-saw mechanism in which the addition of very massive right-handed neutrino states produces the suppression of the left-handed neutrino masses. Such a mechanism can easily be incorporated within the MSSM and indeed many Grand Unified Theories require the existence of right-handed neutrino states.

Chapter 3

A Global Analysis of a supersymmetric Pati-Salam model

In this chapter we present a complete phenomenological analysis of a realistic string-inspired model based on the supersymmetric Pati-Salam $SU(4) \times SU(2)_L \times SU(2)_R$ gauge group supplemented by a $U(1)$ family symmetry, and present predictions for all observables including muon $g-2$, $\tau \to \mu\gamma$, and the CHOOZ angle. Our analysis demonstrates the compatibility of such a model with all laboratory data including charged fermion masses and mixing angles, LMA MSW and atmospheric neutrino masses and mixing angles, and $b \to s\gamma$, allowing for small deviations from third family Yukawa unification. We show that in such models the squark and slepton masses may be rather light compared to similar models with exact Yukawa unification.

The work presented in this chapter has been published in [23].

3.1 Preliminaries

Understanding the origin of fermion masses and mixing angles is one of the most interesting theoretical aspects of particle physics. In the post-SuperKamiokande era this puzzle has become more intriguing than ever before. We saw in section 2.3 that experimental results from SuperKamiokande [15], SNO [17] and KamLAND [18] imply the existence of massive neutrinos with large solar and atmospheric mixing angles. Such large mixings imply a low-energy structure of lepton masses markedly different from those of the quark sector. In this chapter we assume that the smallness of neutrino masses can be explained by the see-saw mechanism involving very heavy right-handed neutrino states, and that the see-saw mechanism is implemented using single right-handed neutrino dominance which can explain in a natural way the coexistence of large neutrino mixing angles with a mass hierarchy. It then becomes a flavour problem to fit together the neutrino mass puzzle with the pieces provided by the long-known pattern of quark and charged lepton masses.

The flavour problem cannot be fully addressed without unification. However, unification has its own challenges. These include the unification of gauge couplings and third family Yukawa couplings and the introduction of supersymmetry. In the previous chapter we saw that supersymmetry facilitates gauge coupling unification, stabilises the hierarchy between the high energy scale and the weak scale, and allows a radiative mechanism of electroweak symmetry breaking. Within the natural framework of supersymmetric unification, the larger high energy gauge group in turn increases the predictive power of the theory in the flavour sector, for example by leading to group theoretical mass relations between quark and lepton masses of the same family. Relations between quarks and leptons of different families require an additional family symmetry, however. In this way it becomes possible to address both the flavour problem and the unification problem, within a single framework.

Having defined the framework, it is by no means guaranteed that models exist which satisfy all the phenomenological constraints provided by current data, and comply with all the theoretical requirements such as successful electroweak symmetry breaking, and approximate gauge and Yukawa unification, while reproducing the known observables. It is therefore important to know that at least some models exist which satisfy all the constraints, as an existence proof that such a procedure can be implemented consistently.

In this chapter we shall study a particular example of a complete supersymmetric unified model of flavour, based on the Pati-Salam $SU(4) \times SU(2)_L \times SU(2)_R$ gauge group [33] extended by an additional $U(1)$ family symmetry. Accepting minimality as a model building principle this group has the following nice features: it establishes the third family Yukawa unification, places the right-handed neutrinos into non-trivial multiplets and does not introduce unwanted exotic states in the multiplets containing the Standard Model fermions and two Higgs doublets required by its SUSY extension. The Pati-Salam group can emerge from a simple gauge group like $SO(10)$ or $E(6)$. However, from a string theory perspective, it is not necessary in order to achieve unification that there should be a unified field theory based on a simple group. A partially unified gauge group can equally well emerge directly from string theory, and in the case of the Pati-Salam gauge group this possibility has been explored extensively both in the case of weakly coupled fermionic string theories [24] and in the case of type I strings with D-branes [25].

Although models based on the Pati-Salam gauge group have been extensively examined, the work presented in this chapter currently represents the only complete and up to date phenomenological study of this model in the literature. For instance [26] investigated constraints from Lepton Flavour Violation(LFV) in a Pati-Salam model with small neutrino mixing angles. Subsequently a Pati-Salam model was proposed [27], using single right-handed neutrino dominance [22] to achieve naturally large neu-

trino mixing angles, but the question of LFV was not re-addressed and it was later shown [28] that the $\mu \to e\gamma$ branching ratio is too large. Moreover, only the negative μ parameter was considered in [27, 29] which is currently disfavoured by the muon $g-2$. In other works such as [30] and [31] the neutrino sector is absent all together. The complete lepton sector is studied in great detail in a global analysis in [28], but the quark mass matrices used [27] were obtained for the opposite sign of μ, and the analysis gives imperfect fits for the branching ratio $Br(b \to s\gamma)$ or b quark mass m_b which both get potentially significant contributions from SUSY loops proportional to μ. To summarise, a completely phenomenologically acceptable supersymmetric Pati-Salam model does not currently exist in the literature. This illustrates the broader point that while many models exist in the literature, it is less common for the analysis of any such model to be complete.

In this chapter, then, we shall construct a "4221" model, following the approach of [27], and demonstrate its phenomenological viability. The model has approximate third family Yukawa unification perturbed by higher order terms and assumes non-universal soft Higgs masses. To demonstrate the viability of such a model, we perform a top down global analysis of the parameter space carried out on 24 observables. In the leptonic sector the observables include the muon $g-2$ and solar and atmospheric neutrino data. A complete list of observables and their σ values, which are used to calculate the χ^2 function can be found in table 3.3. In the analysis we ensure that the upper limits on the branching ratio for the lepton flavour violating processes $\tau \to \mu\gamma$, $\mu \to e\gamma$ and $\tau \to e\gamma$ are not exceeded as well as the limit on the 13 neutrino mixing angle. In addition to this an experimental lower bound on each sparticle mass was imposed.

Having constructed the model and demonstrated its phenomenological viability, we then discuss the following three aspects of the model in more detail:

- The first such aspect, as first pointed out in [28], is lepton flavour violation

arising from the large 23 neutrino mixing through a neutrino Yukawa texture of the form

$$Y^{\nu}_{LR} \sim \begin{pmatrix} 0 & 0 & 0 \\ 0 & 0 & 1 \\ 0 & 0 & 1 \end{pmatrix}. \tag{3.1}$$

Owing to large $\tan\beta$ additional features emerge when studying correlations among observables like $\mathrm{Br}(b \to s\gamma)$, $\mathrm{Br}(\tau \to \mu\gamma)$ and muon $g-2$. Most notably, two distinct minima are found with similar χ^2 values for the best fits. These conclusions are new since study [28] did not investigate a complete model and all other previous works did not involve global analysis.

- The preference for positive μ, given by the sign of the muon $g-2$ discrepancy, implies positive gluino corrections to m_b thus leading to difficulties in obtaining $t-b-\tau$ Yukawa unification. Hence a second focus of the present work is to study the required deviation from third family Yukawa unification in the best fits. [1]

- Thirdly we focus on the effects of future experimental advances, in the form of direct Higgs searches, a lepton flavour violating $\tau \to \mu\gamma$ measurement and a refinement of the muon $g-2$ discrepancy, upon our global fits, indicating how further experimental progress in these areas will constrain the parameter space of the model.

The remainder of this chapter is arranged as follows. Section 3.2 briefly reviews our construction of a string-inspired Pati-Salam model. Section 3.3 contains a brief description of the numerical technique used in the analysis. A discussion of our main results can be found in section 3.4, with concluding remarks in section 3.5.

[1] This was also recently studied from a somewhat different point of view in [30].

3.2 A supersymmetric Pati-Salam Model

The model considered in this chapter is based on the Pati-Salam gauge group [33], supplemented by a local $U(1)$ family symmetry,

$$\mathrm{SU}(4) \times \mathrm{SU}(2)_L \times \mathrm{SU}(2)_R \times U(1). \tag{3.2}$$

The left-handed quarks and leptons are accommodated in the following representations,

$$F_i^{a\alpha} = (4,2,1) = \begin{pmatrix} u^R & u^B & u^G & \nu \\ d^R & d^B & d^G & e^- \end{pmatrix}_i , \tag{3.3}$$

$$\bar{F}_{i\,x\alpha} = (\bar{4},1,\bar{2}) = \begin{pmatrix} \bar{u}^R & \bar{u}^B & \bar{u}^G & \bar{\nu} \\ \bar{d}^R & \bar{d}^B & \bar{d}^G & e^+ \end{pmatrix}_i , \tag{3.4}$$

where $\alpha = 1 \ldots 4$ is an SU(4) index, $a, x = 1,2$ are $\mathrm{SU}(2)_{L,R}$ indices, and $i = 1 \ldots 3$ is a family index. The first/second gauge index should be read as corresponding to the row/column of the matrix. Furthermore the up/down indices are related to the gauge transformation properties of the multiplet, e.g. the raised a and α signifies that F transforms in the **2** representation of $\mathrm{SU}(2)_L$ and the **4** of SU(4), whereas the lower index x and α signifies that $\bar{F}$ transforms in the $\bar{\mathbf{2}}$ of $\mathrm{SU}(2)_R$ and $\bar{\mathbf{4}}$ of SU(4) .

The Higgs fields are contained in the following representation,

$$h_a{}^x = (1,\bar{2},2) = \begin{pmatrix} h_u{}^0 & -h_d{}^- \\ -h_u{}^+ & h_d{}^0 \end{pmatrix}. \tag{3.5}$$

This can also be made more familiar by writing it as a **2** of $\mathrm{SU}(2)_L$ rather than a $\bar{\mathbf{2}}$,

$$h^{ax} = \epsilon^{ab} h_b^{\alpha} = (1,2,2) = \begin{pmatrix} h_u{}^+ & -h_d{}^0 \\ h_u{}^0 & -h_d{}^- \end{pmatrix}. \tag{3.6}$$

Where $\epsilon_{12} = -\epsilon^{12} = +1$. The signs in eq. (3.6) have been chosen so that contraction of the fields $F^{a\alpha}\bar{F}_{x\alpha}h_a{}^x$ gives a contribution to the Yukawa couplings. This means that we can identify the left and right components as the low energy Higgs doublets of the MSSM.

There are also two heavy Higgs representations [24]

$$H^{b\alpha} = (4,1,2) = \begin{pmatrix} u_H^R & u_H^B & u_H^G & \nu_H \\ d_H^R & d_H^B & d_H^G & e_H^- \end{pmatrix}, \tag{3.7}$$

and

$$\bar{H}_{x\alpha} = (\bar{4},1,\bar{2}) = \begin{pmatrix} \bar{u}_{\bar{H}}^R & \bar{u}_{\bar{H}}^B & \bar{u}_{\bar{H}}^G & \bar{\nu}_{\bar{H}} \\ \bar{d}_{\bar{H}}^R & \bar{d}_{\bar{H}}^B & \bar{d}_{\bar{H}}^G & e_{\bar{H}}^+ \end{pmatrix}. \tag{3.8}$$

These Higgs fields are assumed to develop VEVs,

$$< H > \equiv < \nu_H > \sim M_{GUT}, \quad < \bar{H} > \equiv < \bar{\nu}_H > \sim M_{GUT}, \tag{3.9}$$

leading to the symmetry breaking at M_{GUT} [2]

$$\mathrm{SU}(4) \otimes \mathrm{SU}(2)_L \otimes \mathrm{SU}(2)_R \longrightarrow \mathrm{SU}(3)_C \otimes \mathrm{SU}(2)_L \otimes \mathrm{U}(1)_Y, \tag{3.10}$$

in the usual notation. So that we can write,

$$H^{b\alpha} = (v + H)\delta_1^b\delta_4^\alpha, \quad \bar{H}_{x\alpha} = (\bar{v} + \bar{H})\delta_x^1\delta_\alpha^4, \tag{3.11}$$

The group $SU(3)_C$ emerges from the breaking of $SU(4)$ with the remaining $U(1)$

[2]The Pati-Salam model presented in this section has its origins as a string inspired model where the 422 group emerges as the GUT gauge group directly from a string theory construction. Alternatively such a model could emerge from SO(10) unification, in such a case the Pati-Salam breaking scale may be lower than M_{GUT}.

subgroups of $SU(4)$ and $SU(2)_R$ combining to form the hypercharge $U(1)_Y$ with,

$$\frac{Y}{2} = T_{3R} + \frac{B-L}{2}. \tag{3.12}$$

Under the symmetry breaking in eq. (3.10), the Higgs field h in eq. (3.6) splits into the two MSSM Higgs doublets h_u, h_d whose neutral components subsequently develop weak scale VEVs,

$$< h_u^0 >= v_u, \quad < h_d^0 >= v_d, \tag{3.13}$$

with $\tan\beta \equiv v_u/v_d$.

Owing to the unification of quarks and leptons into a single representation F and the two MSSM Higgs doublets into h we have GUT scale Yukawa Unification,

$$Y_F^{ij} = Y_u^{ij} = Y_d^{ij} = Y_e^{ij} = Y_\nu^{ij}, \tag{3.14}$$

where Y_F is the Yukawa coupling of the superpotential term, $F_i \bar{F}_j h$, which after the symmetry breaking of eq. (3.10) produces the quark and lepton superpotential terms of eq. (2.59).

With a large value of $\tan\beta \sim m_t/m_b$ this works rather well for the third family masses [34]. Unfortunately it does not work quite so well for the masses and mixings of the lighter generations. The approach we adopt in order to overcome this problem is to allow only the third family to acquire masses from the renormalisable operators in the superpotential. The remaining masses and mixings are generated through a set of non-renormalisable operators with coefficients that are suppressed by some large scale. In this way we benefit from the efficiency of Yukawa unification but are also able to explain the mixings and mass hierarchy among the lighter generations.

Therefore in order to construct the quark and lepton mass matrices we make use of

non-renormalisable operators [35] of the form:

$$i) \qquad (F^i\overline{F}^j)h\left(\frac{H\overline{H}}{M^2}\right)^n\left(\frac{\theta}{M}\right)^{p_{ij}} \tag{3.15}$$

$$ii) \qquad (\overline{F}^i\overline{F}^j)\left(\frac{HH}{M^2}\right)\left(\frac{H\overline{H}}{M^2}\right)^m\left(\frac{\theta}{M}\right)^{q_{ij}}. \tag{3.16}$$

The θ fields are Pati-Salam singlets which carry $U(1)$ family charge and develop VEVs which break the $U(1)$ family symmetry. They are required to construct U(1)-invariant operators. After the H and θ fields acquire VEVs, they generate a hierarchy in $i)$ effective Yukawa couplings and $ii)$ Majorana masses. These operators are assumed to originate from additional interactions at the scale $M > M_{GUT}$. The value of the powers p_{ij} and q_{ij} are determined by the assignment of $U(1)$ charges, with $X_\theta = -1$ then $p_{ij} = (X_{F^i} + X_{\overline{F}^j} + X_h)$ and $q_{ij} = (X_{\overline{F}^i} + X_{\overline{F}^j} + X_h)$. To ensure anomaly cancellation we must have that the sum of the F charges is equal to the sum of the $\bar{F}$ charges, see [27].

The contribution to the third family Yukawa coupling is assumed to be only from the renormalisable operator with $n = p = 0$ leading to Yukawa unification. The contribution of an operator, with a given power n, to the matrices $Y_{f=u,d,\nu,e}$, and M_{RR} is determined by the relevant Clebsch-Gordan factors coming from the gauge contractions within that operator[3]. A list of Clebsch factors for all $n = 1$ operators can be found appendix D. These Clebsch factors give zeros for some matrices and not for others[4], hence a choice of operators can be made such that a large 23 entry can be given to Y_ν and not $Y_{u,d,e}$. We shall write,

$$\delta = \frac{< H >< \overline{H} >}{M^2} = 0.22, \quad \epsilon = \frac{< \theta >}{M} = 0.22, \tag{3.17}$$

then we can identify δ with mass splitting within generations and ϵ with splitting

[3]Appendix D explains the method of calculating the Clebsch Gordan coefficients for all $n = 1$ operators.

[4]For example $\mathcal{O}^{Ee}$ gives, $x_u = x_d = x_e = 0$, but $x_\nu = 2$.

	X_{F_1}	X_{F_2}	X_{F_3}	$X_{\bar{F}_1}$	$X_{\bar{F}_2}$	$X_{\bar{F}_3}$	X_h	X_H	$X_{\bar{H}}$
$U(1)$	$\frac{11}{6}$	$\frac{5}{6}$	$\frac{5}{6}$	$\frac{19}{6}$	$\frac{7}{6}$	$-\frac{5}{6}$	0	$\frac{5}{6}$	$-\frac{5}{6}$

Table 3.1: List of U(1) family charges that determine the family structure of the Yukawa and Neutrino Majorana matrices. To ensure amomaly cancellation we must have $\sum X_F = \sum X_{\bar{F}}$.

between generations.

The pattern of Yukawa couplings and Majorana mass matrix is then completely determined by the choice of U(1) charges and non-renormalisable operators,

$$\begin{aligned} Y_{f_{ij}} &\sim \lambda^{\delta}_{ij}\,\lambda^{\epsilon}_{ij} \\ M_{RRij} &\sim M_{RR}{}^{\delta}_{ij}\,M_{RR}{}^{\epsilon}_{ij}. \end{aligned} \tag{3.18}$$

Here the matrices M^{ϵ}_{RR} and λ^{ϵ} contain powers of ϵ determined by the choice of U(1) charges. They can therefore be written as $M_{RR}{}^{\epsilon}_{ij} = \epsilon^{q_{ij}}$ and $\lambda^{\epsilon}_{ij} = \epsilon^{p_{ij}}$. For example, if we choose the charges as $X_{F_i} = (4,1,1)$, $X_{\bar{F}_i} = (3,2,1)$ and $X_h = -2$, then the form of λ^{ϵ} would be,

$$\lambda^{\epsilon} = \begin{pmatrix} \epsilon^5 & \epsilon^4 & \epsilon^3 \\ \epsilon^2 & \epsilon^1 & \epsilon^0 \\ \epsilon^2 & \epsilon^1 & \epsilon^0 \end{pmatrix} \tag{3.19}$$

and M_{RR} would be of the form,

$$M_{RR}{}^{\epsilon} = \begin{pmatrix} \epsilon^6 & \epsilon^5 & \epsilon^4 \\ \epsilon^5 & \epsilon^4 & \epsilon^3 \\ \epsilon^4 & \epsilon^3 & \epsilon^2 \end{pmatrix} \tag{3.20}$$

In addition the matrices M^{δ}_{RR} and λ^{δ} contain powers of δ determined by the choice of non-renormalisable operators.

Our choice of $U(1)$ charges are as in [27], and are summarised in table 3.1. This fixes the powers of ϵ in each entry of the Yukawa matrix, but does not specify the complete operator. The Yukawa couplings are specified by the choice of operators,

$$Y_f(M_{GUT}) = \begin{pmatrix} (a_{11}\mathcal{O}^{Fc} + a''_{11}\mathcal{O}''^{Ae})\epsilon^5 & (a_{12}\mathcal{O}^{Ee} + a'_{12}\mathcal{O}'^{Cb})\epsilon^3 & (a'_{13}\mathcal{O}'^{Cf})\epsilon \\ (a_{21}\mathcal{O}^{Dc})\epsilon^4 & (a_{22}\mathcal{O}^{Bc} + a'_{22}\mathcal{O}'^{Ff})\epsilon^2 & (a_{23}\mathcal{O}^{Ee} + a'_{23}\mathcal{O}'^{Bc}) \\ (a_{31}\mathcal{O}^{Fc})\epsilon^4 & (a_{32}\mathcal{O}^{Ac} + a'_{32}\mathcal{O}'^{Fe})\epsilon^2 & a_{33} \end{pmatrix}. \tag{3.21}$$

The operators were initially defined in [27], although the selection of operators here is different from that work. The notation is such that $\mathcal{O}$, $\mathcal{O}'$ and $\mathcal{O}''$ are $n = 1$, $n = 2$ and (extremely small) $n = 3$ operators respectively where n refers to the powers of $(H\overline{H})$, thus [5]

$$\mathcal{O} \sim (H\overline{H}) \sim \delta, \quad \mathcal{O}' \sim (H\overline{H})^2 \sim \delta^2, \quad \mathcal{O}'' \sim (H\overline{H})^3 \sim \delta^3. \tag{3.22}$$

The order unity coefficients $a_{ij}, a'_{ij}, a''_{ij}$ multiply the operators $\mathcal{O}, \mathcal{O}', \mathcal{O}''$ in the ij position. The Majorana operators are assumed to arise from an $m = 0$ operator in the 33 position and $m = 1$ operators elsewhere. The Neutrino Majorana matrix therefore takes the form,

$$\frac{M_{RR}(M_{GUT})}{M_R} = \begin{pmatrix} A_{11}\mathcal{O}\epsilon^8 & A_{12}\mathcal{O}\epsilon^6 & A_{13}\mathcal{O}\epsilon^4 \\ A_{12}\mathcal{O}\epsilon^6 & A_{22}\mathcal{O}\epsilon^4 & A_{23}\mathcal{O}\epsilon^2 \\ A_{13}\mathcal{O}\epsilon^4 & A_{23}\mathcal{O}\epsilon^2 & A_{33} \end{pmatrix}. \tag{3.23}$$

Throughtout our analysis the right handed neutrino scale, M_R, is fixed at 3×10^{14}.

The operator choice in eq. (3.21) leads to the quark and lepton mass matrices in table 3.2. For example the Clebsch coefficients from the leading $\mathcal{O}^{Bc}$ operator in the 22

[5] The $n = 3$ operators can, to a very good approximation, be neglected. Their inclusion here serves only to fill the 11 entries of the $Y_{u,\nu}$ Yukawa matrices, thereby ensuring (for example) that the up quark is given a very small mass.

position give the ratio $0:1:3$ in the $Y_{u,d,e}$ matrices. This ratio along with sub-leading corrections provides the correct $m_c : m_s : m_\mu$ ratio.

In the neutrino sector the matrices in table 3.2 satisfy the condition of sequential dominance [22] in which a neutrino mass hierarchy naturally results with the dominant third right-handed neutrino being mainly responsible for the atmospheric neutrino mass, and the sub-dominant second right-handed neutrino being mainly responsible for the solar neutrino mass. Notice that Y_ν in eq. (3.2) takes the approximate form of eq. (2.110). As discussed in eq. (2.111) the atmospheric mixing angle is then determined approximately as a ratio of $Y_\nu^{23} : Y_\nu^{33}$, and the solar mixing angle is determined by a ratio of Y_ν^{12} to a linear combination of Y_ν^{22} and Y_ν^{32}, while the CHOOZ angle is determined by a more complicated formula [36]. Note that the dominant right-handed neutrino in this model is the heaviest one, corresponding to heavy sequential dominance (HSD) and LFV has been considered in general in this class of models [37].

In the previous analysis [28] the matrix elements, Y_e^{12}, $Y_{e,\nu}^{13}$ were suppressed artificially to keep $Br(\mu \to e\gamma)$ within its experimental limit without substantially changing the predictions of fermion masses and mixings. In this new analysis we have built this suppression into the model with our new choice of operators, whose Clebsch coefficients give zeros in the desired matrix elements as can be seen in table 3.2. This can be understood analytically from [37].

Notice that the sub-leading operators in the 33 position are not shown explicitly in eq. (3.21), but are expected to lead to significant deviations from exact Yukawa unification. This effect is parametrised by the ratios

$$r_t \equiv \frac{Y_u(M_{GUT})_{33}}{Y_e(M_{GUT})_{33}}, \quad r_b \equiv \frac{Y_d(M_{GUT})_{33}}{Y_e(M_{GUT})_{33}}, \quad r_\nu \equiv \frac{Y_\nu(M_{GUT})_{33}}{Y_e(M_{GUT})_{33}}. \tag{3.24}$$

$$
Y_u(M_{GUT}) = \begin{pmatrix} \sqrt{2}\, a''_{11}\delta^3\epsilon^5 & \sqrt{2}\, a'_{12}\delta^2\epsilon^3 & \frac{2}{\sqrt{5}}\, a'_{13}\delta^2\epsilon \\ 0 & \frac{8}{5\sqrt{5}}\, a'_{22}\delta^2\epsilon^2 & 0 \\ 0 & \frac{8}{5}\, a'_{32}\delta^2\epsilon^2 & r_t a_{33} \end{pmatrix}
$$

$$
Y_d(M_{GUT}) = \begin{pmatrix} \frac{8}{5}\, a_{11}\delta\epsilon^5 & -\sqrt{2}\, a'_{12}\delta^2\epsilon^3 & \frac{4}{\sqrt{5}}\, a'_{13}\delta^2\epsilon \\ \frac{2}{\sqrt{5}}\, a_{21}\delta\epsilon^4 & \sqrt{\frac{2}{5}}\, a_{22}\delta\epsilon^2 + \frac{16}{5\sqrt{5}}\, a'_{22}\delta^2\epsilon^2 & \sqrt{\frac{2}{5}}\, a'_{23}\delta^2 \\ \frac{8}{5}\, a_{31}\delta\epsilon^5 & \sqrt{2}\, a_{32}\delta\epsilon^2 & r_b a_{33} \end{pmatrix}
$$

$$
Y_e(M_{GUT}) = \begin{pmatrix} \frac{6}{5}\, a_{11}\delta\epsilon^5 & 0 & 0 \\ \frac{4}{\sqrt{5}}\, a_{21}\delta\epsilon^4 & -3\sqrt{\frac{2}{5}}\, a_{22}\delta\epsilon^2 + \frac{12}{5\sqrt{5}}\, a'_{22}\delta^2\epsilon^2 & -3\sqrt{\frac{2}{5}}\, a'_{23}\delta^2 \\ \frac{6}{5}\, a_{31}\delta\epsilon^5 & \sqrt{2}\, a_{32}\delta\epsilon^2 & a_{33} \end{pmatrix}
$$

$$
Y_\nu(M_{GUT}) = \begin{pmatrix} \sqrt{2}\, a''_{11}\delta^3\epsilon^5 & 2\, a_{12}\delta\epsilon^3 & 0 \\ 0 & \frac{6}{5\sqrt{5}}\, a'_{22}\delta^2\epsilon^2 & 2\, a_{23}\delta \\ 0 & \frac{6}{5}\, a'_{32}\delta^2\epsilon^2 & r_\nu a_{33} \end{pmatrix}
$$

$$
\frac{M_{RR}(M_{GUT})}{M_R} = \begin{pmatrix} A_{11}\delta\epsilon^8 & A_{12}\delta\epsilon^6 & A_{13}\delta\epsilon^4 \\ A_{12}\delta\epsilon^6 & A_{22}\delta\epsilon^4 & A_{23}\delta\epsilon^2 \\ A_{13}\delta\epsilon^4 & A_{23}\delta\epsilon^2 & A_{33} \end{pmatrix}
$$

Table 3.2: The quark and lepton Yukawa matrices and neutrino Majorana mass matrix as used in the analysis. In our numerical analysis we set $M_R = 3 \cdot 10^{14}$ GeV. The Yukawa matrices follow from eq. (3.21) and the Clebsch factors arising from each operator are shown numerically above. Clebsch zeroes play an important part in suppressing the leading operator contribution in a particular element of the matrix, or in simply giving a zero if all the operators are suppressed. The Clebsch coefficients in the Majorana sector are set equal to unity, with A_{ij} being independent order unity coefficients.

3.3 Numerical Procedure

In our numerical analysis we have adopted a complete top-down approach [38]. At the GUT scale the MSSM gauge couplings are related to the GUT scale couplings as $\alpha_{2L} = \alpha_1 = \alpha_{GUT}$ and $\alpha_3 = \alpha_{GUT}(1 + \epsilon_3)$, where ϵ_3 sums up the effects of GUT scale threshold corrections. The particular choice of the Yukawa couplings, table 3.2, follows from the higher dimensional operators in eq. (3.21) as the latter are matched to the MSSM lagrangian. The parameters

$$\begin{aligned} &M_{GUT},\ \alpha_{GUT},\ \epsilon_3,\ \delta,\ \epsilon,\ a\text{'s and } A\text{'s},\ r_t,\ r_b,\ r_\nu, \\ &M_{1/2},\ A_0,\ \mu,\ B\mu,\ m_F^2,\ m_{\overline{F}}^2,\ m_h^2 \text{ and } D^2 \end{aligned} \tag{3.25}$$

are then defined by the boundary conditions at the GUT scale. They parametrise the imprint of a complete Pati-Salam theory together with the SUSY sector (second line) on the MSSM and stand for the inputs of the model.

$$\begin{aligned} m_{\tilde{Q}}^2 &= m_F^2 + g_4^2\, D^2 \\ m_{\tilde{u}_R}^2 &= m_{\overline{F}}^2 - (g_4^2 - 2g_{2R}^2)\, D^2 \\ m_{\tilde{d}_R}^2 &= m_{\overline{F}}^2 - (g_4^2 + 2g_{2R}^2)\, D^2 \\ m_{\tilde{L}}^2 &= m_F^2 - 3g_4^2\, D^2 \\ m_{\tilde{e}_R}^2 &= m_{\overline{F}}^2 + (3g_4^2 - 2g_{2R}^2)\, D^2 \\ m_{\tilde{\nu}_R}^2 &= m_{\overline{F}}^2 + (3g_4^2 + 2g_{2R}^2)\, D^2 \\ m_{H_u}^2 &= m_h^2 - 2g_{2R}^2\, D^2 \\ m_{H_d}^2 &= m_h^2 + 2g_{2R}^2\, D^2. \end{aligned} \tag{3.26}$$

In the SUSY sector, the soft SUSY breaking parameters are for simplicity introduced at the same scale. The gaugino masses are assumed universal (equal to $M_{1/2}$) and so are the trilinear couplings: $\mathbf{A}_i = A_0\, \mathbf{Y}_i$, for $i = u,\ d,\ e,\ \nu$. The soft scalar masses of the MSSM superfields include the D terms from the breaking of the Pati-Salam gauge

group [29][6] and are shown in eq. (3.26). Notice that as $D^2 = \frac{1}{8}\left(|\overline{H}_\nu|^2 - |H_\nu|^2\right)$ [29] it is possible for this quantity to be both positive or negative.

We now describe minor simplifications to the input in eq. (3.25) which were assumed in the actual numerical analysis. We have kept equality between the two order parameters δ and ϵ as in eq. (3.17) and the soft SUSY breaking scalar masses m_F and $m_{\overline{F}}$ have been held equal to each other as well, therefore m_F^2 plays the role of the universal scalar mass m_0^2. Furthermore we exploited the fact that determining $\mu(M_{GUT})$ and $B\mu$ at the GUT scale is equivalent to determining the low energy values $\mu(M_Z)$ and $\tan\beta$, respectively, as discussed in eq. (2.74) and (2.75). Thus instead of eq. (3.25) our numerical analysis uses

$$\begin{aligned} &M_{GUT},\ \alpha_{GUT},\ \epsilon_3,\ \delta,\ a\text{'s and } A\text{'s},\ r_t,\ r_b,\ r_\nu, \\ &M_{1/2},\ A_0,\ \mu(M_Z),\ \tan\beta,\ m_F^2,\ m_h^2 \text{ and } D^2 \end{aligned} \tag{3.27}$$

as input parameters. The top down approach implies that we can freely vary or hold fixed any one of them and then investigate the fit properties. This is one of the advantages of doing the analysis top down. For example, in more traditional bottom up approaches it is difficult to control the size of the dimensionless GUT scale parameters. One usually sets up a sample of randomly scattered points and then searches through it to identify a sub-sample with physically interesting GUT scale properties. In our case we can set up the interesting GUT relations explicitly right at the start — as we have done for instance in section 3.4.3 where the fits with r_b and r_t approaching unity are studied.

We note that taking advantage of the top-down approach we kept $\delta = 0.22$, $r_\nu = 1$, $A_0 = 0$ and $\tan\beta = 50$ fixed throughout the analysis. We also kept the μ parameter at scale M_Z fixed to two different values as is explained below.

[6] Appendix E gives a brief outline of the origin of the D-term mass contributions in eq. (3.26).

Two-loop RGEs for the dimensionless couplings and one-loop RGEs for the dimensionful couplings were used to run all couplings down to the scale M_{3R} where the heaviest right-handed neutrino is decoupled from the RGEs. Similar steps were taken for the lighter M_{2R} and M_{1R} scales, and finally with all three right-handed neutrinos decoupled the solutions for the MSSM couplings and spectra were computed at the Z scale. This includes full one loop SUSY threshold corrections to the fermion mass matrices and all Higgs masses while the sparticle masses are obtained at tree level.

m_h and D in eq. (3.26) were varied to optimise radiative electroweak symmetry breaking (REWSB), which was checked at one loop with the leading m_t^4 and m_b^4 corrections included following the effective potential method in [39]. It was shown in [39] that the leading logarithm correctioned Higgs spectrum, evaluated at the top mass scale, is in very good agreement with that of the virtually scale independent Next-to-leading-log result. We note that as $\tan\beta$ determines the Higgs bilinear parameter $B\mu$, there is a redundancy in our procedure since two input parameters, m_h and D, determine one condition for the Higgs VEV of 246 GeV. This approach enabled us to control the μ parameter and we explored regions with μ low ($\mu = 120$ GeV) and high ($\mu = 300$ GeV) [7].

An experimental lower bound on each sparticle mass was imposed. In particular, the most constraining are: the LEP limits on the charged SUSY masses ($m_{\tilde{\chi}^\pm}, m_{\tilde{\tau}} > 105$ GeV), the CDF limit on the mass of the CP odd Higgs state ($m_{A^0} > 105$-110 GeV, valid for $\tan\beta \approx 50$) [32], and the requirement that the lightest SUSY particle should be neutral. Finally, the χ^2 function $\sum(X_i^{th} - X_i^{exp})^2/\sigma_i^2)$ is evaluated based on the agreement between the theoretical predictions and 24 experimental observables collected in table 3.3. In addition to the constraints listed above and in [28], we make a full analysis of the quark sector mass and mixings, in particular we have included

[7] For $\tan\beta$ as large as 50, $\mu \gg 300$ GeV leads to too large SUSY threshold corrections to the masses of the third generation fermions τ and b unless the sparticles in the loop have masses well above the 1 TeV region. [40, 41, 38]

the important constraint set by $\mathrm{Br}(b \to s\gamma)$.

3.4 Results and Discussion

The numerical results from the global analysis are presented in the form of contour plots in the $(m_F, M_{1/2})$ plane and are produced for two different values of the μ parameter $\mu = 120\,\mathrm{GeV}$ and $\mu = 300\,\mathrm{GeV}$. Before we address the details we would like to discuss two different viewpoints of our analysis, namely the flavour sector on the one hand and the unification sector of the other hand. In our discussion we would like to distinguish between the two viewpoints. The main distinction is that in the MSSM analysis the flavour parameters a_{ij} (with the exception of a_{33}) and A_{ij} can be considered fixed at unity or at a value of order unity. Up to a_{33}, which enters the large Yukawa couplings their exact values do not affect the fit of the SUSY spectra or SUSY-related observables like the muon $g-2$ or branching ratio $b \to s\gamma$. They neither perturb gauge coupling unification nor change the running of the large Yukawa couplings. This means that the discussion of our results is naturally split into a part dealing with the flavour structure of the Pati-Salam model where the variation of the coefficients of the higher dimensional operators matters, and a part where the MSSM analysis is presented and the conclusions do not depend on the variation of the a and A parameters (up to a_{33}).

Concerning the flavour sector, our results can be used to show how well the model, i.e. the set of higher dimensional operators specified by eq. (3.21), describes the observed fermion masses and mixings. Taking this viewpoint all parameters listed in eq. (3.27) represent the input of the analysis. The results in each of the four panels in fig. (3.1) show that the model gives a very good agreement with the data. The minimum of the total χ^2 is less than unity, obtained for $\mu = 120\,\mathrm{GeV}$ in the upper left panel. This means that it is possible to fit every observable to better than a $1\,\sigma$ accuracy.

Observable	Mean	σ_i
α_{EM}	$1/137.036$	$7.30 \cdot 10^{-6}$
G_μ	$1.16639 \cdot 10^{-5}\,\mathrm{GeV}^{-2}$	$1.12 \cdot 10^{-7}$
$\alpha_s(M_Z)$	0.1181	0.0020
M_t	174.3 GeV	5.1
$m_b(m_b)$	4.20 GeV	0.20
$M_b - M_c$	3.4 GeV	0.2
$m_s(2\mathrm{GeV})$	0.110 GeV	0.035
$(m_d^2 - m_u^2)/m_s^2$	$2.03 \cdot 10^{-3}$	$2.0 \cdot 10^{-4}$
m_d/m_s	0.05	0.015
M_τ	1.777 GeV	$1.8 \cdot 10^{-3}$
M_μ	0.106 GeV	$1.1 \cdot 10^{-4}$
M_e	$5.11 \cdot 10^{-4}$ GeV	$5.1 \cdot 10^{-7}$
$\lvert V_{us}\rvert$	0.2196	0.0023
$\lvert V_{cb}\rvert$	0.0402	0.003
$\lvert V_{ub}\rvert/\lvert V_{cb}\rvert$	0.09	0.02
M_Z	91.1882 GeV	0.091
M_W	80.419 GeV	0.08
ρ_{NEW}	-0.0002	0.0011
$Br(b \to s\gamma)$	$3.47 \cdot 10^{-4}$	$0.45 \cdot 10^{-4}$
$\delta a_\mu^{\mathrm{NEW}}$	$34.7.6 \cdot 10^{-10}$	$11 \cdot 10^{-10}$
Δm^2_{ATM}	$2.5 \cdot 10^{-3}\,\mathrm{eV}^2$	$0.8 \cdot 10^{-3}$
$\sin^2 2\theta_{ATM}$	0.99	0.06
Δm^2_{SOL}	$7.0 \cdot 10^{-5}\,\mathrm{eV}^2$	$3 \cdot 10^{-5}$
$\sin^2 2\theta_{SOL}$	0.8	0.09

Table 3.3: Table of observables and σ values used to calculate the χ^2 function. The observable $\delta a_\mu^{\mathrm{NEW}} = a_\mu^{\mathrm{exp}} - a_\mu^{\mathrm{SM}}$, is the present discrepancy between the experimental measurement and SM prediction for the anomalous magnetic moment of the muon. $\rho_{new} = \frac{\Pi^{WW}_{new}(0)}{M_W^2} - \frac{\Pi^{ZZ}_{new}(0)}{M_Z^2}$ where $\Pi^{ZZ}_{new}(0)$ and $\Pi^{WW}_{new}(0)$ stand for contributions of physics beyond the standard model to the vector self-energies at zero momentum. Upper and lower case masses denote pole and running masses respectively.

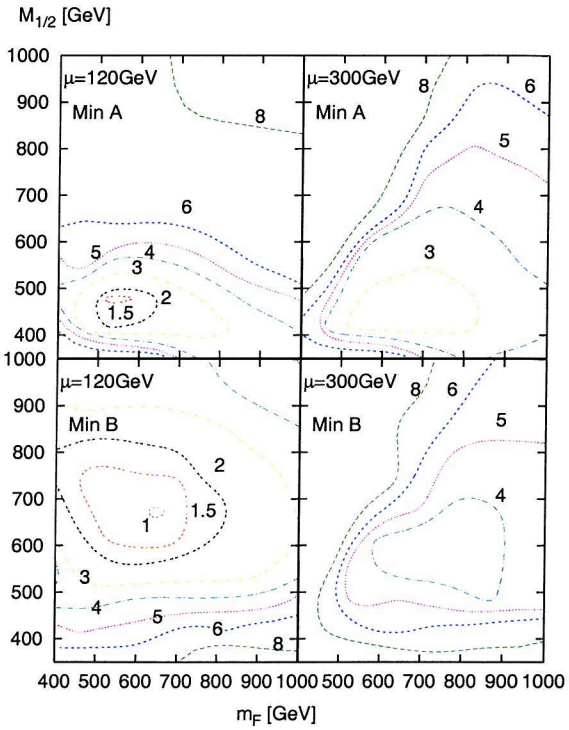

Figure 3.1: χ^2 contour plots in the plane of $(m_F, M_{1/2})$. The four plots, are obtained from the two minima, minimum A and minimum B with $\mu = 120$ and 300 GeV as labelled. All points in the top left corner with approximately $M_{1/2} > 700$ GeV and $m_F < 700$ GeV are unphysical due to the lightest stau becoming the LSP.

Concerning the unification sector, the conclusions are much stronger as there are effectively much fewer input parameters after the a's and A's decouple from the analysis. Indeed, the set of the effective input parameters in this sector is reduced to

$$\begin{aligned} &M_{GUT},\ \alpha_{GUT},\ \epsilon_3,\ a_{33},\ r_t,\ r_b, \\ &M_{1/2},\ m_F^2,\ m_h^2 \text{ and } D^2. \end{aligned} \tag{3.28}$$

With this input the low energy Higgs and SUSY spectra are determined. The conventional present-day observables include α_{EM}, G_μ, $\alpha_s(M_Z)$, M_t, $m_b(m_b)$, M_τ, M_Z, M_W,

ρ_{NEW}, $Br(b \to s\gamma)$ and δa_μ. The unification sector observables are insensitive to the small Yukawa coupling, except for Br$(b \to s\gamma)$ which is sensitive to $\tilde{t} - \tilde{c}$ mixing and V_{cs}. The a_{ij} and A_{ij} input parameters are all of order one and their exact values are always adjusted to fit the first two generation masses and mixings well while these variations do not affect the fit of the observables listed above.

We study many details of the MSSM analysis, in particular the dependence of the fit on m_F^2 and $M_{1/2}$, best fit results for muon $g-2$, and $Br(\tau \to \mu\gamma)$ predictions. The numerical results also contain studies of a deviation from Yukawa unification and a future measurement of $Br(\tau \to \mu\gamma)$. The effect of a change to the present muon $g-2$ discrepancy was studied and also the effect of future direct Higgs searches, the results of which can be found in the following sections.

From our global analysis we found that there are two χ^2 minima as shown in fig. (3.1). In this model there are two conditions, see eqs. (2.74), (2.75) and three free variables, m_h^2, D^2, and $B\mu$, for electroweak symmetry breaking to be achieved. The two minima hence are independent solutions to these conditions. Minimum A has D^2 negative and smaller m_h, $B\mu$. Minimum B on the other hand has D^2 positive and larger m_h, $B\mu$. The relative size of $B\mu$ results in a different Higgs spectrum, particularly the CP odd pseudoscalar Higgs, A^0, which will be lighter for minimum A and heavier for minimum B. The difference between the sign of D^2, which contributes to the soft scalar masses as shown in eq. (3.26), means that minimum B will have lighter right squarks and left sleptons, along with heavier left squarks and right sleptons, than minimum A. This difference in sign of D^2 has some interesting phenomenological consequences for the two minima which will now be discussed.

The upper and lower plots shown in fig. (3.1), display the χ^2 contours for these two minima. Each of the figures display results for both $\mu = 120$ and 300 GeV in the relative left and right positions. The contours in fig. (3.1) are bounded from the lower m_F region due to the lightest stau becoming the LSP and from the lower $M_{1/2}$ region

Inputs				
	$\mu = 120$ **GeV**		$\mu = 300$ **GeV**	
	Min A	Min B	Min A	Min B
$M_{1/2}$	450	650	450	650
m_F	500	650	500	650
μ	120	120	300	300
D^2	$-6.4 \cdot 10^4$	$17 \cdot 10^4$	$-10 \cdot 10^4$	$13 \cdot 10^4$
m_h^2	$6 \cdot 10^5$	$16 \cdot 10^5$	$4.5 \cdot 10^5$	$14 \cdot 10^5$
r_t	1.01	1.07	1.03	1.02
r_b	0.75	0.72	0.66	0.64
a_{33}	0.55	0.55	0.55	0.56
a_{11}	-0.93	-0.92	-0.92	-0.93
a_{12}	0.20	0.33	0.31	0.30
a_{21}	1.67	1.67	1.67	1.75
a_{22}	1.13	1.12	1.13	1.13
a_{23}	0.98	0.89	1.05	0.85
a_{31}	-0.20	-0.21	-0.20	-0.28
a_{32}	2.18	2.08	2.32	2.53
a'_{12}	0.77	0.77	0.71	0.71
a'_{13}	0.60	0.53	0.46	0.46
a'_{22}	0.66	0.66	0.64	0.62
a'_{23}	0.41	0.40	0.36	0.36
a'_{32}	1.16	1.80	1.56	1.72
a''_{11}	0.32	0.278	0.20	0.23
A_{11}	0.63	0.94	0.63	0.94
A_{12}	0.74	0.48	0.69	0.52
A_{13}	1.75	2.10	1.73	2.04
A_{22}	0.97	0.52	0.93	0.55
A_{23}	2.49	1.79	2.23	1.91
A_{33}	1.97	1.88	1.97	1.88

Table 3.4: Table of inputs for the best fit points for each of the global χ^2 minima with $\mu = 120$ and 300 GeV.

Outputs				
	$\mu = 120$ **GeV**		$\mu = 300$ **GeV**	
	Min A	Min B	Min A	Min B
m_{A^0}	102	818	102	822
m_{h^0}	106	114	106	114
m_{H^0}	112	891	113	888
m_{H^+}	136	861	135	861
M_1	186	270	186	271
M_2	371	537	371	537
M_3	1175	1671	1175	1671
$M_{\chi_1^+}$	114	117	272	290
$M_{\chi_2^+}$	390	549	408	554
$M_{\tilde{N}_1}$	98	107	179	249
$M_{\tilde{N}_2}$	130	127	277	305
$M_{\tilde{N}_3}$	198	278	307	311
$M_{\tilde{N}_4}$	390	549	408	554
$M_{\tilde{Q}_{1,2}}$	1166	1679	1159	1673
$M_{\tilde{Q}_3}$	979	1345	960	1356
$M_{\tilde{U}_{1,2}}$	1131	1623	1124	1617
$M_{\tilde{U}_3}$	798	1147	805	1160
$M_{\tilde{D}_{1,2}}$	1182	1510	1204	1529
$M_{\tilde{D}_3}$	923	1192	1044	1251
$M_{\tilde{L}_1}$	673	611	715	656
$M_{\tilde{L}_2}$	665	595	707	644
$M_{\tilde{L}_3}$	580	334	638	425
$M_{\tilde{E}_1}$	496	766	473	752
$M_{\tilde{E}_2}$	495	765	473	751
$M_{\tilde{E}_3}$	201	370	188	325
$\tau \to \mu\gamma$	$2 \cdot 10^{-7}$	$3 \cdot 10^{-6}$	$8 \cdot 10^{-8}$	$5 \cdot 10^{-7}$
$\tau \to e\gamma$	$1 \cdot 10^{-14}$	$3 \cdot 10^{-13}$	$6 \cdot 10^{-15}$	$5 \cdot 10^{-14}$
$\mu \to e\gamma$	$3 \cdot 10^{-14}$	$1 \cdot 10^{-13}$	$1 \cdot 10^{-14}$	$3 \cdot 10^{-14}$
$\sin\theta_{13}$	0.053	0.078	0.037	0.10
$\sin(\beta - \alpha)$	0.22	1.0	0.15	1.0
$\cos(\beta - \alpha)$	-0.98	0.0	-0.99	0.0

Table 3.5: Table of outputs for the best fit points for each of the global χ^2 minima with $\mu = 120$ and 300 GeV. The input parameters are as defined in table 3.4.

due to an increasing χ^2 penalty coming from $Br(b \to s\gamma)$.

The upper minima of fig. (3.1), minimum A, has a preferred region in the lower $(m_F, M_{1/2})$ plane, with $M_{1/2} = 400 - 500$ GeV and $m_F = 500 - 700$ GeV. The lower minima of fig. (3.1), Minima B, has its preferred region nearer $M_{1/2} = 550 - 650$ GeV and $m_F = 600 - 800$ GeV. A list of inputs and outputs for the best fit point in each minimum can be found in tables 3.4 and 3.5. The Higgs masses and CP even Higgs mixings found for minimum A in table 3.5 are discussed in detail in section 3.4.4.

3.4.1 Muon $g-2$

Fig. (3.2), shows contour plots for the SUSY contributions to the anomalous magnetic moment of the muon. Both minimum A and minimum B (upper and lower plots respectively) give good fits to the present discrepancy between experiment and Standard Model prediction. As expected, a larger contribution to the muon $g-2$ is obtained in the lower left corner of the $(m_F, M_{1/2})$ plane where the SUSY spectrum is lightest and decreases as we move towards a heavier spectrum in the top right corner. It is also clear that for any one point in the $(m_F, M_{1/2})$ plane, minimum B gives a larger contribution than the corresponding point in minimum A. This relative enhancement can be ascribed to the dominant chargino-sneutrino diagram via the presence of a lighter muon sneutrino for the case of minimum B, as can be seen in fig. (3.3).

The present muon $g-2$ discrepancy lies at 34×10^{-10} but over the past 12 months it has varied from a 1.5σ to 3σ effect. Also the size of the present discrepancy depends on the experimental data used in the calculation of the Standard model prediction. The value we have used throughout our analysis [43] makes use of e^+e^- data. On the other hand it is possible to do the same calculation making use of τ decay data [44], which gives a lower discrepancy of 9.4×10^{-10}. As a result we think it worth

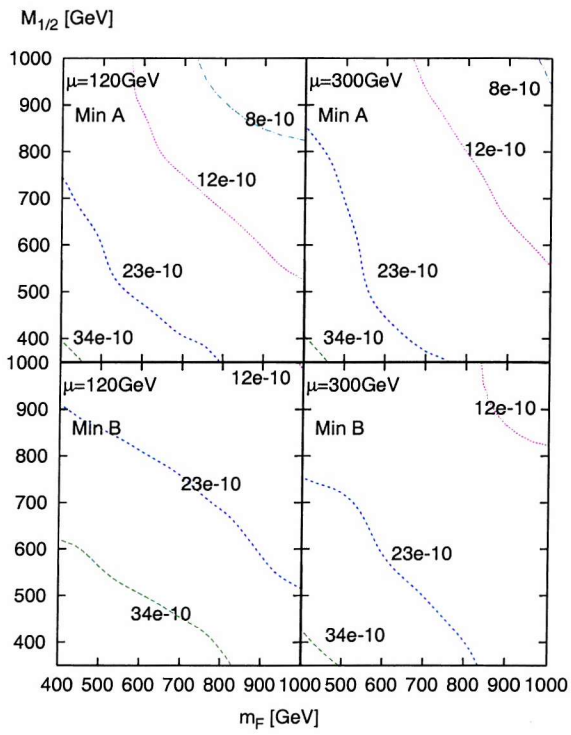

Figure 3.2: Muon $g-2$ contour plot in the plane of $(m_F, M_{1/2})$. The four plots, are obtained from the two minima, minimum A and minimum B with $\mu = 120$ and 300 GeV as labelled. All points to the left of the solid red line are unphysical due to the lightest stau becoming the LSP. The present discrepancy stands at $34(11)\times10^{-10}$ with the above plots showing 1 and 2 σcontours.

while looking into how our best fit regions would change if a lower discrepancy was assumed. For simplicity we took just 3 points in the $(m_F, M_{1/2})$ plane of minimum A with $\mu = 120$ GeV and gradually changed the $g-2$ discrepancy from 34×10^{-10} down to 0. The results are presented in fig. (3.4) as a plot of χ^2 against the muon $g-2$ discrepancy, a_μ^{New}.

With the discrepancy held at 34×10^{-10} the best fit point is near $M_{1/2} = 450$ GeV and $m_F = 550$ GeV. Following the curve corresponding to this point in parameter space, we can see, in fig. (3.4), that as the muon $g-2$ discrepancy is lowered the χ^2 gradually

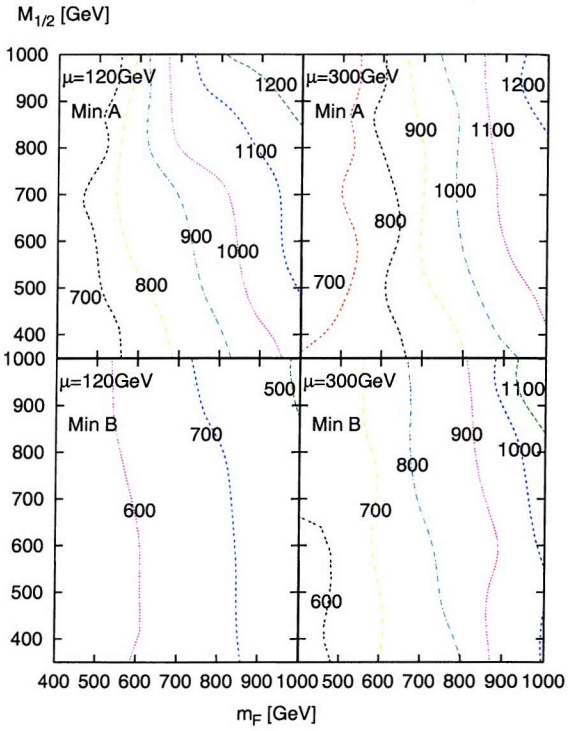

Figure 3.3: Contours of the second generation sneutrino mass, $m_{\tilde{\nu}_\mu}$, are plotted in the plane of $(m_F, M_{1/2})$. The contours are in the units of GeV. The four plots, are obtained from the two minima, minimum A and minimum B with $\mu = 120$ and 300 GeV as labelled. All points in the top left corner with approximately $M_{1/2} > 700$ GeV and $m_F < 700$ GeV are unphysical due to the lightest stau becoming the LSP.

increased. On the other hand the two curves with larger $M_{1/2}$, m_F have decreasing χ^2. Therefore the best fit point has moved in the positive $M_{1/2}$, m_F direction. Looking at these two other curves in fig. (3.4) we can see that if $a_\mu^{New} \sim 16 \times 10^{-10}$ then the best fit point would move nearer $M_{1/2} = 550$ GeV and $m_F = 650$ GeV. One particular point of interest is $a_\mu^{New} = 9.4 \times 10^{-10}$, the value for the discrepancy as given by the Standard Model prediction from τ decay data. If we make an approximation, based on the curves in fig. (3.4), we can say that the best fit point, for $a_\mu^{New} = 9.4 \times 10^{-10}$, would be in the region $M_{1/2} = 550 - 700$ GeV, $m_F = 650 - 700$ GeV.

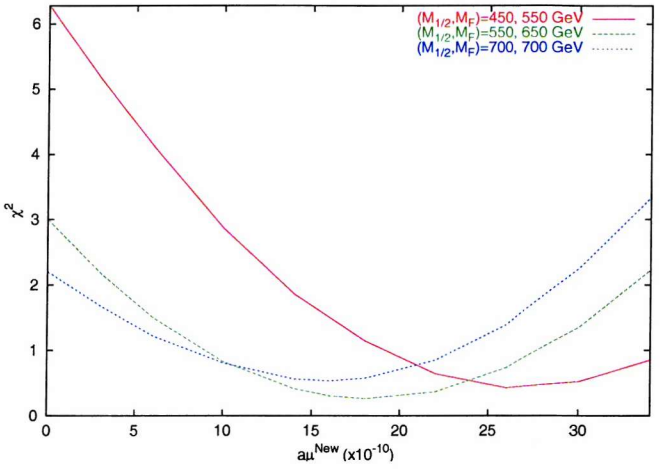

Figure 3.4: This plot displays the effect on χ^2 due to a future change in the value of the muon $g-2$ discrepancy. The value of the muon anomalous magnetic moment is varied from the present value of 34×10^{-10} down to zero. The resulting change in χ^2 is observed for three points in the $(m_F, M_{1/2})$ plane.

3.4.2 $\tau \to \mu\gamma$

Fig. (3.5) displays contours for the quantity $\mathrm{Br}(\tau \to \mu\gamma)$ for both minima with $\mu = 120$ and 300 GeV as labelled. The general pattern of the contours show larger branching ratios for lighter SUSY spectrum and smaller branching ratios for heavier spectrum. This pattern is not strictly obeyed in the bottom left panel which shows results for minimum B with $\mu = 120$ GeV. The reason for this is that our numerical procedure adds a large penalty χ^2 contribution for a $\tau \to \mu\gamma$ branching ratio larger than the BaBar limit of 2.0×10^{-6}[45]. Looking at the bottom left panel in fig. (3.5) we would expect the branching ratio to exceed the present limit as we go to a lighter spectrum. The result of adding this penalty χ^2 is to numerically force an alternative solution to be found which gives lower branching ratio and disrupts the pattern. Re-calculation of this region of parameter space without the additional χ^2 penalty does indeed yield values of $\mathrm{Br}(\tau \to \mu\gamma)$ as large as 6.0×10^{-6}, these points would therefore follow the expected contour pattern but are clearly experimentally excluded.

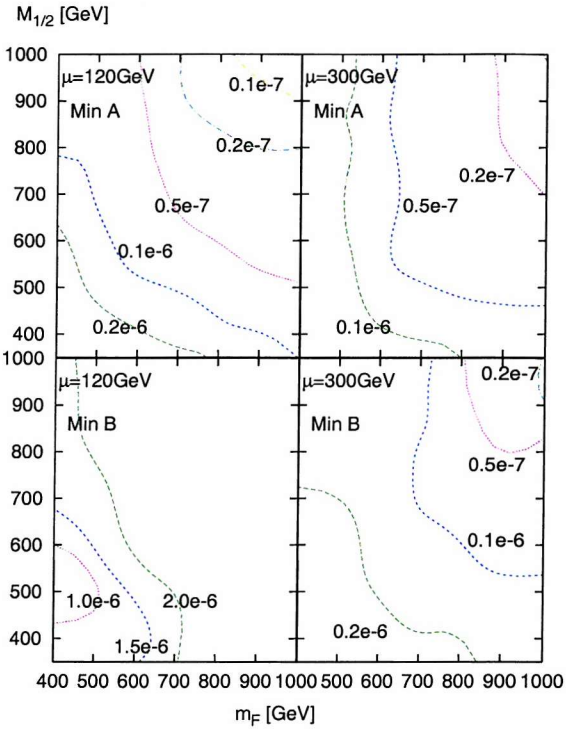

Figure 3.5: Contours of $Br(\tau \to \mu\gamma)$ are plotted in the plane of $(m_F, M_{1/2})$. The four plots, are obtained from the two minima, minimum A and minimum B with $\mu = 120$ and 300 GeV as labelled. All points in the top left corner with approximately $M_{1/2} > 700$ GeV and $m_F < 700$ GeV are unphysical due to the lightest stau becoming the LSP.

Looking at fig. (3.5), the branching ratio for minimum A with $\mu = 120$ and 300 GeV is at least an order of magnitude below the present experimental bound. On the other hand, the branching ratio for minimum B, with $\mu = 120$ GeV fig. (3.5), is right at the present 90% confidence level bound of 2.0×10^{-6}. For $\mu = 300$ GeV minimum B gives a branching ratio in the range, $0.1 - 0.2 \times 10^{-6}$, just below the present bound. With BaBar expected to search as far as $\mathrm{Br}(\tau \to \mu\gamma) \sim 10^{-8}$ over the next 5 years this certainly provides a means of distinguishing the two minima.

3.4.3 Deviations from Yukawa Unification

The plots shown in fig. (3.6) show contour lines for $r_b = Y_b/Y_\tau$ and those in fig. (3.7), show contour lines for $r_t = Y_t/Y_\tau$ in the best fits over the $(m_F, M_{1/2})$ plane. These

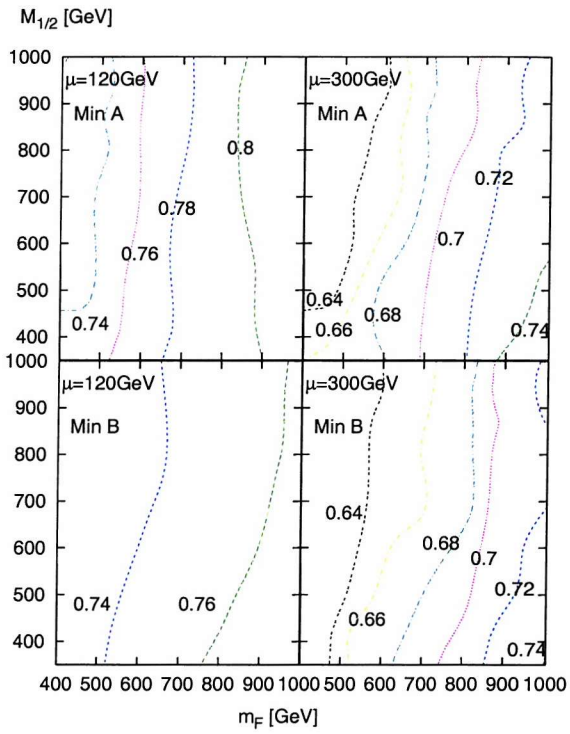

Figure 3.6: Contours of $r_b = Y_b/Y_\tau$ are plotted in the plane of $(m_F, M_{1/2})$. The four plots, are obtained from the two minima, minimum A and minimum B with $\mu = 120$ and 300 GeV as labelled. All points in the top left corner with approximately $M_{1/2} > 700$ GeV and $m_F < 700$ GeV are unphysical due to the lightest stau becoming the LSP.

parameters allow the deviation of the top, bottom and tau Yukawa couplings away from unification($r_b = r_t = 1$). Both parameters show significant dependence upon m_F and weak dependence upon $M_{1/2}$, with increasing $r_{t,b}$ values as we move towards larger m_F. The plots show that the level of deviation from Yukawa unification required for a good χ^2 fit to be obtained is of the order of 20-35% in r_b and 0-10% in r_t. It is possible

to account for this level of deviation through the presence of sub-leading operators, of the type mentioned in eq. (3.22), in the 33 element of the Yukawa matrices. Hence the 33 element in eq. (3.21) should read,

$$Y_{33} = a_{33} + \mathcal{O} + \mathcal{O}' + \ldots \tag{3.29}$$

where the operators $\mathcal{O}$ and $\mathcal{O}'$ are responsible for generating $r_{t,b} \neq 1$. The 23 block of the neutrino Yukawa matrix has already shown us that a contribution to the Yukawa matrices from a sub-leading operator can actually be comparable to those from a

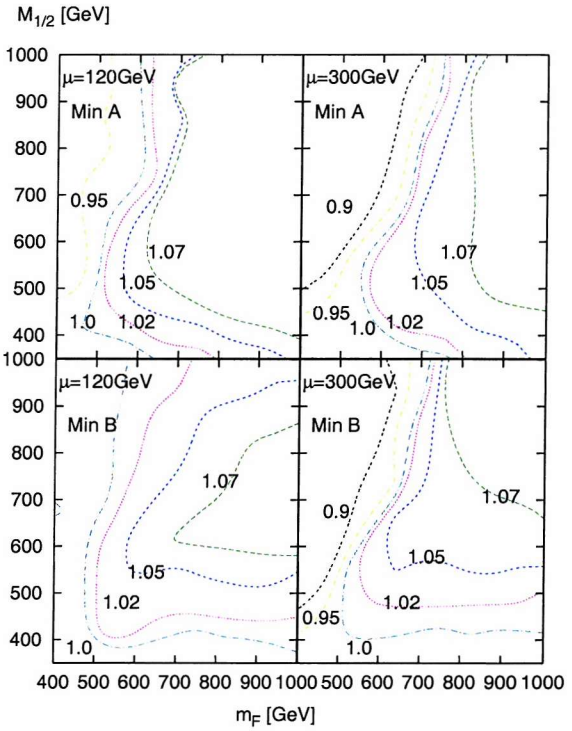

Figure 3.7: Contours of $r_t = Y_t/Y_\tau$ are plotted in the plane of $(m_F, M_{1/2})$. The four plots, are obtained from the two minima, minimum A and minimum B with $\mu = 120$ and 300 GeV as labelled. All points in the top left corner with approximately $M_{1/2} > 700$ GeV and $m_F < 700$ GeV are unphysical due to the lightest stau becoming the LSP.

leading operator. This occurs in the 23 element of the neutrino Yukawa matrix, where there is a contribution from the operator $\mathcal{O}^{Ee}$ and the neutrino matrix is the only one that receives a non-zero Clebsch-Gordan coefficient as can be seen in table 3.2. This leads to the relative sizes of the elements $Y_\nu^{23} \sim 0.44$ and $Y_\nu^{33} \sim 1$. A similar sub-leading contribution to the 33 element of the up and down quark Yukawa matrices could easily account for a deviation from third family Yukawa unification at the level discovered in our study.

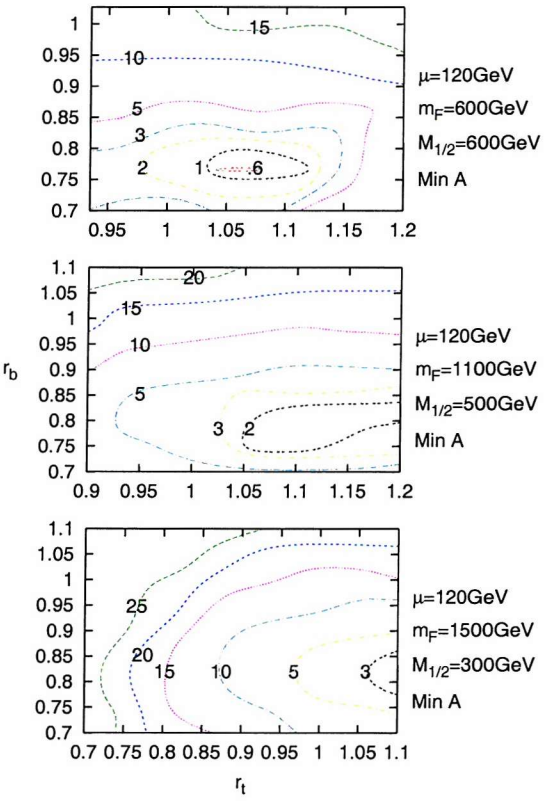

Figure 3.8: χ^2 contours in the $r_t - r_b$ plane. The plots are generated with $\mu = 120$ GeV and for minimum A. The three plots are each generated with fixed $M_{1/2}$, m_F as labelled. The plots display the χ^2 penalty which is required for exact Yukawa unification to be achieved.

Here we do not study the region in the parameter space $m_F > 2\,\text{TeV}$, $A_0 \approx -2\,m_F$ where the exact unification might work [46]. Instead, we carried out a study of the

additional χ^2 penalty incurred due to demanding exact Yukawa unification in the region $m_F < 2\,\text{TeV}$ and $A_0 = 0$. Fig. (3.8) shows the result as χ^2 contour plots in the $r_t - r_b$ plane corresponding to the best fits. The three panels were obtained from three points in the $(m_F, M_{1/2})$ plane and show that a very heavy penalty $\delta\chi^2 > 10$ is paid when requiring exact Yukawa unification in this SUSY region.

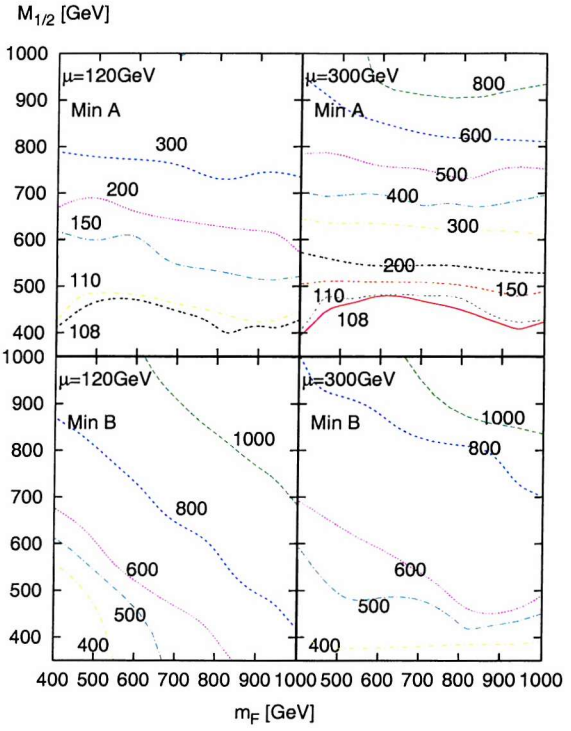

Figure 3.9: Contours of the CP odd Pseudoscalar Higgs mass, m_{A^0}, are plotted in the plane of $(m_F, M_{1/2})$. The contours are in the units of GeV. The four plots, are obtained from the two minima, minimum A and minimum B with $\mu = 120$ and 300 GeV as labelled. All points in the top left corner with approximately $M_{1/2} > 700$ GeV and $m_F < 700$ GeV are unphysical due to the lightest stau becoming the LSP.

3.4.4 Future Higgs searches

Fig. (3.9) shows mass contours of the CP odd pseudoscalar Higgs, m_{A^0}. These plots show that for the Pseudoscalar Higgs mass minimum A prefers values approximately $200 - 300$ GeV lower than minimum B. In fig. (3.9) we see that for both $\mu = 120$ and 300 GeV, minimum A gives a very light pseudoscalar Higgs mass, $m_{A^0} \sim 108$ GeV, in the low $M_{1/2}$, m_F region.

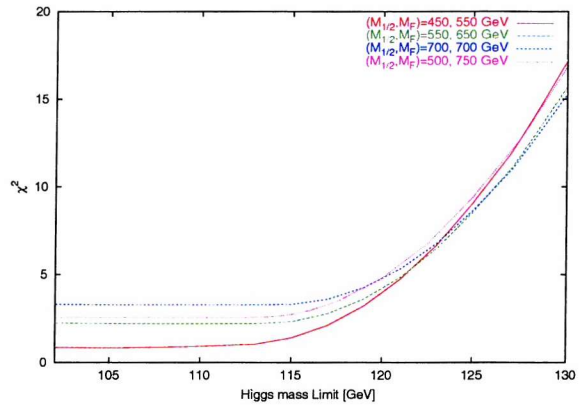

Figure 3.10: This plot displays the effect on χ^2 due to an increase in the lower bound on the Higgs mass from direct searches. As in fig. (3.4) the variation in χ^2 is observed through individual points in the $(m_F, M_{1/2})$ plane.

This is in fact the same region in which minimum A provides its lowest χ^2. In fact table 3.5 shows that for the best fit point in minimum A we have a pseudoscalar mass of 102 GeV and a light CP even mass of 106 GeV. With the TeVatron now taking data there is a high probability that the present lower bound on Higgs masses will be pushed higher. Hence we have undertaken a study of the effect this would have on our best fits. The plot in fig. (3.10) shows the increase in χ^2, for four points in the $(m_F, M_{1/2})$ plane of minimum A, due to an increase in the lower bound on the Higgs masses m_{A^0}, m_{h^0}. It clearly shows that all four of the points can accommodate an increase in the lower bound up to approximately 120 GeV, above this the χ^2 increases

sharply due the inability to accommodate such a large lower bound.

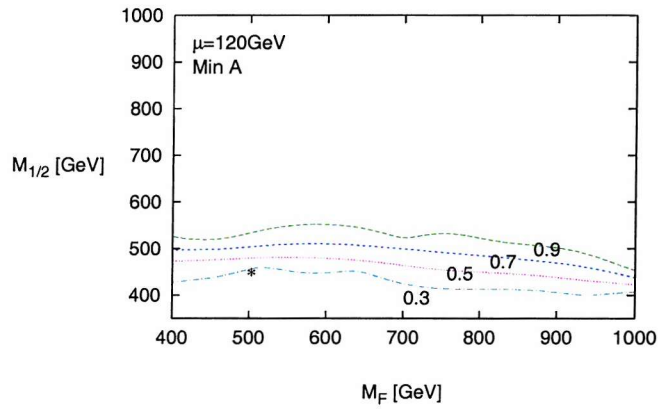

Figure 3.11: Contours of $\sin(\beta - \alpha)$, which defines the strength of the Z boson coupling to the Higgs h^0 relative to that of H^0. For values of $\sin(\beta - \alpha)$ near one the $Z - h^0$ coupling is large and for small values the $Z - H^0$ coupling is large. The contours are plotted using data from minimum A with $\mu = 120$ GeV. The the best fit point at $M_{1/2} = 450$ GeV, $m_f = 500$ GeV is marked with an asterisk.

The coupling of the light CP even Higgs, h^0, to the Z boson is proportional to $\sin(\beta - \alpha)$, as seen in table 2.3 in section 2.2.2, and that of the heavy CP even Higgs, H^0, is proportional to $\cos(\beta - \alpha)$, where α is the mixing angle for the CP even Higgs states. In fig. (3.11), which shows contours of $\sin(\beta - \alpha)$ for points in minimum A, we see that in the low $M_{1/2}$ region $\sin(\beta - \alpha)$ is small and hence the Z couples dominantly to the heavier Higgs state H^0, rather that the lighter h^0. Therefore, in this region it is the heavier state, H^0, which is the standard model like Higgs and so the LEP limit will apply to the larger m_{H^0} and not m_{h^0}. Table 3.5 shows that we have exactly this situation for the best fit points of minimum A where $\sin(\beta - \alpha) \sim 0.2$, therefore the standard model like Higgs is the heavier state H^0 for these points with a mass of 113 GeV. Assuming a 3 GeV error in our numerical calculation means we

are compatible with the present LEP limit of 114.4 GeV.

3.4.5 CHOOZ angle, θ_{13}

We are interested in using our best fit points to make further predictions for unknown observables as we have already done for $\mathrm{Br}(\tau \to \mu\gamma)$ in section 3.4.2. One further observable we would like to study is the neutrino mixing angle θ_{13}. As mentioned

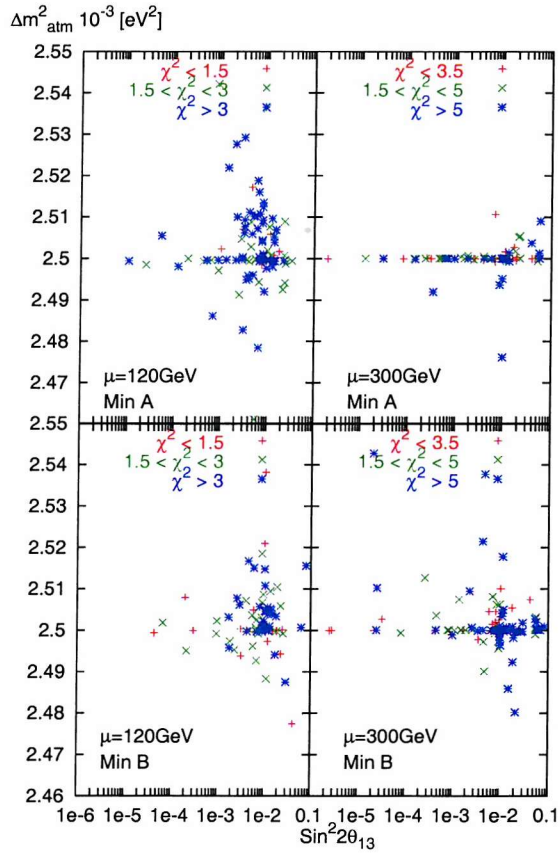

Figure 3.12: The four panels contain scatter plots of the values of Δm^2_{Atm} against $\sin^2 2\theta_{13}$ coming from the best fit points in the $(m_F, M_{1/2})$ plane. Each plot shows results obtained from either minimum A or minimum B, with $\mu = 120$ or 300 GeV as labelled. The points are grouped according to their χ^2 values as indicated.

in chapter 2 this mixing angle is still unknown although a bound has been set by the reactor experiment CHOOZ. The model we are studying is typical of a larger class of models and fits all present experimental constraints and so its predictions are characteristic of this broader group of models.

Fig. (3.12) shows scatter plots of $\sin^2 2\theta_{13}$ against Δm^2_{Atm} for both minimum A and minimum B with $\mu = 120$ and 300 GeV. Each point denotes a value obtained from an individual point in the $(m_F, M_{1/2})$ plane, with points grouped according to the value of χ^2. These plots show that the Model can easily yield values of θ_{13} that are within the present CHOOZ limit, $\theta_{13} \lesssim 0.22$. Each of the plots in fig. (3.12) shows that the best fit points, denoted by a "+" symbol, give a range of values of $\sin^2 2\theta_{13}$ from, 10^{-6} to 0.1. Although our results do not give any firm prediction for the value of θ_{13}, it can be seen that the model favours the region, $10^{-4} < \sin\theta_{13} < 0.1$, just below the present CHOOZ limit.

3.5 Summary and Conclusion

We have performed a complete global phenomenological analysis of a realistic string-inspired model based on the supersymmetric Pati-Salam $SU(4) \times SU(2)_L \times SU(2)_R$ gauge group supplemented by a $U(1)$ family symmetry. Global contour plots in the $(m_F,\ M_{1/2})$ plane have been presented in fig. (3.1), showing two χ^2 minima. These two distinct minima differ numerically by the relative sign of the D-term. This gives interesting phenomenological differences between the two minima, notably one has $Br(\tau \to \mu\gamma)$ near the present limit and a heavy pseudoscalar Higgs m_{A^0}, while the other has $Br(\tau \to \mu\gamma)$ well below the present bound but a light pseudoscalar Higgs m_{A^0}. Both minima give a good fit to the present muon $g-2$ discrepancy over a large region of parameter space and give $\sin^2 2\theta_{13}$ over the range $10^{-5} - 0.1$. Our best fit predictions for the superpartner masses for each of the two minima for two different

μ values are summarised in table 3.5.

We emphasise again that our analysis really should be considered as consisting of two distinct parts, associated with flavour physics on the one hand and unification and electroweak symmetry breaking on the other hand. For the flavour part, we have proposed a complete model in table 3.2 which gives an accurate description of all fermion masses and mixing angles, including the LMA MSW neutrino solution. We have shown that improved limits on $Br(\tau \to \mu\gamma)$ could begin to rule out one of our two minima. The conclusions on $Br(\tau \to \mu\gamma)$ are applicable to a wide class of models which achieve approximate maximal atmospheric neutrino mixing via the see-saw mechanism in the MSSM with a large 23 entry in the neutrino Yukawa matrix. On the other hand $Br(\mu \to e\gamma)$ is predicted to be about two orders of magnitude below the current limit, which is a consequence of the specific flavour structure of the model in table 3.2.

Regarding unification, the model predicts approximate third family Yukawa unification and hence large $\tan\beta \sim 50$. Electroweak symmetry breaking was achieved with the help of D-terms and non-universal soft Higgs mass, which allows small μ values. The property of exact Yukawa unification was relaxed throughout the analysis and it was found that a deviation of 20-35% for the bottom Yukawa coupling and 0-10% for the top Yukawa coupling are required for a good fit to be obtained. We showed that relaxing Yukawa unification has the effect of allowing small values of the soft scalar mass m_F, and lighter squark and slepton masses as a consequence.

Further studies of the effects of future direct Higgs searches and a change to the present muon $g-2$ discrepancy are shown in fig. (3.4) and (3.10). We found that our best fit points, for the minima with lighter Higgs masses, can accommodate a lower bound on Higgs masses up to about 120 GeV. For these points the coupling of the lighter CP even Higgs state to the Z boson is suppressed, leaving the heavier of the two CP even states acting as the standard model like Higgs.

In conclusion, we have constructed and analysed a complete supersymmetric Pati-Salam model which agrees with all laboratory observables and constraints. Using a global analysis we identify the most preferred regions of the SUSY parameter space, and find a rather light superpartner spectrum corresponding to $(m_F, M_{1/2}) \sim (600, 600)$ (in GeV) well within reach at the LHC.

Chapter 4

The Implications of $B_s \to \mu^+\mu^-$

In this chapter we examine the potentially very promising signal $B_s \to \mu^+\mu^-$ in supersymmetry with large $\tan\beta$ in a *top-down* approach starting from the best fits of the $SO(10)$-like model studied in the previous chapter. In fact our predictions are to a large extent model independent, being similar to those based on minimal supergravity, but we include contributions which go beyond those investigated in previous works. In particular, in the effective flavour changing coupling we include terms not explicitly proportional to V_{ts} which have been neglected in previous studies based on minimal supergravity. We show that the absolute best fits provide a signal for $B_s \to \mu^+\mu^-$ at the borderline of the present limits and hence the ongoing search at the TeVatron will start having an impact on the global analysis of this class of SUSY models. We discuss the implications of a measurement of $B_s \to \mu^+\mu^-$ for restricting the parameter space of gauginos and sfermion masses, and of signals in other channels $B_{d,s} \to \ell^+\ell^-$. We also discuss correlations of $B_s \to \mu^+\mu^-$ with the CP-odd Higgs mass, $\sin(\beta-\alpha)$ and $b \to s\gamma$ in $SO(10)$-like models.

The work presented in this chapter may be found in ref. [47].

4.1 Preliminaries

Ideas of unification and the origin of flavour have been under investigation for a long time and many different models have been proposed in the last twenty years. Yet in the diversity of different approaches a class of unification models can be recognised which is remarkably simple at the unification scale. We call this class SO(10)-like unification models. In these models the effective theory at the unification scale assumes that the Standard Model (SM) gauge couplings unify to a per cent level, third family Yukawa couplings are all of order unity and the remaining flavour structure originates in a small set of higher-dimensional superpotential operators keeping the supersymmetry (SUSY) breaking sector of a model flavour blind. We note that actual models which fall into this category often assume lower symmetry than SO(10), e.g. models based on the Pati-Salam gauge group or the MSSM gauge group generated by a string theory in higher dimensions are often found in this class of models.

It has been recently pointed out that if the Minimal Supersymmetric Standard Model (MSSM) is the effective theory describing nature above the scale 100 GeV and $\tan\beta \equiv \langle H_u^0 \rangle / \langle H_d^0 \rangle \equiv v_u/v_d$ is large, a pure leptonic $B_s \to \mu^+\mu^-$ decay has a very strong case to emerge among the first indirect signals of supersymmetry (SUSY) [48]. This is because the decay signal should be very clear at the TeVatron or LHC and also because the SM branching fraction is suppressed down to 10^{-9} while the rate can be enhanced when considering SUSY extensions. In particular, this occurs due to large couplings of the down-type quarks and charged leptons to the MSSM higgs states if $\tan\beta$ is large. Thus it is important to analyse this decay in a full SUSY theory and not just in terms of the minimal flavour violation that assumes that V_{cb} is the only source of the 32 transition, as has been done in the past. In the full context of complete unification models it means that the 32 flavour structure is restricted by the fermion mass ratios m_μ/m_τ, m_s/m_b and m_c/m_t, small value of V_{cb}, large $U_{\mu 3}$, $b \to s\gamma$ branching ratio and possibly other low energy observables and constraints.

Although these constraints do not determine the 32 sector uniquely they do provide for a realistic prediction of observables like the $B_s \to \ell^+\ell^-$ decay rates.

In the following sections of this chapter we present the results of such a complete *top-down* investigation based on the best fit predictions obtained in the global analysis of a complete SO(10)-like model presented in chapter 3 and published in [23]. The best fits obtained in this work give a very good agreement with the observables related to the 32 flavour sector and satisfy all laboratory experimental constraints on superpartner masses. Here they serve as our starting point since they provide us with all the MSSM couplings at the low-energy scale. Within this framework we study the implications of a possible measurement $B_s \to \mu^+\mu^-$. In particular, we discuss the related processes $B_s \to \tau^+\tau^-$, $B_d \to \mu^+\mu^-$, $B_d \to \tau^+\tau^-$, and show the correlations with $B_s \to \mu^+\mu^-$. We discuss the implications of a measurement of $B_s \to \mu^+\mu^-$ for restricting the parameter space of gauginos and sfermion masses, and also discuss correlations of $B_s \to \mu^+\mu^-$ with $b \to s\gamma$ and the CP-odd Higgs mass.

We emphasise that our work is general and applies to any mSUGRA model with universal sfermion masses at the unification scale and the Higgs spectrum similar to the one considered here. In such a framework it is well known that, for a given choice of low energy fermion masses and CKM mixing angles, the flavour predictions are independent of the precise nature of the Yukawa matrices selected at high energy since different choices of Yukawa matrices can be rotated into each other. Apart from being general, the present study contains a number of new features not present in previous works. One novel feature is to present results that are based on a top-down global analysis. [1] In a top-down approach of this kind the complete Yukawa and sfermion mass matrices are known at the low energy scale and no extra iteration (sometimes called resummation of large $\tan\beta$ terms) is needed to extract the couplings which enter the one-loop SUSY integrals. Another new aspect is a more complete

[1] This approach was also considered by Dermisek *et al.*in [48].

analysis of the process $B_s \to \mu^+\mu^-$. The previous analyses of SO(10)-like models (see, e.g. Dedes et al in [48]) only considered minimal flavour violation with the rate $B_s \to \mu^+\mu^-$ explicitly proportional to the low-energy value V_{ts}^2 while our results also include the contributions from diagrams like in fig. (4.4) that are not proportional to $V_{ts}(M_Z)$. Such contributions, which arise from squark mixing effects, have so far been ignored in mSUGRA based analyses, yet can give significant contributions to the rate, as discussed later.

After this introduction the chapter continues in section 4.2 with a brief theoretical section on the evaluation of $B_s \to \ell^+\ell^-$ decay rate in the *top-down* approach. In section 4.3 we discuss our top down approach after which section 4.4 presents our numerical results, and discusses the implications of a signal for $B_s \to \mu^+\mu^-$. Section 4.5 concludes the chapter.

4.2 $B_s \to \mu^+\mu^-$

We emphasise that in a *top-down* approach the tree-level MSSM couplings are determined from high energy boundary conditions, and do not have to be determined by an iterative procedure as in bottom-up approaches. In particular, in terms of effective vertices f and g, which are matrices in flavour space, after heavy sparticles are integrated out the lagrangian can be written down as

$$\mathcal{L}_{eff} = -\overline{d}_R^{(0)} \left[Y_d^{(0)\mathrm{diag}\,\dagger} H_d^0 + f^\dagger H_d^0 + g^\dagger H_u^{0*} \right] d_L^{(0)} + h.c.. \tag{4.1}$$

At tree level down-type quarks $d_{L,R}$ only couple to down-type Higgs H_d^0 and $f = g = 0$. Yukawa couplings $Y_d^{(0)}$ can be read out as a straightforward prediction of a unified model. $Y_d^{(0)}$ and the mass matrix $m_d^{(0)} = Y_d^{(0)} v_d$ can then be simultaneously diagonalised with eigenvectors $d_{R,L}^{(0)}$. At one-loop level f and g have to be computed

and the mass terms relevant for this discussion become [2]

$$\mathcal{L}_{mass} = -\overline{d}_R^{(0)} \left[m_d^{(0)diag\,\dagger} + f^\dagger v_d + g^\dagger v_u \right] d_L^{(0)}, \tag{4.2}$$

using the same basis. Clearly, if $v_u \gg v_d$ sizeable corrections to the mass eigenvalues [40] and mixing matrices [41] are generated. Furthermore the 3-point functions in eq. (4.1) and mass matrix in eq. (4.2) cannot be simultaneously diagonalised [50]. If we write eq. (4.1) as

$$-\overline{d}_R^{(0)} \left[Y_d^{(0)diag\,\dagger} + f^\dagger + g^\dagger \frac{v_u}{v_d} \right] d_L^{(0)} H_d^0 \; - \; \overline{d}_R^{(0)} \left[g^\dagger \left(H_u^{0*} - \frac{v_u}{v_d} H_d^0 \right) \right] d_L^{(0)}, \tag{4.3}$$

then the first bracket of eq. (4.3) is in a form which is similar to that of the mass matrix and therefore is diagonal when $d_{L,R}^{(0)}$ are rotated into corrected mass eigenstates $d_{L,R}^{(1)} = V_d^{L,R\,(1)} d_{L,R}^{(0)}$. This is not true for the last bracket which becomes a source of flavour changing,

$$\mathcal{L}_{FCNC} \; = \; -\overline{d}_{Ri}^{(1)} \left[V_d^{R\,(1)} g^\dagger \left(H_u^{0*} - \frac{v_u}{v_d} H_d^0 \right) V_d^{L\,(1)\,\dagger} \right]_{ij} d_{Lj}^{(1)} + h.c.. \tag{4.4}$$

It is now explicit that its origin comes from the interaction $\overline{d}_R^0 H_u^{0*} d_L^0$, not present at tree level. Moreover, the flavour changing couplings get enhanced by an explicit factor $\tan\beta$ on top of any $\tan\beta$ scaling present in g. In the leading order in $\tan\beta$ the g matrix can in fact be related in a simple way to the finite non-logarithmic mass matrix corrections, $g_{ij} = (\delta m_d^{finite})_{ij}/v_u$, computed for the first time in [41]. Due to $H_u^0 = v_u + (H^0 s_\alpha + h^0 c_\alpha + i A^0 c_\beta + i G^0 s_\beta)/\sqrt{2}$ and $H_d^0 = v_d + (H^0 c_\alpha - h^0 s_\alpha + i A^0 s_\beta - i G^0 c_\beta)/\sqrt{2}$ we can write

$$H_u^{0*} - \frac{v_u}{v_d} H_d^0 \; = \; \frac{1}{\sqrt{2}} \frac{1}{c_\beta} \left[H^0 s_{\alpha-\beta} + h^0 c_{\alpha-\beta} - i\, A^0 \right], \tag{4.5}$$

[2] Terms due to wavefunction renormalisation do not contribute to flavour changing.

where $s_\alpha \equiv \sin\alpha$, $c_\alpha \equiv \cos\alpha$, *etc.* We can thus identify effective vertices $\bar{b}_R s_L H^0$, $\bar{b}_R s_L h^0$ and $\bar{b}_R s_L A^0$ involving b to s transitions mediated by neutral physical higgs states. We note that with large $\tan\beta$ the coupling to the pseudoscalar A^0 is always large while the CP-even states, h^0 and H^0, have couplings which depend on the CP-even higgs mixing angle α. The Goldstone mode is cancelled in the equation above and thus the effective vertex with the Z boson is absent at this level.

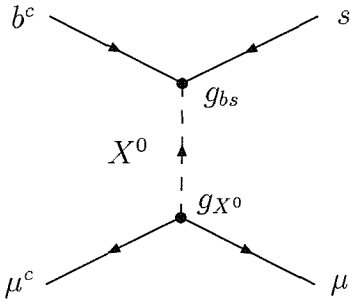

Figure 4.1: Higgs penguin contribution to the flavour changing neutral current process, $B_s \to \mu^+\mu^-$. The coupling g_{bs} is an effective vertex generated from loops where the heavy SUSY partners have been integrated out. The mediating X^0 stands for neutral Higgs mass eigenstates, h^0, H^0, A^0.

In the MSSM with large $\tan\beta$ the dominant contribution to $B_s \to \ell^+\ell^-$ comes from the penguin diagram where the dilepton pair is produced from a virtual Higgs state [48]. After the SUSY partners are integrated out we are left with the effective vertices determined above. Thus in combination with the standard tree-level term $\mathcal{L}_{\ell\ell H} = -y_\ell \overline{\ell_R} \ell_L H_d^0 + h.c.$ the dominant $\tan\beta$ enhanced contribution to the branching ratio

turns out to be

$$Br(B_s^0 \to \mu^+\mu^-) = 1.75 \times 10^{-3} \left|\frac{\delta m^\dagger_{d\,32}}{m_b V_{ts}}\right|^2 \left[\frac{V_{ts}}{0.04}\right]^2 \left[\frac{y_\mu}{0.0311}\right]^2 \left[\frac{M_{170}}{v_u}\right]^2 \left[\frac{\tan\beta}{50}\right]^2 \times \left[\left(\frac{c_\alpha s_{\alpha-\beta}}{\left(\frac{M_{H^0}}{M_{100}}\right)^2} - \frac{s_\alpha c_{\alpha-\beta}}{\left(\frac{M_{h^0}}{M_{100}}\right)^2}\right)^2 + \frac{s_\beta^2}{\left(\frac{M_{A^0}}{M_{100}}\right)^4}\right], \quad (4.6)$$

where matrix $\delta m_d^\dagger$ is in the $\{d^{(1)}_{L,R}\}$ basis, and is defined by

$$\delta m_d^\dagger = V_d^{R\,(1)}(f^\dagger v_d + g^\dagger v_u) V_d^{L\,(1)\dagger}, \quad (4.7)$$

m_b is the b quark mass at scale M_Z in the effective $SU(3)_c \times U(1)_{em}$ theory, the constants are $M_{100} = 100\,\text{GeV}$ and $M_{170} = 170\,\text{GeV}$. The numerical factor in eq. (4.6) arises from:

$$1.75 \times 10^{-3} = \frac{\tau_B f_B^2 M_B^5}{128\pi} \frac{0.04^2\, 0.0311^2\, 50^2}{M_{100}^4\, M_{170}^2}. \quad (4.8)$$

Note that $Br(B_s^0 \to \mu^+\mu^-)$ in eq. (4.6) is not proportional to V_{ts}^2. This formula therefore differs from that used in previous mSUGRA analyses, as mentioned previously.

Modification for other $B^0_{d_i} \to \ell^+\ell^-$ decays is trivial. We note that each of these branching fractions actually scales down as $\tan^6\beta$ [49] for lower values of $\tan\beta$: additional powers of $\tan\beta$ enter due to the explicit presence of lepton Yukawa coupling y_ℓ^2 and mass matrix corrections $\delta m_d^{finite}/m_b$ (or, equivalently, Yukawa coupling y_{d_i} in g).

4.3 Top-down approach

Our results are based on the model analysed in [23]. The model was defined below the $SO(10)$ breaking scale, where the gauge group was broken to its maximal Pati-Salam

subgroup, and the flavour structure of the model was determined by operators which respected the Pati-Salam symmetry. Universal gaugino masses $M_{1/2}$ and sfermion masses m_F were assumed, and we allowed for D-terms and non-universal scalar Higgs masses. Throughout this work the trilinear parameter was kept fixed at $A_0(M_{GUT}) = 0$. We note that the Yukawa unification is not exact, with y_b for example dropping down to $0.7y_t$ for the best fits, although we keep the low energy value $\tan\beta = 50$ fixed in our analysis. As we have already emphasised, since the soft sfermion masses are assumed to be universal, the physical effects arising from flavour violation in the quark sector are independent of the choice of high energy quark Yukawa matrices. However in the lepton sector this is not the case due to heavy right-handed neutrino mass thresholds.[3] The essential features of the model in the lepton sector include a large off-diagonal neutrino Yukawa coupling $Y^{\nu}_{23} \sim 1$, to generate the large atmospheric mixing angle. Since the soft SUSY breaking sfermion mass matrices at M_{GUT} are proportional to the unit matrix the main difference between this model and standard mSUGRA is that here we consider a non-universal Higgs mass and D-terms which allow for a larger flexibility for the Higgs spectra.

4.4 Results

We first summarise the experimental limits for the processes of interest:

$$\mathrm{Br}(B_s \to \mu\mu) \;<\; 2.0 \times 10^{-6}\,[\mathrm{CDF}] \tag{4.9}$$

$$\mathrm{Br}(B_d \to \mu\mu) \;<\; 6.1 \times 10^{-7}\,[\mathrm{Babar}], \tag{4.10}$$

with no bounds yet established for the τ final state processes. Looking to the future, the TeVatron will bring us further results for B_s decays with the prospect of a CDF bound in the region of $\mathrm{Br}(B_s \to \mu\mu) < 10^{-7}$. By comparison the standard model

[3] See for example [37].

predicts $\mathrm{Br}(B_s \to \mu\mu)_{\mathrm{SM}} \sim 3.5 \times 10^{-9}$ [51].

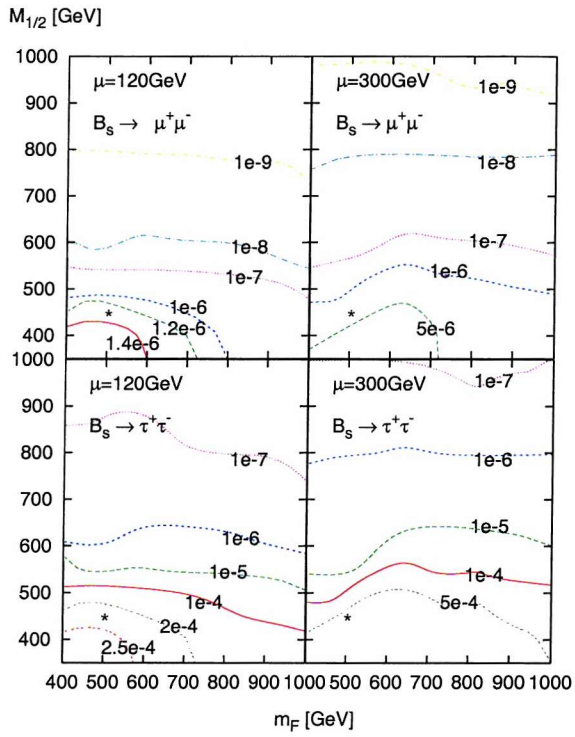

Figure 4.2: Contour plots for the branching ratios of the FCNC processes, $B_s \to \mu^+\mu^-$ and $B_s \to \tau^+\tau^-$. Each branching ratio is plotted with two different values of the μ parameter. The $\star$ marks the best fit point.

To obtain predictions for such processes, we have performed a *top-down* global analysis of the $SO(10)$-like model outlined in the previous chapter. This analysis yields two distinct best fits, which we call Minimum A and Minimum B. The higgs spectrum in Minimum B is heavy, mostly near the TeV scale and will not be considered in the discussion below. The Higgs spectrum of Minimum A was found to be more interesting for our present study with masses at the 100 GeV scale. Hence it is the results from the unaltered fits of Minimum A which are presented in this chapter.

The numerical results for the processes $B_s \to \mu^+\mu^-$ and $B_s \to \tau^+\tau^-$ are displayed

in fig. (4.2). Similar results for $B_d \to \mu^+\mu^-, \tau^+\tau^-$ are given in fig. (4.3). These results are presented as contour plots in the $m_F - M_{1/2}$ plane with a fixed value of $\mu = 120$ GeV(left panels) and $\mu = 300$ GeV(right panels). When comparing these contours with eq. (4.6) we find that a significant suppression is obtained from the ratio

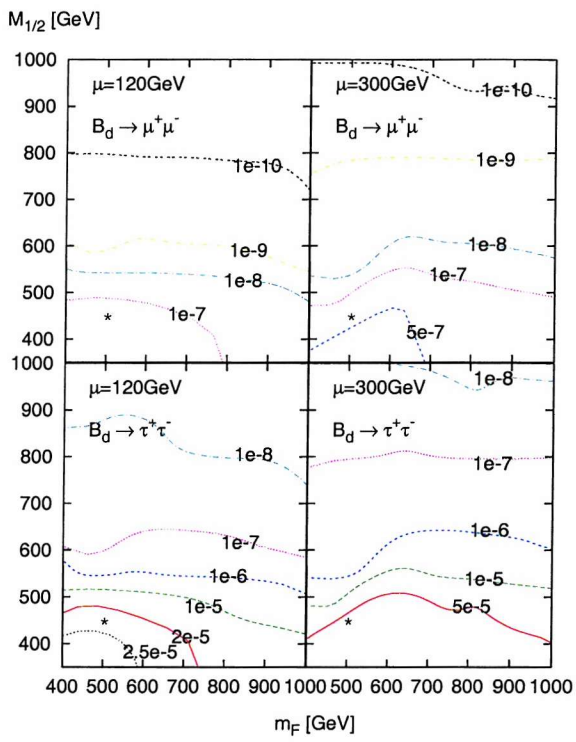

Figure 4.3: Contour plots for the branching ratios of the FCNC processes, $B_d \to \mu^+\mu^-$ and $B_d \to \tau^+\tau^-$. Each branching ratio is plotted with two different values of the μ parameter. The $\star$ marks the best fit point.

$(\delta m_d)_{32}/m_b V_{ts}$. This comes purely from fitting the b quark mass, V_{cb} and $b \to s\gamma$. At this point it is of interest to enquire how large are the non-minimal flavour violating effects represented by the diagrams in fig. (4.4). For the best fit point we have checked that the second diagram in fig. (4.4) is 25% as large as a similar diagram without the mass insertion on the squark line, but with V_{ts} inserted at the vertex instead. This gives an indication that the non-minimal flavour violating effects we include are

significant.

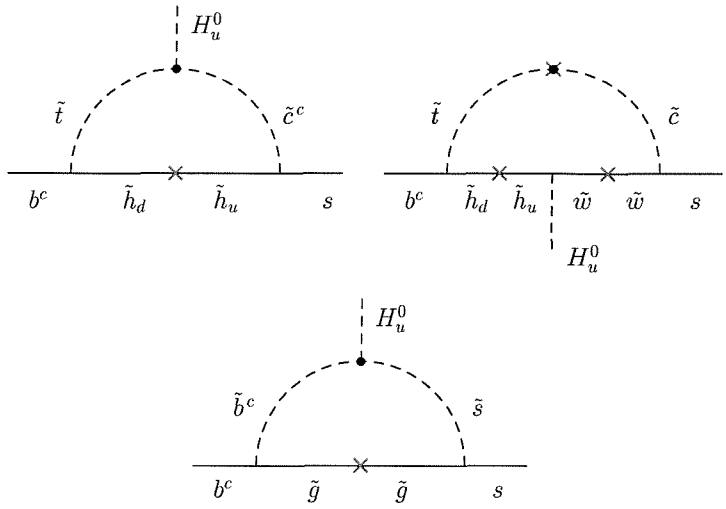

Figure 4.4: Examples of Feynman diagrams contributing to the effective bsH_u^0 coupling that are not proportional to $V_{ts}(M_Z)$. Black dots indicate flavour-changing vertices while crosses stand for mass insertions for interaction eigenstates.

The upper two panels of fig. (4.2) display contours of $\mathrm{Br}(B_s \to \mu\mu)$ with $\mu = 120$ and 300 GeV, and show values quite close to the current limits, and well above the standard model predictions. The Higgs mediated contribution in the SUSY model clearly dominates over the standard model contribution and for $\mu = 300$ GeV, with low $M_{1/2}$, it can even exceed the present CDF limit. An improved limit of 10^{-7} would be very restricting and could probe Higgs masses into the range, $m_{A^0} = 150{-}300$ GeV. As for the process, $B_d \to \mu\mu$, fig. (4.3) shows that the present bound is satisfied by both μ values over the entire displayed plane.

Inspection of figs. (4.2) and (4.3), reveals that the branching ratios for $B_{s,d} \to \mu^+\mu^-, \tau^+\tau^-$ are sensitive to the universal gaugino mass $M_{1/2}$, but not to the universal sfermion mass m_F. Inspecting the m_{A^0} panels of fig. (4.5) we see that it has

a very similar $M_{1/2}$, m_F dependence. This can be understood as a consequence of a lighter mediating Higgs which leads to larger branching ratios.

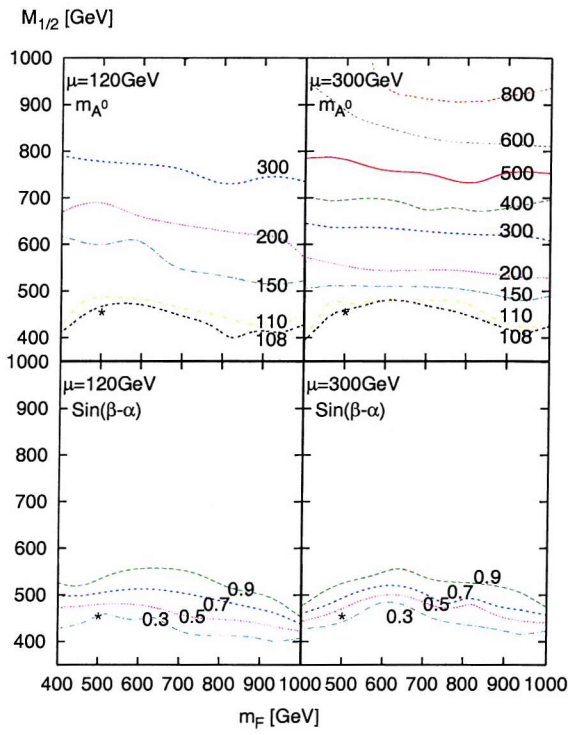

Figure 4.5: The upper two panels contain contours of the CP odd Pseudoscalar Higgs mass, plotted in the $m_F - M_{1/2}$ plane. The lower panels contain contours of, $\sin(\beta - \alpha)$, which determines the strength of the Z-boson coupling to, h^0, the lighter CP even Higgs. Again the plots are displayed at different values of μ. The $\star$ marks the best fit point.

The branching ratio for $B_{s,d} \to \tau\tau$ is enhanced by a factor of $(y_\tau/y_\mu)^2 \sim 100$ compared to the muon final state processes, as can be seen in the lower panels of fig. (4.2) and (4.3). This makes the tau final state processes very attractive for experimental discovery. The difficulty comes with the required detector resolution to measure tau decays. If this problem could be solved at future experiments then these tau final state processes could become the primary signal for indirect SUSY searches.

Fig. (4.5) contains corresponding contours of m_{A^0} in the upper panels and the quantity $\sin(\beta-\alpha)$, which controls the coupling of the lightest CP-even Higgs scalar coupling to the Z, in the lower panels. The numerical predictions for the best fit point at $M_{1/2} = 450$, $m_F = 500$ GeV (indicated by an asterisk in the figures) are given in table 4.1.

	$\mu = 120$ GeV	$\mu = 300$ GeV
$M_{1/2}$ [GeV]	450	450
m_F [GeV]	500	500
$B_s \to \mu\mu$	1.5×10^{-6}	5.9×10^{-6}
$B_s \to \tau\tau$	2.6×10^{-4}	1×10^{-3}
$B_d \to \mu\mu$	1.5×10^{-7}	5.8×10^{-7}
$B_d \to \tau\tau$	2.7×10^{-5}	1×10^{-4}
m_{A^0} [GeV]	102	102
$\sin(\beta-\alpha)$	0.22	0.15

Table 4.1: Table of branching ratios for $B_{s,d} \to \mu^+\mu^-, \tau^+\tau^-$, CP-odd pseudoscalar mass m_{A^0}, and $\sin(\beta-\alpha)$ which governs the lightest CP-even scalar coupling to the Z, for the best fit point.

We now turn to the implications of a possible measurement (or an improved experimental limit) of the branching fraction of $B_s \to \mu\mu$ for $SO(10)$-like models. Fig. (4.6) and (4.7) show the effect on various quantities of varying the branching ratio for $B_s \to \mu\mu$ for three fixed points in the $m_F - M_{1/2}$ plane.

The upper panels of fig. (4.6) show the variation of χ^2 as $\mathrm{Br}(B_s \to \mu\mu)$ is varied. As $\mathrm{Br}(B_s \to \mu\mu)$ decreases the χ^2 increases initially slowly and later rapidly. The initial slow increase is understood from fig. (3.10) in the previous chapter, where it was observed that the value of χ^2 for the best fit points are insensitive to changes of a few GeV in the Higgs spectrum, which implies an insensitivity to small changes in the branching ratio for $B_s \to \mu\mu$. Hence the points which presently exceed the CDF bound can be forced to satisfy it with only a small(~ 0.5) increase in χ^2. But if the bound was to be lowered to 10^{-7} then this would no longer be possible with $\Delta\chi^2 \sim 3$.

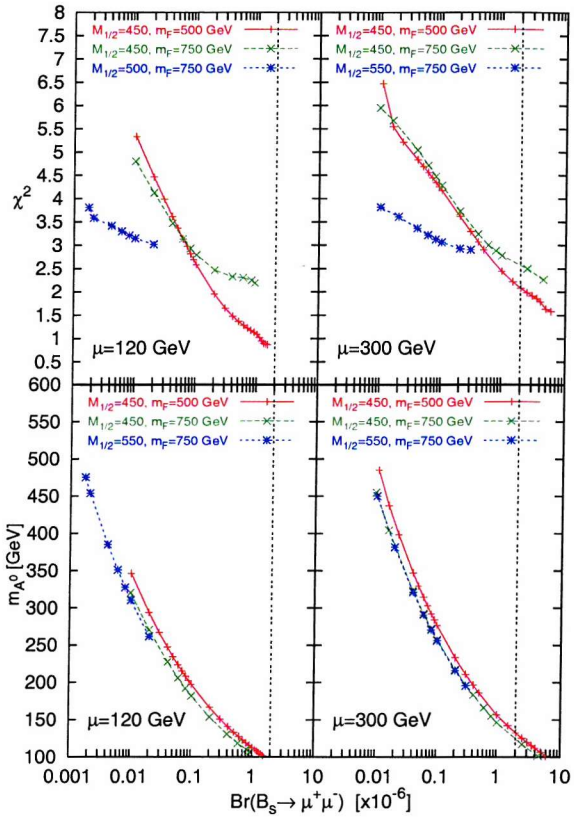

Figure 4.6: This figure shows the variation of χ^2 and the Pseudoscalar Higgs mass, m_{A^0}, as the branching ratio of $B_s \to \mu\mu$ varies from 10^{-5} down to 10^{-8}. Each of the three curves are drawn with fixed values of $M_{1/2}$, m_F. The vertical dashed line represents the present CDF bound on $B_s \to \mu^+\mu^-$.

Hence the low $M_{1/2}$ region of the $\mu = 300$ GeV plane will be ruled out and the best fit region would move toward larger $M_{1/2}$.

The lower panels of fig. (4.6) display the variation of m_{A^0} as $\mathrm{Br}(B_s \to \mu\mu)$ is varied. As expected m_{A^0} increases smoothly as $\mathrm{Br}(B_s \to \mu\mu)$ decreases. Note the strong correlation of the CP-odd Higgs mass with $\mathrm{Br}(B_s \to \mu\mu)$, which for a fixed value of μ is quite insensitive to m_F and $M_{1/2}$.

It is well known in SUSY models with large $\tan\beta$ that $b \to s\gamma$ provides a strong

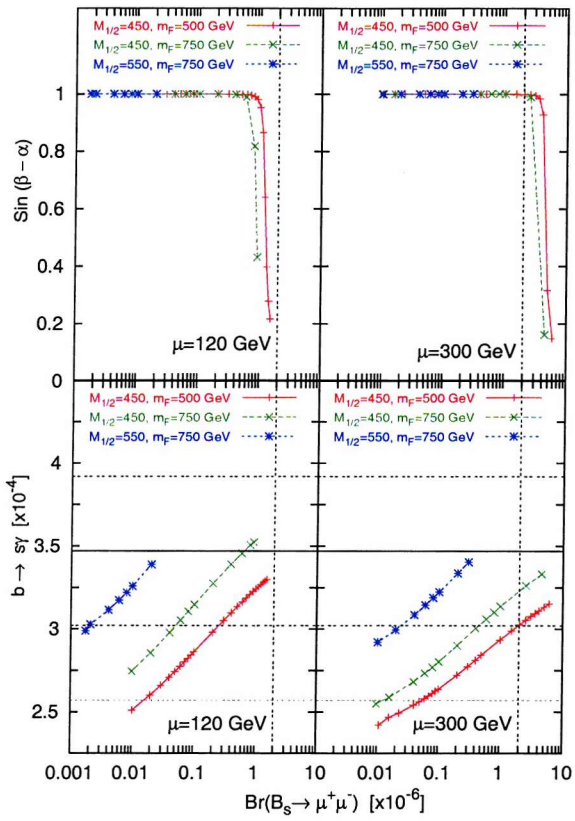

Figure 4.7: This figure shows the variation of $\sin(\beta - \alpha)$ and the branching ratio for $b \to s\gamma$, against $B_s \to \mu\mu$. The vertical dashed line represents the present CDF bound on $B_s \to \mu^+\mu^-$. The horizontal lines show the central measured value(solid) of $\mathrm{Br}(b \to s\gamma)$ along with the 1σ(dashed) and 2σ(light dashed) regions.

constraint on parameter space [52]. In fig. (4.6) the main contribution to the increase in χ^2 seen is due to $b \to s\gamma$ not being fit well. The lower panels of fig. (4.7) show the variation of $\mathrm{Br}(b \to s\gamma)$ against $\mathrm{Br}(B_s \to \mu\mu)$ and show a clear correlation. This correlation can be understood as the SUSY contribution to each of these processes involves the 23 mixings in the squark mass matrix. For example the dominant chargino contributions to each process, shown in fig. (4.4) and fig. (2.6), are closely related. These panels also show why $b \to s\gamma$ is the main contribution to the change in χ^2 as the fit to $b \to s\gamma$ changes from within 1σ to almost 2σ.

The upper panels of fig. (4.7) show the variation of $\sin(\beta - \alpha)$ as $\mathrm{Br}(B_s \to \mu\mu)$ is varied. In the low $M_{1/2}$ region, where $\mathrm{Br}(B_s \to \mu\mu)$ is near the current limit, $\sin(\beta-\alpha)$ is small and hence the Z-boson couples predominantly to the heavier CP-even Higgs H^0, rather than the lighter Higgs h^0. However $\sin(\beta - \alpha)$ very quickly approaches unity as the $\mathrm{Br}(B_s \to \mu\mu)$ decreases, corresponding to the standard model limit where the h^0 couples like the standard model Higgs boson.

4.5 Conclusions

We have examined the potentially very promising signal $B_s \to \mu^+\mu^-$ in supersymmetry with large $\tan\beta \sim 50$ in a *top-down* approach starting from the best fits of an $SO(10)$-like model presented in chapter 3. However our predictions are to a large extent model independent, being similar to those based on minimal supergravity, but we include all additional contributions which go beyond the minimal flavour violation investigated in previous works. In particular, in the effective flavour changing coupling we include terms not explicitly proportional to V_{ts} which have been neglected in previous studies based on minimal supergravity, and which we have shown are significant. The results in this chapter therefore go beyond those based on minimal flavour violation in mSUGRA investigated previously. Our results show that the absolute best fits provide for the $B_s \to \mu^+\mu^-$ signal at the borderline of the present limits and hence the ongoing search at the TeVatron will start having an impact on the global analysis of this class of SUSY models.

We have discussed the implications of a measurement (or an improved limit) of $B_s \to \mu^+\mu^-$ for restricting the parameter space of gauginos and sfermion masses, and of signals in other channels $B_{d,s} \to \ell^+\ell^-$. We have also discussed correlations of $B_s \to \mu^+\mu^-$ with $b \to s\gamma$ and the CP-odd Higgs mass. An improved limit for $\mathrm{Br}(B_s \to \mu\mu)$ of around 10^{-7} would be very restricting and could probe Higgs masses into the

range, $m_{A^0} = 150 - 300$ GeV, with the Higgs coupling strength $\sin(\beta - \alpha)$ varying very quickly around this region. The possible non-observation of $B_s \to \mu^+\mu^-$ at the levels suggested by our study would by no means rule out $SO(10)$-like models. In the context of the analysis in chapter 3 this would simply highlight Minimum B, with its heavier Higgs spectrum and $\mathrm{Br}(B_s \to \mu\mu) \sim 10^{-10}$, as the favoured solution. On the other hand we have seen that an actual observation of $B_s \to \mu^+\mu^-$ at the 10^{-7} level is quite plausibly expected in SUSY $SO(10)$-like models, with interesting phenomenological and theoretical consequences.

5.1 Preliminaries

Observations of neutrino oscillations at SuperKamiokande [15], SNO [17] and KamLAND [18] imply the existence of massive neutrinos with large solar and atmospheric mixing angles. The small neutrino masses are most naturally explained via the see-saw mechanism with heavy singlet neutrinos. Models incorporating the see-saw mechanism will contain Yukawa couplings for both the neutrinos, Y_ν and charged leptons, Y_e and a Majorana mass for the singlet neutrinos, M_R. It is possible to work in a basis where both Y_e and M_R are diagonal in flavour space. In such a basis Y_ν is always left as a possible source of flavour violation. In SUSY models this flavour violation can be communicated to the slepton sector through renormalisation group running. The initial communication is from running between the GUT scale and the scale of M_R. Although the scale M_R is far above the weak scale its effects leave a lasting impression on the mass squared matrices of the sleptons. Subsequently flavour violation can enter into the charged lepton sector through loop diagrams involving the sleptons and indeed such effects have been used to predict large branching ratios for $\tau \to \mu\gamma$ and $\mu \to e\gamma$ within the MSSM [26, 28, 37, 53].

We have seen in the previous chapter that such flavour changing can appear in the couplings of the neutral Higgs bosons and is enhanced by large $\tan\beta$. In the quark sector interactions of the form, $\bar{d}_R d_L H_u^{0*}$, are generated at one-loop [40, 41] and at large $\tan\beta$ can become comparable to the tree-level interaction, $\bar{d}_R d_L H_d^0$. We saw in the previous chapter that these two contributions cannot be simultaneously diagonalised and lead to potentially large Higgs-mediated flavour changing processes such as $B_s \to \mu\mu$ [48, 47].

Similar Higgs-mediated flavour violation can also occur in the lepton sector of SUSY see-saw models through interactions of the form $\bar{e}_R e_L H_u^{0*}$. This leads to the possibility of large branching ratios for the Higgs-mediated LFV processes such as $B_s \to \tau\mu$,

$\tau \to 3\mu$ and flavour violating Higgs decays [54, 55, 56, 57].

In this chapter we extend the work of chapters 3 and 4 to study the lepton flavour violating decays $B_s \to \tau\mu$ and $\tau \to 3\mu$ from the best fit points of the SO(10)-like model studied in chapter 3. These processes are correlated and highly constrained by those of $B_s \to \mu\mu$ and $\tau \to \mu\gamma$. Such correlations will therefore be studied in detail. The remaining sections of this chapter are as follows, section 5.2 contains a discussion of the theoretical origin of the lepton flavour violating Higgs couplings in the *top-down* approach, section 5.3 presents our results for the processes mentioned above and finally section 5.4 concludes the chapter.

5.2 Lepton Flavour violating Higgs couplings

As we saw in section 2.3.2 a SUSY see-saw model will have lagrangian terms of the form,

$$\mathcal{L} \supset \bar{e}_R Y_e L_L H_d - \bar{\nu}_R Y_\nu L_L H_u - \nu_R^{\mathrm{T}} M_R \nu_R. \tag{5.1}$$

We can diagonalise the charged lepton Yukawa and neutrino Majorana mass matrices such that,

$$M_R = V_R^\nu \, M_R^{\mathrm{diag}} \, V_R^{\nu\,\mathrm{T}}, \qquad Y_e = V_R^e \, Y_e^{\mathrm{diag}} \, V_L^{e\,\dagger}. \tag{5.2}$$

In this basis we must also rotate the the neutrino Yukawa matrix using the unitary matrices V_R^ν and V_L^e. Hence we have,

$$Y_\nu \to V_R^{\nu\,\mathrm{T}} \, Y_\nu \, V_L^e. \tag{5.3}$$

Clearly Y_ν need not be diagonal and represents a source of flavour violation in the lepton sector. This flavour violation is communicated to the sleptons via renormalisation group flow from the GUT scale to the scale at which the right-handed neutrinos are decoupled. The relevant renormalisation group equation for the slepton soft mass squared matrix can be written as,

$$\mu\frac{d}{d\mu}(m^2_{\tilde{L}})_{ij} = \left(\mu\frac{d}{d\mu}(m^2_{\tilde{L}})_{ij}\right)_{\text{diag}} + \frac{1}{16\pi^2}\left[m^2_{\tilde{L}}Y_\nu Y_\nu^\dagger + Y_\nu Y_\nu^\dagger m^2_{\tilde{L}} + 2\left(Y_\nu m^2_{\tilde{\nu}_R}Y_\nu^\dagger + m^2_{H_u}Y_\nu Y_\nu^\dagger + A_\nu A_\nu^\dagger\right)\right]_{ij}. \quad (5.4)$$

The first term here represents the lepton flavour conserving terms. As Y_ν is non-diagonal the combinations $Y_\nu^\dagger Y_\nu$ will induce off-diagonal contributions to $m^2_{\tilde{L}}$. Therefore even for universal soft terms, as discussed in eq. (2.67), large flavour changing may be induced in the slepton sector. Eq. (5.4) can be solved approximately for the flavour mixing part with,

$$(\Delta m^2_{\tilde{L}})_{ij} \approx -\frac{\ln(M_{\text{GUT}}/M_R)}{16\pi^2}(6m_0^2 + 2A_0^2)(Y_\nu Y_\nu^\dagger)_{ij}. \quad (5.5)$$

Here, m_0 is the universal scalar mass at the GUT scale, the trilinear coupling is $A_\nu = A_0 Y_\nu$ and $i \neq j$. The class of models we are studying, see eq. (3.2), has a neutrino Yukawa matrix of the approximate form,

$$Y_\nu \sim \begin{pmatrix} 0 & 0 & 0 \\ 0 & 0 & 1 \\ 0 & 0 & 1 \end{pmatrix}. \quad (5.6)$$

In such a model eq. (5.5) leads to sizable off-diagonal components of the slepton mass squared matrix. Through loops involving sleptons this flavour violation can be fed into the charged leptons. Hence, as in section 4.2, we can write effective vertices f

and g after heavy sparticles are integrated out of the lagrangian so that,

$$\mathcal{L}_{eff} = -\bar{e}_R^{(0)} \left[Y_e^{(0)diag\,\dagger} H_d^0 + f^\dagger H_d^0 + g^\dagger H_u^{0\,*} \right] e_L^{(0)} + h.c.. \tag{5.7}$$

There are also mass term contributions of the same form but with the Higgs fields replaced by their VEVs.

Following the logic of section 4.2 we see that at tree-level $f = g = 0$ and the Yukawa couplings and mass matrix for the charged leptons can be simultaneously diagonalised. At one-loop level f and g are to be computed and it follows that the one-loop 3-pt couplings and mass matrices are no longer simultaneously diagonalisable. The cause of this is the term, $\bar{e}_R^{(0)} g^\dagger H_u^{0\,*} e_L^{(0)}$, not present at tree-level. Fig. (5.1) shows the dominant contributions to the effective vertex g. The flavour changing part of the

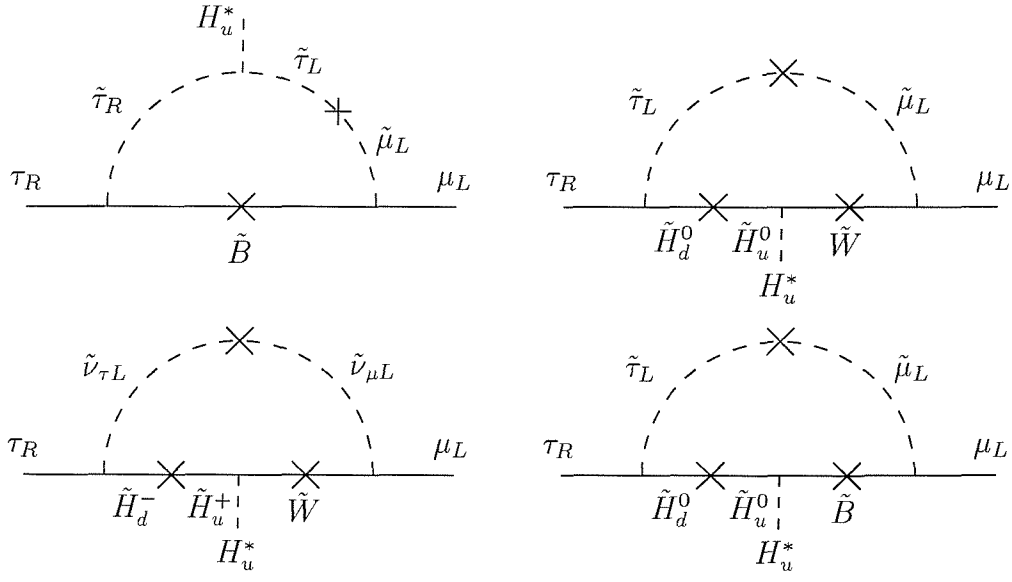

Figure 5.1: Diagrams that contribute to the coupling $\tau_R \mu_L H_u^*$. The crosses on the internal slepton lines represents mass insertions of off-diagonal components of $\Delta m_{\tilde{L}}^2$.

lagrangian therefore takes the form,

$$\mathcal{L}_{LFV} = -\bar{e}^{(1)}_{Ri}\left[V^{e\,(1)}_{R} g^{\dagger}\left(H^{0*}_{u} - \frac{v_u}{v_d}H^{0}_{d}\right)V^{e\,(1)\,\dagger}_{L}\right]_{ij} e^{(1)}_{Lj} + h.c., \tag{5.8}$$

with,

$$H^{0*}_{u} - \frac{v_u}{v_d}H^{0}_{d} = \frac{1}{\sqrt{2}}\frac{1}{c_\beta}\left[H^0 s_{\alpha-\beta} + h^0 c_{\alpha-\beta} - i\,A^0\right]. \tag{5.9}$$

Here the matrices $V^{e\,(1)}_{L,R}$ rotate the fields from tree-level mass eigenstates $e^{(0)}_{L,R}$ to the one-loop mass eigenstates, $e^{(1)}_{L,R} = V^{e\,(1)}_{L,R}\, e^{(0)}_{L,R}$. As for the down quarks of the previous chapter we can relate the matrix g, at leading order in $\tan\beta$, to the finite non-logarithmic corrections to the charged lepton mass matrix, $g_{ij} = (\delta m_e^{\text{finite}})_{ij}/v_u$.

We can make use of the LFV lagrangian term of eq. (5.8) to study the Higgs mediated contributions to the process $\tau \to 3\mu$. The dominant Higgs contributions will come from the penguin diagram shown in fig. (5.2a). There is of course a contribution from the photon penguin which can be related to the branching ratio of $\tau \to \mu\gamma$ as [57],

$$\frac{\text{Br}(\tau \to 3\mu)_\gamma}{\text{Br}(\tau \to \mu\gamma)} \approx 0.003. \tag{5.10}$$

This relation is model independent and so it is possible for us to apply a bound of $\text{Br}(\tau \to 3\mu)_\gamma < 3.3\times10^{-9}$ on the photon penguin contribution from the present bound of $\text{Br}(\tau \to \mu\gamma) < 1.1 \times 10^{-6}$ [3]. The present experimental bound of $\text{Br}(\tau \to 3\mu) < 1.9 \times 10^{-6}$ [3] is at present far from this level, but in the future any measurements that significantly deviate from this relation, eq. (5.10), would be a clear signal that additional contributions, such as Higgs mediation, are present.

In the MSSM with large $\tan\beta$ the dominant contribution to the branching ratio of

$\tau \to 3\mu$ turns out to be,

$$\mathrm{Br}(\tau \to 3\mu) = \frac{\tau_\tau}{4096\pi^3} m_\tau^5 \left(\frac{(\delta m_e)_{23}}{v_u}\frac{\lambda_\mu}{2c_\beta}\right)^2 \left[\left(\frac{c_\alpha s_{\alpha-\beta}}{M^2_{H^0}} - \frac{s_\alpha c_{\alpha-\beta}}{M^2_{h^0}}\right)^2 + \left(\frac{s_\beta}{M^2_{A^0}}\right)^2\right] . \quad (5.11)$$

Here τ_{tau} is the lifetime of the tau lepton and λ_μ is the Yukawa coupling of the muon. It has also been noted [58] that the related process $\tau \to \mu\eta$ would in fact yield a larger branching ratio. The enhancement of this process comes from a factor of 3 for colour and a factor of $(m_s/m_\mu)^2$ for the Yukawa coupling. In addition to this the cross diagram in the muon case lowers the rate by a factor 3/2, hence the overall enhancement is by $\frac{9m_s^2}{2m_\mu^2} \sim 10$. The present experimental bound is given as $\mathrm{Br}(\tau \to \mu\eta) < 9.6 \times 10^{-6}$ [3] and so it is clearly more constraining than $\tau \to 3\mu$.

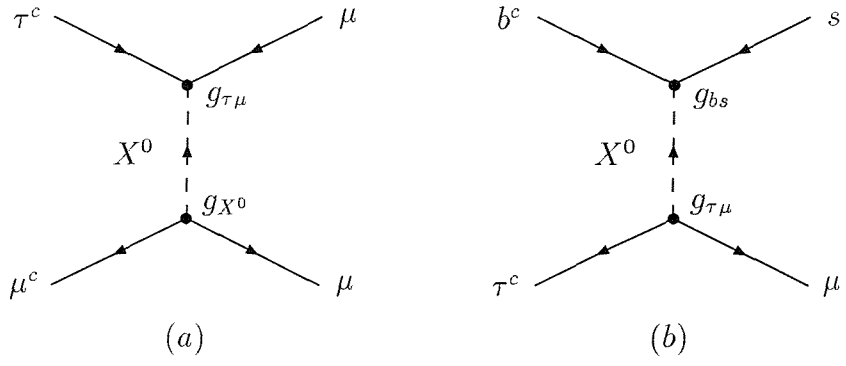

Figure 5.2: Higgs Penguin contributions to the processes $(a)\,\tau \to 3\mu$ and $(b)B_s \to \tau\mu$. The effective vertices g_{bs} and $g_{\tau\mu}$ are generated from loop involving SUSY partners which are then integrated out. The mediating X^0 stands for neutral Higgs mass eigenstates, h^0, H^0, A^0.

The lepton flavour violating Higgs coupling discussed above can also be combined with the quark flavour charging coupling studied in the previous chapter. In this way we can also study the LFV and FCNC process $B_s \to \tau\mu$. In the MSSM with large $\tan\beta$ the dominant Higgs contribution will again come from the penguin diagram mediated by the Higgs as shown in fig. (5.2b). The branching ratio may be written

as,

$$\mathrm{Br}(B_s \to \tau^+\mu^-) = \frac{\tau_{B_s}}{256\pi}\frac{(\delta m_b)^2_{23}}{v_u^2}\frac{(\delta m_e)^2_{23}}{v_u^2}\frac{1}{c_\beta^4} f^2_{B_s}\frac{M_B^5}{m_b^2}$$
$$\times\left[\frac{s^2_{\alpha-\beta}}{M^2_{H^0}} + \frac{c^2_{\alpha-\beta}}{M^2_{h^0}} + \frac{1}{M^2_{A^0}}\right]^2 (1-x_\mu-x_\tau)\sqrt{1-2(x_\tau+x_\mu)+(x_\tau-x_\mu)^2}. \quad (5.12)$$

Here $x_i = (m_i/M_{B_s})^2$. We have concentrated here on the final state $\tau^+\mu^-$ because the contribution for $\tau^-\mu^+$ goes like, $\left[\frac{s^2_{\alpha-\beta}}{M^2_{H^0}} + \frac{c^2_{\alpha-\beta}}{M^2_{h^0}} - \frac{1}{M^2_{A^0}}\right]^2$, and approximately vanishes at large $\tan\beta$. It is worth noting that at present there are no experimental bounds set on the process $B_s \to \tau\mu$ and only a weak bound set on the related process $\mathrm{Br}(B_d \to \mu\tau) < 8.3 \times 10^{-4}$.

We shall now make use of the best fit points obtained from the global χ^2 analysis of an SO(10)-like model presented in chapter 3. In particular we choose to study the best fit points of minimum A. We make this choice because the Higgs spectrum, see fig. (3.9), of minimum B is greater than 500 GeV whilst that of minimum A is rather lighter. As the branching ratio scales like $1/M_A^4$ minimum A will yield much more promising results.

5.3 Results and Discussion

Our numerical results for the branching ratio $B_s \to \mu\mu$ and $\tau \to 3\mu$ are presented in fig. (5.3)-(5.7) in the form of contour and scatter plots. The contour plot, fig. (5.3) is plotted in the m_F, $M_{1/2}$ plane (here m_F is equivalent to the standard universal scalar mass m_0) and with two values of $\mu = 120$ GeV(left panels) and $\mu = 300$ GeV(right panels). The scatter plots of fig. (5.4)-(5.7) are presented to display the correlation of various decay processes. These too are presented for the two different values of μ. The points are grouped in terms of their χ^2 values, the best fit point is also clearly marked.

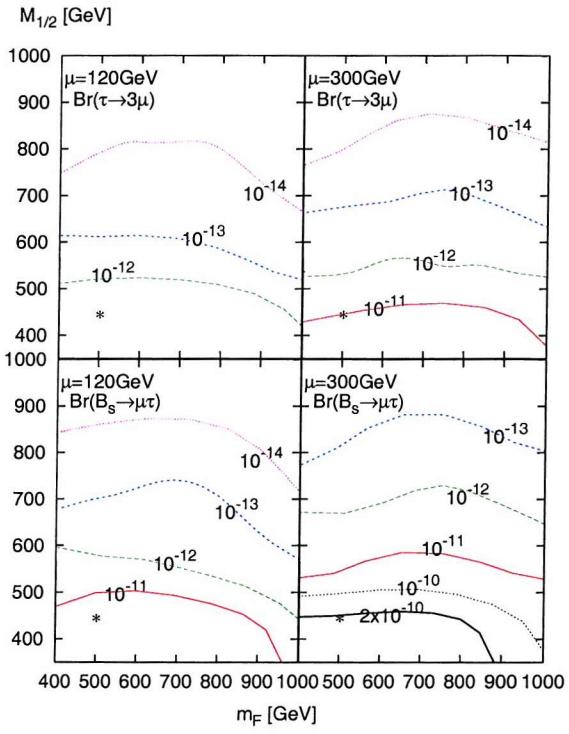

Figure 5.3: Contours of the Higgs-mediated contribution to the processes $Br(\tau \to 3\mu)$ and $Br(B_s \to \tau\mu)$ in the $m_F - M_{1/2}$ plane with $\mu = 120$ GeV(left panels) and 300 GeV(right panels). The $\star$ marks the best fit point.

Fig. (5.3) contains contour plots of branching ratios for both $B_s \to \tau\mu$(lower panels) and $\tau \to 3\mu$(upper panels). The $\tau \to 3\mu$ contours are some 5 orders of magnitude below the present experimental bound. We find that $\mathrm{Br}(\tau \to 3\mu) < 2 \times 10^{-11}$. This is clearly disappointing as other authors [55] reported a much larger prediction of $\mathrm{Br}(\tau \to 3\mu) \sim 10^{-7}$. The $B_s \to \tau\mu$ panels of fig. (5.3) fair no better with $\mathrm{Br}(B_s \to \tau\mu) < 2 \times 10^{-10}$. Our results for both processes are in much better agreement with those of [56] who also predict small branching ratios for both processes. Ref. [56] calculates the branching ratio for $\tau \to 3\mu$ following the same procedure as in ref. [55] and so the discrepancy between these two results is not yet understood.

Scatter plots for the branching ratios of $B_s \to \tau\mu$ and $\tau \to 3\mu$ against the Pseu-

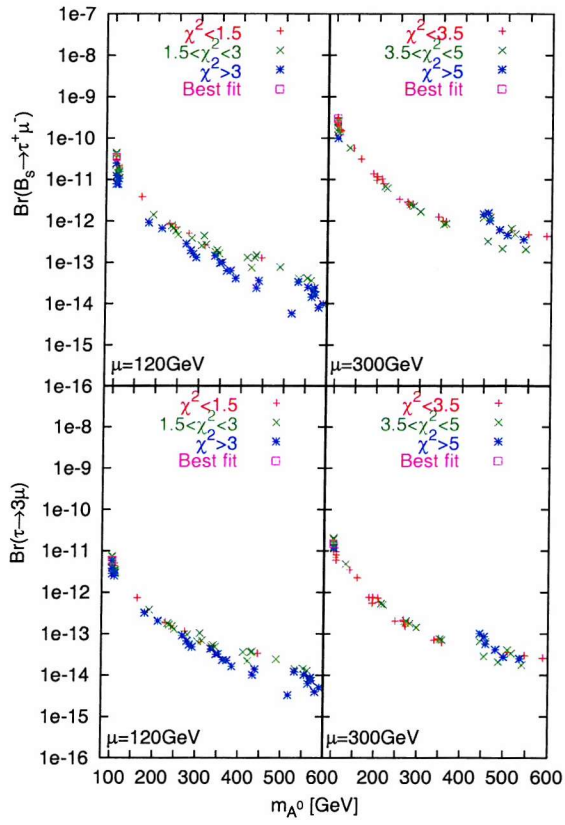

Figure 5.4: Scatter plots of Higgs-mediated contribution to the processes $Br(\tau \to 3\mu)$(lower panels) and $Br(B_s \to \tau\mu)$(upper panels) against the Pseudoscalar Higgs mass m_{A^0} for $\mu = 120$ GeV(left panels) and 300 GeV(right panels). The points are colour coded depending on their χ^2 values with the best fit point also highlighted.

doscalar Higgs mass are shown in fig. (5.4). Again each process is shown for the two values of μ. These plots show very nicely the strong dependence upon the Higgs spectrum. It is clear that lighter mediating Higgs bosons lead to a larger branching ratio in each case.

It is interesting to study the correlations of these LFV processes with one another and other related processes such as $\tau \to \mu\gamma$ and $B_s \to \mu\mu$. Fig. (5.5) contains a scatter plot of $\tau \to 3\mu$ against $B_s \to \tau\mu$ again with $\mu = 120$ GeV and $\mu = 300$ GeV. These

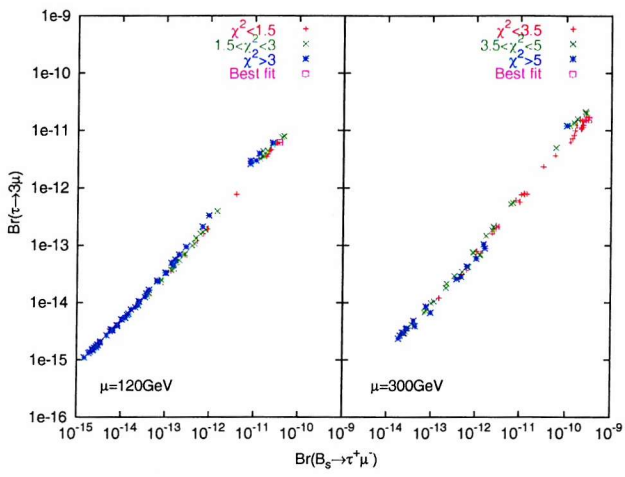

Figure 5.5: Scatter plot of Higgs-mediated contribution to the processes $Br(\tau \to 3\mu)$ against $Br(B_s \to \tau\mu)$ for $\mu = 120$ GeV(left panels) and 300 GeV(right panels). The points are colour coded depending on their χ^2 values with the best fit point also highlighted.

two LFV Higgs-mediated contributions are clearly strongly correlated. It is useful to note that our global analysis prefers the largest attained branching ratios.

There is expected to be a strong correlation between the processes $B_s \to \tau\mu$, $\tau \to 3\mu$ and $B_s \to \mu\mu$, $\tau \to \mu\gamma$. With this in mind fig. (5.6) presents scatter plots of $B_s \to \tau\mu$ and $\tau \to 3\mu$ against $B_s \to \mu\mu$. These Higgs-mediated contributions are all strongly correlated and this is shown very well in this figure with large $\mathrm{Br}(B_s \to \mu\mu)$ coinciding with large branching ratios for $B_s \to \tau\mu$ and $\tau \to 3\mu$. The scatter plots in fig. (5.7) are plotted against $\mathrm{Br}(\tau \to \mu\gamma)$. The best fit points of our model predict $\mathrm{Br}(\tau \to \mu\gamma) \sim 10^{-8} - 10^{-7}$, see fig. (3.5), which through eq. (5.10) can be related to a photon penguin contribution $\mathrm{Br}(\tau \to 3\mu)_\gamma \sim 10^{-11} - 10^{-10}$ and it is clear therefore that this will dominate over the Higgs-mediated contribution in our model. The correlation shown in fig. (5.7) appears to be weaker than that shown in fig. (5.6) for $B_s \to \mu\mu$. This implies that there is a stronger dependence on the Higgs mass than on the LFV coupling.

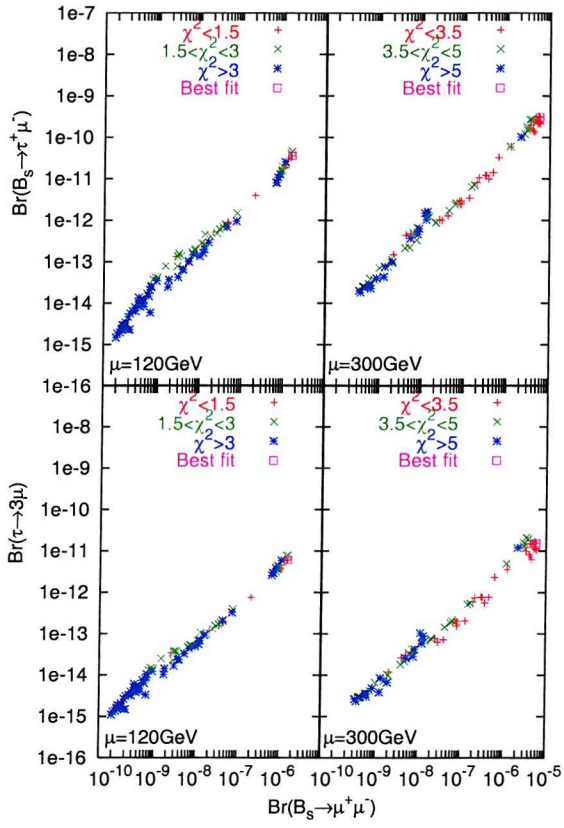

Figure 5.6: Scatter plots of Higgs-mediated contribution to the processes $Br(\tau \rightarrow 3\mu)$(lower panels) and $Br(B_s \rightarrow \tau\mu)$(upper panels) against $Br(B_s \rightarrow \tau\mu)$ for $\mu = 120$ GeV(left panels) and 300 GeV(right panels). The points are colour coded depending on their χ^2 values with the best fit point also highlighted.

5.4 Conclusion

The observation of neutrino oscillations and therefore flavour violation in the lepton sector has motivated the ongoing study of rare flavour violating processes involving charged lepton. In the past much attention has been given to the well known processes $\tau \rightarrow \mu\gamma$ and $\mu \rightarrow e\gamma$. More recently it has been suggested that in addition Higgs-mediated contributions to $\tau \rightarrow 3\mu$ and $B_s \rightarrow \tau\mu$ could also be of interest in SUSY models. Higgs-mediation has been shown to give potentially large contributions to

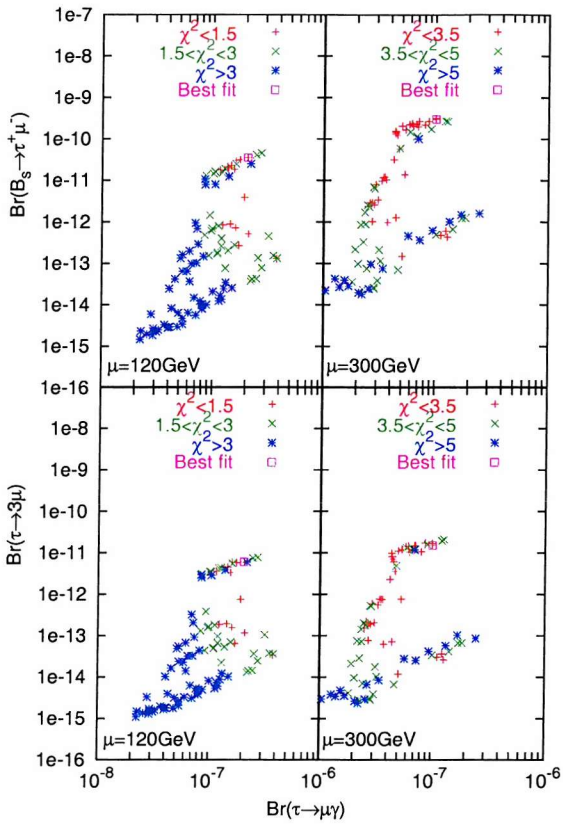

Figure 5.7: Scatter plots of Higgs-mediated contribution to the processes $Br(\tau \to 3\mu)$(lower panels) and $Br(B_s \to \tau\mu)$(upper panels) against $Br(\tau \to \mu\gamma)$ for $\mu = 120$ GeV(left panels) and 300 GeV(right panels). The points are colour coded depending on their χ^2 values with the best fit point also highlighted.

flavour changing neutral currents such as $B_{s,d} \to \mu\mu$. In this chapter the work of chapter 3 has been extended to study the lepton flavour violating decays $B_s \to \tau\mu$ and $\tau \to 3\mu$. We have found that our predictions for these branching ratios are disappointingly small with $\mathrm{Br}(\tau \to 3\mu) \sim 10^{-15} - 10^{-11}$ and $\mathrm{Br}(B_s \to \tau\mu) \sim 10^{-15} - 10^{-10}$. The correlation of such processes to $B_s \to \mu\mu$ was shown to be very strong, but the dependence on $\tau \to \mu\gamma$ showed a much weaker correlation.

The predictions made in the previous chapter for the Higgs-mediated contribution

to $B_s \to \mu\mu$ should therefore be highlighted. We found that the branching ratio for this process is well within reach at future colliders. In contrast the conclusions of the present chapter are far less promising, $(B_s \to \tau\mu)$ is clearly suffering from heavy suppression from the additional loop and small LFV.

In conclusion we have made use of the best fit points found in the global analysis of the SO(10)-like model presented in chapter 3 to make predictions for the rare processes $\tau \to \mu\gamma$ and $(B_s \to \tau\mu)$. We found that unlike $B_s \to \mu\mu$ of the previous chapter the branching ratios are highly suppressed. Therefore greater emphasis should be put on the results of chapter 4.

Chapter 6

Overview and Conclusions

The aim of the work in this thesis has been to study a complete model of fermion masses and mixing and the low-energy phenomenological predictions that can be deduced. To this end we began in chapter 3 by performing a complete global phenomenological analysis of a realistic string-inspired model based on the supersymmetric Pati-Salam $SU(4) \times SU(2)_L \times SU(2)_R$ gauge group supplemented by a $U(1)$ family symmetry. The results of our global analysis determined that there were two χ^2 minima with interesting phenomenological differences. Notably minimum B has $Br(\tau \to \mu\gamma)$ near the present limit and a heavy pseudoscalar Higgs m_{A^0}, while minimum A has $Br(\tau \to \mu\gamma)$ well below the present bound but a light pseudoscalar Higgs m_{A^0}. $\sin^2 2\theta_{13}$ predictions of both minima are in the range $10^{-5} - 0.1$. It is important to notice that improved limits on $Br(\tau \to \mu\gamma)$ could begin to rule out minimum B.

The property of exact Yukawa unification was relaxed throughout the analysis and it was found that a deviation of 20-35% for the bottom Yukawa coupling and 0-10% for the top Yukawa coupling are required for a good fit to be obtained.

Questions of the effects of future direct Higgs searches and a change to the present muon $g-2$ discrepancy were addressed. We found that our best fit points for minimum

A, with light Higgs masses, can accommodate a lower bound on Higgs masses up to about 120 GeV. Also we found that in the very light Higgs mass region the coupling of the lighter CP even Higgs state to the Z boson is suppressed, leaving the heavier of the two CP even states acting as the standard model like Higgs.

Realising that the light Higgs spectrum of minimum A may lead to interesting phenomenological consequences, in chapter 4 we examined the potentially very promising signal $B_s \to \mu^+\mu^-$. We studied this process using the best fits from minimum A found in the global analysis of the Pati-Salam model of chapter 3. The results of chapter 4 go beyond minimal flavour violation to include contributions not depending on V_{ts} which have previously been neglected. Our results show that the absolute best fits predict a $B_s \to \mu^+\mu^-$ signal at the borderline of the present limits and hence the ongoing search at the TeVatron will start having an impact on the global analysis of this class of SUSY models. We also studied the prospects of signals in other channels such as $B_{d,s} \to \ell^+\ell^-$. Correlations of $B_s \to \mu^+\mu^-$ with $b \to s\gamma$ and the CP-odd Higgs mass were found to be particularly strong. An improved limit for $\mathrm{Br}(B_s \to \mu\mu)$ of around 10^{-7} would be very restricting to the parameter space of our minimum A solution. An experimental limit in this region could probe Higgs masses into the range, $m_{A^0} = 150 - 300$ GeV. The most exciting conclusion from the work presented in chapter 4 is that a signal of $B_s \to \mu^+\mu^-$ at the 10^{-7} level is quite plausibly expected in SUSY $SO(10)$-like models.

Chapter 5 extends the work of chapters 3 and 4 to study the lepton flavour violating decays $\tau \to 3\mu$ and $B_s \to \tau\mu$. It was recently suggestioned that Higgs-mediated contributions to these processes could also be of interest in SUSY models. However our disappointing results don't add weight to this claim with branching ratios at the level $10^{-11} - 10^{-10}$. In fact we have found that it is the photon penguin which dominates and not the Higgs-mediation for the process $\tau \to 3\mu$. The correlation of these rare decays to the related processes $\tau \to \mu\gamma$, $B_s \to \mu\mu$ were studied and

showed a stronger dependence on the Higgs spectrum than on the lepton flavour violating coupling. The disappointing results in this chapter should further highlight the exciting prospects for indirect SUSY discovery found in chapter 4.

The origin of fermion mass and mixing is a great puzzle and has been for a number of years. In recent times low-energy experimental discovery has given vital clues to the solution of this problem, yet it could be argued that these clues have also made the situation even more interesting. It is extremely important that complete models are constructed that reproduce all present experimental observations so that they enable accurate predictions to be made and for the theory parameter space to be thoroughly explored. In this way theorists are able to begin to find the answers to such fundamental questions. The work in this thesis contributes in part to this grander goal.

Appendix A

Grassmann Numbers

Let θ be a 2-component *Grassmann* Number, that is a numbers which anti-commutes,

$$\begin{aligned} &\theta_\alpha, \quad \alpha = 1,2 \qquad \text{and} \qquad \bar{\theta}_{\dot{\beta}}, \quad \dot{\beta} = 1,2 \\ &\{\theta_\alpha, \theta_\beta\} = 0, \quad \{\bar{\theta}_{\dot{\alpha}}, \bar{\theta}_{\dot{\beta}}\} = 0, \quad \{\theta_\alpha, \bar{\theta}_{\dot{\beta}}\} = 0 \\ &. \end{aligned} \tag{A.1}$$

It is now important for the operations of differentiation and integration with respect to Grassmann numbers to be defined.

Grassmann derivative

Let us define the derivative with respect to a Grassmann number a_i as,

$$\frac{\partial a_i}{\partial a_j} = \delta_i^j, \quad \forall\, i,j = 1,\ldots,N. \tag{A.2}$$

It is important to remember that derivatives with respect to Grassmann numbers must also anti-commute,

$$\left\{\frac{\partial}{\partial a_i}, \frac{\partial}{\partial a_j}\right\} = 0. \tag{A.3}$$

To simplify notation we write the derivatives as,

$$\begin{aligned} \partial_\alpha &= \frac{\partial}{\partial\theta^\alpha} & \partial^\alpha &= \frac{\partial}{\partial\theta_\alpha} \\ \bar{\partial}_{\dot{\alpha}} &= \frac{\partial}{\partial\bar{\theta}^{\dot{\alpha}}} & \bar{\partial}^{\dot{\alpha}} &= \frac{\partial}{\partial\bar{\theta}_{\dot{\alpha}}}. \end{aligned} \tag{A.4}$$

From eq. (A.2) we can write the action of the derivative in terms of our new notation as,

$$\begin{aligned} \partial_\alpha\theta^\beta &= \delta^\beta_\alpha & \partial^\alpha\theta_\beta &= \delta^\alpha_\beta \\ \bar{\partial}_{\dot{\alpha}}\bar{\theta}^{\dot{\beta}} &= \delta^{\dot{\beta}}_{\dot{\alpha}} & \bar{\partial}^{\dot{\alpha}}\bar{\theta}_{\dot{\beta}} &= \delta^{\dot{\alpha}}_{\dot{\beta}} \\ \partial_\alpha\theta_\beta &= -\epsilon_{\alpha\beta} & \bar{\partial}_{\dot{\alpha}}\bar{\theta}_{\dot{\beta}} &= -\epsilon_{\dot{\alpha}\dot{\beta}}. \end{aligned} \tag{A.5}$$

Here the tensor $\epsilon^{\alpha\beta}$ is as defined in eq. (B.2) of appendix B Using the identities in eq. (A.5) it is a straightforward exercise to derive the conventions for raising and lowering the indices of the Grassmann derivatives,

$$\begin{aligned} \epsilon^{\alpha\beta}\partial_\beta &= -\partial^\alpha & \epsilon_{\alpha\beta}\partial^\beta &= -\partial_\alpha \\ \epsilon^{\dot{\alpha}\dot{\beta}}\bar{\partial}_{\dot{\beta}} &= -\bar{\partial}^{\dot{\alpha}} & \epsilon_{\dot{\alpha}\dot{\beta}}\bar{\partial}^{\dot{\beta}} &= -\bar{\partial}_{\dot{\alpha}}. \end{aligned} \tag{A.6}$$

The anti-commutation of Grassmann variables, as in eq. (A.3), implies that,

$$\{\partial_\alpha,\, \partial_\beta\} = 0 \qquad \left\{\bar{\partial}_{\dot{\alpha}},\, \bar{\partial}_{\dot{\beta}}\right\} = 0. \tag{A.7}$$

The Grassmann Integral

Let us define the Grassmann integral as a functional,

$$I\,[f] = \int f(a)\, da. \tag{A.8}$$

Here f is a function of a single Grassmann number a. Unlike the standard integral we cannot associate this with the area under the curve $f(a)$ and nor can any meaning

be attached to the upper and lower limited of the integral. In addition we demand that the integral be translational invariant,

$$\int f(a+b)\,da = \int f(a)\,da, \tag{A.9}$$

and that it be linear,

$$\int (\alpha f(a) + \beta g(a))\,da = \alpha \int f(a)\,da + \beta \int g(a)\,da. \tag{A.10}$$

We can Taylor expand the function f in a series with only two terms

$$f(a) = f(0) + a.f' \qquad \text{since } a^2 = 0. \tag{A.11}$$

Here if we define $f(a)$ as a normal number then so must $f(0)$, but a and f' are Grassmann numbers. Then we can rewrite eq. (A.8) as,

$$\begin{aligned} I[f] &= f(0)\int 1\,.\,da + \left(\int a\,da\right).f' \\ &= (f(0) + f'b)\int 1\,.\,da + \left(\int a\,da\right).f'. \end{aligned} \tag{A.12}$$

Where in the last line of eq. (A.12) we have used the translational invariance of the integral to shift $a \to a + b$. It is clear from eq. (A.12) that we must define,

$$\int 1\,.\,da = 0 \quad \text{and} \quad \int a\,da = 1. \tag{A.13}$$

Hence the action of Grassmann integration and differentiation have the same effect.

$$\frac{\partial}{\partial a} f(a) = \int f(a)\,da = f'. \tag{A.14}$$

These results can be extended from this 1-dimensional algebra to an n-dimensional

Grassmann algebra,

$$\begin{aligned} \{\theta_i,\, \theta_j\} = 0 \quad &, \quad \{d\theta_i,\, d\theta_j\} = 0 \\ \int d\theta_i = 0 \quad &, \quad \int d\theta_i\, \theta_j = \delta_{ij}. \end{aligned} \tag{A.15}$$

It will be useful to define the multidimensional integrals,

$$\begin{gathered} \int d^2\theta\ \theta^2 = 1, \quad \int d^2\bar{\theta}\ \bar{\theta}^2 = 1 \\ \int d^2\theta\, d^2\bar{\theta}\ \ \theta^2\, \bar{\theta}^2 = 1. \end{gathered} \tag{A.16}$$

The volume elements are therefore defined as,

$$\begin{aligned} d^2\theta &\equiv -\tfrac{1}{4} d\theta^\alpha d\theta^\beta \epsilon_{\alpha\beta} \\ d^2\bar{\theta} &\equiv -\tfrac{1}{4} d\bar{\theta}_{\dot{\alpha}} d\bar{\theta}_{\dot{\beta}} \epsilon^{\dot{\alpha}\dot{\beta}}. \end{aligned} \tag{A.17}$$

Appendix B

Weyl and Dirac Spinors

B.1 2 component Weyl spinor notation

Throughout this thesis we assume the space-time metric, $\eta_{\mu\nu} = \text{diag}(1, -1, -1, -1)$. If we define a 2×2 matrix M with determinant 1, i.e. $M \in SL(2, C)$. Then the matrices M and M^* provide inequivalent representations of $SL(2, C)$. These matrices can be used to represent the action of the Lorentz group on two-component Weyl spinors as follows,

$$\begin{array}{l|l} \psi'_\alpha = M_\alpha^\beta \psi_\beta & \bar{\psi}'_{\dot{\alpha}} = (M^*)_{\dot{\alpha}}^{\dot{\beta}} \bar{\psi}_{\dot{\beta}} \\ \psi'^\alpha = (M^{-1})_\beta^\alpha \psi^\beta & \bar{\psi}'^{\dot{\alpha}} = (M^{*-1})_{\dot{\beta}}^{\dot{\alpha}} \bar{\psi}^{\dot{\beta}}. \end{array} \tag{B.1}$$

Here, α, $\beta = 1, 2$, and, $\dot{\alpha}$, $\dot{\beta} = 1, 2$. The dotted indices and undotted indices are used to remind us that ψ and $\bar{\psi} = \psi^\dagger$ [1] transform in different representations of $SL(2, C)$, $(0, \frac{1}{2})$ and $(\frac{1}{2}, 0)$ respectively.

[1] This definition is sometimes written as $\dot{\psi} = \psi^\dagger$ in other sources.

It is useful to define the tensors $\epsilon^{\alpha\beta}$ and $\epsilon^{\dot{\alpha}\dot{\beta}}$

$$\epsilon^{\alpha\beta} = \epsilon^{\dot{\alpha}\dot{\beta}} = i\sigma^2 = \begin{pmatrix} 0 & 1 \\ -1 & 0 \end{pmatrix}, \qquad \epsilon_{\alpha\beta} = \epsilon_{\dot{\alpha}\dot{\beta}} = -i\sigma^2 = \begin{pmatrix} 0 & -1 \\ 1 & 0 \end{pmatrix}, \tag{B.2}$$

which are used to raise and lower indices as follows:

$$\psi^\alpha = \epsilon^{\alpha\beta}\psi_\beta \ , \quad \psi_\alpha = \epsilon_{\alpha\beta}\psi^\beta \ , \quad \bar{\psi}^{\dot{\alpha}} = \epsilon^{\dot{\alpha}\dot{\beta}}\bar{\psi}_{\dot{\beta}} \ , \quad \bar{\psi}_{\dot{\alpha}} = \epsilon_{\dot{\alpha}\dot{\beta}}\bar{\psi}^{\dot{\beta}} \ . \tag{B.3}$$

The tensor $\epsilon^{\alpha\beta}$ is invariant under Lorentz transformations, $\epsilon_{\alpha\beta} = M_\alpha^\gamma M_\beta^\delta \epsilon_{\gamma\delta}$. The Pauli matrices are defined as,

$$\begin{aligned} \sigma^0 = \bar{\sigma}^0 = \begin{pmatrix} 1 & 0 \\ 0 & 1 \end{pmatrix} \quad \sigma^1 = -\bar{\sigma}^1 = \begin{pmatrix} 0 & 1 \\ 1 & 0 \end{pmatrix} \\ \sigma^2 = -\bar{\sigma}^2 = \begin{pmatrix} 0 & -i \\ i & 0 \end{pmatrix} \quad \sigma^3 = -\bar{\sigma}^3 = \begin{pmatrix} 1 & 0 \\ 0 & -1 \end{pmatrix}. \end{aligned} \tag{B.4}$$

These matrices form a basis for 2×2 complex matrices. The spinor index structure for the Pauli matrices is, $\sigma^\mu_{\alpha\dot{\beta}} = (\mathbf{1}, \sigma_i)$. Raising the indices using the ϵ tensors yields

$$(\bar{\sigma}^\mu)^{\dot{\alpha}\alpha} = \epsilon^{\dot{\alpha}\dot{\beta}}\epsilon^{\alpha\beta}(\sigma^\mu)_{\beta\dot{\beta}} = (\mathbf{1}, -\sigma_i)^{\dot{\alpha}\alpha}. \tag{B.5}$$

When dealing with expressions involving more than one spinor it is important to remember that spinors anti-commute. So for 2-component spinors we have, $\psi_1\chi_2 = -\chi_2\psi_1$ and $\psi_1\bar{\chi}_2 = -\bar{\chi}_2\psi_1$ etc. The products $\psi\chi$ and $\bar{\psi}\bar{\chi}$ are defined as,

$$\begin{aligned} \psi\chi \equiv \psi^\alpha\chi_\alpha = \epsilon^{\alpha\beta}\psi_\beta\chi_\alpha = -\epsilon^{\alpha\beta}\psi_\alpha\chi_\beta = -\psi_\alpha\chi^\alpha = \chi^\alpha\psi_\alpha \equiv \chi\psi \\ (\chi\psi)^\dagger = \bar{\psi}\bar{\chi} \equiv \bar{\psi}_{\dot{\alpha}}\bar{\chi}^{\dot{\alpha}} = \ldots = \bar{\chi}_{\dot{\alpha}}\bar{\psi}^{\dot{\alpha}} \equiv \bar{\chi}\bar{\psi}, \end{aligned} \tag{B.6}$$

are Lorentz invariant products. Note that by convention undotted indices are always contracted from upper left to lower right, while dotted indices are always contracted

from lower left to upper right. Notice however that this rule does not apply when rising or lowering spinor indices with the ϵ-tensor. With this rule we also have

$$\psi\sigma^{\mu}\bar{\chi} = \psi^{\alpha}(\sigma^{\mu})_{\alpha\dot{\beta}}\bar{\chi}^{\dot{\beta}} \quad , \quad \bar{\psi}\bar{\sigma}^{\mu}\chi = \bar{\psi}_{\dot{\alpha}}(\bar{\sigma}^{\mu})^{\dot{\alpha}\beta}\chi_{\beta}. \tag{B.7}$$

One can then prove a certain amount of useful identities which we summarise here:

$$\begin{aligned} \chi\sigma^{\mu}\bar{\psi} &= -\bar{\psi}\bar{\sigma}^{\mu}\chi \quad , \quad \chi\sigma^{\mu}\bar{\sigma}^{\nu}\psi = \psi\sigma^{\nu}\bar{\sigma}^{\mu}\chi \\ (\chi\sigma^{\mu}\bar{\psi})^{\dagger} &= \psi\sigma^{\mu}\bar{\chi} \quad , \quad (\chi\sigma^{\mu}\bar{\sigma}^{\nu}\psi)^{\dagger} = \bar{\psi}\bar{\sigma}^{\nu}\sigma^{\mu}\bar{\chi} \\ \psi\chi = \chi\psi \quad , \quad \bar{\psi}\bar{\chi} &= \bar{\chi}\bar{\psi} \quad , \quad (\psi\chi)^{\dagger} = \bar{\psi}\bar{\chi} \end{aligned} \tag{B.8}$$

.

After some work, it is also possible to prove the identities,

$$\begin{aligned} (\theta\phi)(\theta\psi) = -\tfrac{1}{2}(\theta\theta)(\phi\psi), \quad (\bar{\theta}\bar{\phi})(\bar{\theta}\bar{\psi}) &= -\tfrac{1}{2}(\bar{\theta}\bar{\theta})(\bar{\phi}\bar{\psi}) \\ (\theta\sigma^{\mu}\bar{\theta})(\theta\sigma^{\nu}\bar{\theta}) &= \tfrac{1}{2}\eta^{\mu\nu}(\theta\theta)(\bar{\theta}\bar{\theta}) \\ \theta^{\alpha}\theta^{\beta} = -\tfrac{1}{2}\epsilon^{\alpha\beta}\theta\theta, \qquad & \bar{\theta}^{\dot{\alpha}}\bar{\theta}^{\dot{\beta}} = \tfrac{1}{2}\epsilon^{\dot{\alpha}\dot{\beta}}\bar{\theta}\bar{\theta} \\ \theta_{\alpha}\theta_{\beta} = \tfrac{1}{2}\epsilon_{\alpha\beta}\theta\theta, \qquad & \bar{\theta}_{\dot{\alpha}}\bar{\theta}_{\dot{\beta}} = -\tfrac{1}{2}\epsilon_{\dot{\alpha}\dot{\beta}}\bar{\theta}\bar{\theta}. \end{aligned} \tag{B.9}$$

In the Weyl representation it is convenient to define the 4×4 gamma matrices as,

$$\gamma_{\mu} = \begin{pmatrix} 0 & \sigma_{\mu} \\ \bar{\sigma}_{\mu} & 0 \end{pmatrix}, \quad \gamma^{5} = i\gamma^{0}\gamma^{1}\gamma^{2}\gamma^{3} = \begin{pmatrix} -\mathbf{1} & 0 \\ 0 & \mathbf{1} \end{pmatrix}. \tag{B.10}$$

Therefore we can construct a four-component Dirac spinor from a two-component undotted and a two-component dotted spinor, $\psi^{D} = \begin{pmatrix} \psi_{\alpha} \\ \bar{\chi}^{\dot{\alpha}} \end{pmatrix}$ The Dirac spinor ψ_{D} therefore transforms as the reducible representation $(\frac{1}{2}, 0) \otimes (0, \frac{1}{2})$ of the Lorentz group. A Majorana spinor can also be defined as a Dirac spinor with, $\chi = \psi$, hence, $\psi^{M} = \begin{pmatrix} \psi_{\alpha} \\ \bar{\psi}^{\dot{\alpha}} \end{pmatrix}$.

B.2 Dirac and Majorana masses

As we have just seen, it is often useful to define a 4-component Dirac spinor in terms of 2-component Weyl spinors,

$$\psi^D = \begin{pmatrix} \xi_\alpha \\ \bar{\chi}^{\dot{\alpha}} \end{pmatrix}. \tag{B.11}$$

It follows that ξ and χ are chiral projections of ψ,

$$\begin{aligned} \psi_L^D &= P_L \psi^D = (\xi_\alpha,\, 0)^{\mathrm{T}} \\ \psi_R^D &= P_R \psi^D = \left(0,\, \bar{\chi}^{\dot{\alpha}}\right)^{\mathrm{T}} \\ \bar{\psi}_L^D &= \bar{\psi}^D P_R = \left(0,\, \bar{\xi}_{\dot{\alpha}}\right) \\ \bar{\psi}_R^D &= \bar{\psi}^D P_L = \left(\chi^\alpha,\, 0\right), \end{aligned} \tag{B.12}$$

here we have defined the projection operators,

$$P_L = \frac{1}{2}\left(1 - \gamma^5\right), \quad P_R = \frac{1}{2}\left(1 + \gamma^5\right). \tag{B.13}$$

Then we see that the standard Dirac mass will connects χ and ξ,

$$\begin{aligned} \mathcal{L}_{\text{Dirac}} = -m_D \bar{\psi}^D \psi^D &= -m_D \left(\bar{\psi}_L^D \psi_R^D + \bar{\psi}_R^D \psi_L^D\right) \\ &= -m_D \left(\bar{\xi}_{\dot{\alpha}} \bar{\chi}^{\dot{\alpha}} + \chi^\alpha \xi_\alpha\right). \end{aligned} \tag{B.14}$$

Alternatively we can construct a Majorana mass term for the spinor,

$$\psi^M = \begin{pmatrix} \xi_\alpha \\ \bar{\xi}^{\dot{\alpha}} \end{pmatrix}. \tag{B.15}$$

As the upper and lower components of ψ^M carry the same degrees of freedom, ξ,

effectively the Majorana spinor has only one independent helicity state, let us define,

$$\begin{aligned}\psi_L^M &= P_L\,\psi^M = (\xi_\alpha,\,0)^{\mathrm{T}}\\ \bar{\psi}_L^M &= \bar{\psi}^M\,P_R = (0,\,\bar{\xi}_{\dot{\alpha}})\end{aligned} \tag{B.16}$$

.

Then we can construct ψ_R^M from the charge conjugate matrix, $\hat{C}$, in the Weyl representation we have,

$$\hat{C} = -i\gamma^2\gamma^0 = \begin{pmatrix} \epsilon_{\alpha\beta} & 0 \\ 0 & \epsilon^{\dot{\alpha}\dot{\beta}} \end{pmatrix}, \quad \text{with,} \quad \begin{aligned}&\hat{C} = -\hat{C}^{\mathrm{T}} = -\hat{C}^{\dagger} = -\hat{C}^{-1}\\ &\hat{C}^{-1}\gamma^\mu\hat{C} = -(\gamma^\mu)^{\mathrm{T}},\end{aligned} \tag{B.17}$$

such that,

$$\begin{aligned}\psi_R^M &= (\psi_L^M)^c = \hat{C}(\bar{\psi}_L^M)^{\mathrm{T}} = \left(0,\,\bar{\xi}^\alpha\right)^{\mathrm{T}}\\ \bar{\psi}_R^M &= (\bar{\psi}_L^M)^c = (\psi_L^M)^{\mathrm{T}}\hat{C} = (\xi^\alpha,\,0)^{\mathrm{T}}\end{aligned} \tag{B.18}$$

.

Notice that the Majorana spinor is self conjugate, $\psi^M = (\psi^M)^c$, or more precisely, $(\psi_L^M)^c = \psi_R^M$ and $(\psi_R^M)^c = \psi_L^M$. Now we can construct a Majorana mass term which connects ξ with itself,

$$\begin{aligned}\mathcal{L}_{\text{Majorana}} &= -\frac{1}{2}m_M\bar{\psi}^M\psi^M\\ &= -\frac{1}{2}m_M\left[\bar{\psi}_L^M\psi_R^M + \bar{\psi}_R^M\psi_L^M\right] &\text{(B.19)}\\ &= -\frac{1}{2}m_M\left[\bar{\xi}_{\dot{\alpha}}\bar{\xi}^{\dot{\alpha}} + \xi^\alpha\xi_\alpha\right]. &\text{(B.20)}\end{aligned}$$

The Majorana mass term of eq. (B.19) can be written in terms of the charge conjugate

fields defined in eq. (B.18) as,

$$\begin{aligned} &-\tfrac{1}{2} m_M \left[(\bar{\psi}_R^M)^c \psi_R^M + h.c. \right] \\ &\text{or} \\ &-\tfrac{1}{2} m_M \left[\bar{\psi}_L^M (\psi_L^M)^c + h.c. \right]. \end{aligned} \tag{B.21}$$

Therefore we have two possible Majorana masses written in terms of ψ_L^M and ψ_R^M. These mass terms would violate charge conservation for fermions carrying a $U(1)_{\text{em}}$ charge and also they violate fermion number by two units.

Appendix C

Sparticle mixings in the MSSM

This appendix gives details of all the tree-level contributions to the squark and slepton mass squared matrices. The mixings among the charged and neutral gauginos into the mass eigenstate Neutralinos and Charginos is then presented.

C.1 Squark and slepton mixing

Before supersymmetry is broken the fermions and their scalar partners have equal mass. This degeneracy is split by the soft SUSY breaking mass terms of eq. (2.66). There are also contributions from F-terms which give Yukawa strength interactions with the Higgs, for example,

$$-\mathcal{L} \supset \left|\frac{\partial W}{\partial \phi_i}\right|^2 = \ldots + |\tilde{U}_i Y_u^{ij} \tilde{U}_j^c - \mu H_d^0|^2 + |H_u^0 Y_u^{ij} \tilde{U}_j^c|^2 + |H_u^0 \tilde{U}_i Y_u^{ij}|^2. \qquad \text{(C.1)}$$

Similar expressions for the sleptons and down type squarks can easily be derived. Notice that there are diagonal left-left and right-right mass terms and left-right mixings. The trilinear terms $A_{u,d,e}$ also give left-right mixings, whereas the D-terms of

eq. (2.60) provide diagonal mass terms. Putting these together the squark and lepton mass matrices can be summarised as,

$$M_{\tilde{f}}^2 = \begin{pmatrix} m_{LL}^2 & m_{LR}^2 \\ m_{LR}^{2\,\dagger} & m_{RR}^2 \end{pmatrix}, \quad \text{in the basis} \quad \left\{\tilde{f},\, \tilde{f}^c\right\}, \tag{C.2}$$

with a sfermion Lagrangian mass term, $\mathcal{L} \subset -(\tilde{f}^*, \tilde{f}^{c*}) \left(M_{\tilde{f}}^2\right) \begin{pmatrix} \tilde{f} \\ \tilde{f}^c \end{pmatrix}$. Here $m_{LL,\,RR,\,LR}$ are 3×3 matrices in flavour space so that $M_{\tilde{f}}^2$ is a 6×6 matrix. The matrices $m_{LL,RR,LR}$ are summarised as,

$$m_{LL}^2 = m_{\tilde{f}}^2 + m_f^2 + M_Z^2 \cos 2\beta \left[\mathrm{T}_3^f - \mathrm{Q}^f \sin^2\theta_w\right] \tag{C.3}$$

$$m_{RR}^2 = m_{\tilde{f}^c}^2 + m_f^2 + M_Z^2 \cos 2\beta \mathrm{Q}^f \sin^2\theta_w \tag{C.4}$$

$$m_{LR}^2 = v_d A_f - \mu^* m_f \tan\beta \qquad [\text{for } f = d,\, e] \tag{C.5}$$

$$m_{LR}^2 = v_u A_f - \mu^* m_f \cot\beta \qquad [\text{for } f = u]. \tag{C.6}$$

The matrices $m_{\tilde{f}}^2 = m_{\tilde{Q},\tilde{L}}^2$ and $m_{\tilde{f}^c}^2 = m_{\tilde{u},\tilde{d},\tilde{e},}^2$ are the soft scalar masses for the scalar partners of the left and right-handed fermions.

For the scalar partners of the neutrinos we will have a 3×3 mass matrix. As we only have left-handed fields the only mass term will be, $m_{LL}^2 \tilde{\nu}\tilde{\nu}$, with,

$$m_{LL}^2 = m_{\tilde{L}}^2 + \frac{1}{2} M_Z^2 \cos 2\beta. \tag{C.7}$$

The sfermion mass squared matrices are diagonalised by a 6×6 unitary matrix, $V_{\tilde{f}}$, so that,

$$(M_{\tilde{f}}^{\text{diag}})^2 = V_{\tilde{f}}^\dagger\, M_{\tilde{f}}^2\, V_{\tilde{f}}, \tag{C.8}$$

and, $\tilde{f}_i' = V_{\tilde{f}\,ij}^\dagger \tilde{f}_j$, where $\tilde{f}_i'$ are the sfermion mass eigenstates.

C.2 Neutralino and Chargino mixing

In the MSSM the neutral fermions, $\tilde{B}$, $\tilde{W}^3$, $\tilde{H}_u^0$ and $\tilde{H}_d^0$, mix to form four neutralino mass eigenstates, $\tilde{\chi}_i^0$. The tree-level mixing comes from the soft Lagrangian terms of eq. (2.66), the superpotential F-term and the D-term contributions from eq. (2.65). The neutralino mass terms in the Lagrangian are then, $\mathcal{L} = -\frac{1}{2}(\psi^0)^{\mathrm{T}} M_{\tilde{\chi}^0} \psi^0$. with,

$$M_{\tilde{\chi}_i^0} = \begin{pmatrix} M_1 & 0 & -M_Z c_\beta s_w & M_Z s_\beta s_w \\ 0 & M_2 & M_Z c_\beta c_w & -M_Z s_\beta c_w \\ -M_Z c_\beta s_w & M_Z s_\beta s_w & 0 & -\mu \\ M_Z c_\beta c_w & -M_Z s_\beta c_w & -\mu & 0 \end{pmatrix} \qquad \text{(C.9)}$$

$$\text{in the basis} \quad \psi^0 = \left\{\tilde{B}, \tilde{W}^3, \tilde{H}_d^0, \tilde{H}_u^0\right\}.$$

Here, $s_\beta = \sin\beta$ and $c_w = \cos\theta_w$. The lightest neutralino is usually assumed to be the LSP as it is also a good cold dark matter candidate. The neutralino mass matrix is diagonalised by a unitary matrix, $V_{\tilde{\chi}^0}$, with $\tilde{\chi}_i^0 = V_{\tilde{\chi}^0 ij} \psi_j^0$, $i, j = 1 \ldots 2$, so that,

$$M_{\tilde{\chi}^0}^{\text{diag}} = V_{\tilde{\chi}^0}^* \, M_{\tilde{\chi}^0} \, V_{\tilde{\chi}^0}^{-1}. \qquad \text{(C.10)}$$

In an analogous way the charged fermions, $\tilde{W}^\pm$, $\tilde{H}_u^+$ and $\tilde{H}_d^-$ also mix to form charginos, $\tilde{\chi}^\pm$. The chargino mass term is, $\mathcal{L} = -\frac{1}{2}(\psi^\pm)^{\mathrm{T}} M_{\tilde{\chi}^\pm} \psi^\pm$, where we can write,

$$M_{\tilde{\chi}_i^\pm} = \begin{pmatrix} 0 & \mathbf{X}^{\mathrm{T}} \\ \mathbf{X} & 0 \end{pmatrix}, \quad \mathbf{X} = \begin{pmatrix} M_2 & \sqrt{2} s_\beta M_W \\ \sqrt{2} c_\beta M_W & \mu \end{pmatrix} \qquad \text{(C.11)}$$

$$\text{in the basis} \quad \psi^\pm = \{\psi^+, \psi^-\} = \left\{(\tilde{W}^+, \tilde{H}_u^+), (\tilde{W}^-, \tilde{H}_d^-)\right\}.$$

Clearly the mass matrix $M_{\tilde{\chi}_i^\pm}$ have a pair of degenerate eigenvalues. The diagonal chargino mass matrix can be found by diagonalising the mass matrix using two 2×2

unitary matrices, $U_{\tilde{\chi}^-}$, $V_{\tilde{\chi}^+}$, with $\tilde{\chi}_i^+ = V_{\tilde{\chi}^+ ij}\psi_j^+$ and $\tilde{\chi}_i^- = U_{\tilde{\chi}^- ij}\psi_j^-$, $i,j = 1\ldots 2$. Then we have,

$$U_{\tilde{\chi}^-}^* \, X \, V_{\tilde{\chi}^+}^{-1} = \begin{pmatrix} m_{\tilde{\chi}_1} & 0 \\ 0 & m_{\tilde{\chi}_2} \end{pmatrix}. \tag{C.12}$$

Appendix D

Non-renormalisable fermion mass operators

In this appendix we review the process of calculating the Clebsch-Gordan coefficients for all of the $n = 1$ non-renormalisable operators written in eq. (3.15) and (3.16).

D.1 $n = 1$ non-renormalisable operators

Including all gauge indices the complete set of $n = 1$ operators can be written as,

$$\mathcal{O}^{\alpha\rho yw}_{\beta\gamma xz} = F^{\alpha a}\overline{F}_{\beta x}h^{y}_{a}\overline{H}_{\gamma z}H^{\rho w} \tag{D.1}$$

where for simplicity we have ignored the gauge singlet field θ and the factors of $\frac{1}{M^2}$ suppression. The complete set of operators comes from each of the possible contractions of the gauge indices in eq. (D.1).

It is useful to define some $SU(4)$ invariant tensors C, and $SU(2)$ invariant tensors R

as follows:

$$\begin{aligned}
(C_1)^{\alpha}_{\beta} &= \delta^{\alpha}_{\beta} \\
(C_6)^{\rho\gamma}_{\alpha\beta} &= \epsilon^{\rho\gamma\omega\chi}_{\alpha\beta\omega\chi} \\
(C_{10})^{\alpha\beta}_{\rho\gamma} &= \delta^{\alpha}_{\rho}\delta^{\beta}_{\gamma} + \delta^{\alpha}_{\gamma}\delta^{\beta}_{\rho} \\
(C_{15})^{\beta\gamma}_{\alpha\rho} &= \delta^{\beta}_{\rho}\delta^{\gamma}_{\alpha} - \frac{1}{4}\delta^{\beta}_{\alpha}\delta^{\gamma}_{\rho} \\
(R_1)^{x}_{y} &= \delta^{x}_{y} \\
(R_3)^{wx}_{yz} &= \delta^{x}_{y}\delta^{w}_{z} - \frac{1}{2}\delta^{x}_{z}\delta^{w}_{y}
\end{aligned} \tag{D.2}$$

The SU(4) indices on $C_{1,6,10,15}$ are contracted with those on two fields to combine them into **1**, **6**, **10**, **15**, representations of SU(4) respectively. Similarly the $SU(2)_R$ indices on $R_{1,3}$ are contracted with those on two fields to combine into **1**, **3** representations of $SU(2)_R$ respectively. From these we can then construct six independent $SU(4)$ structures:

$$\begin{aligned}
\text{A.} \quad (C_1)^{\beta}_{\alpha}(C_1)^{\gamma}_{\rho} &= \delta^{\beta}_{\alpha}\delta^{\gamma}_{\rho} \\
\text{B.} \quad (C_{15})^{\beta\chi}_{\alpha\sigma}(C_{15})^{\gamma\sigma}_{\rho\chi} &= \delta^{\beta}_{\rho}\delta^{\gamma}_{\alpha} - \frac{1}{4}\delta^{\beta}_{\alpha}\delta^{\gamma}_{\rho} \\
\text{C.} \quad (C_6)^{\omega\chi}_{\alpha\rho}(C_6)^{\beta\gamma}_{\omega\chi} &= 8(\delta^{\beta}_{\alpha}\delta^{\gamma}_{\rho} - \delta^{\gamma}_{\alpha}\delta^{\beta}_{\rho}) \\
\text{D.} \quad (C_{10})^{\omega\chi}_{\alpha\rho}(C_{10})^{\beta\gamma}_{\omega\chi} &= 2(\delta^{\beta}_{\alpha}\delta^{\gamma}_{\rho} + \delta^{\gamma}_{\alpha}\delta^{\beta}_{\rho}) \\
\text{E.} \quad (C_1)^{\beta}_{\rho}(C_1)^{\gamma}_{\alpha} &= \delta^{\beta}_{\rho}\delta^{\gamma}_{\alpha} \\
\text{F.} \quad (C_{15})^{\gamma\chi}_{\alpha\sigma}(C_{15})^{\beta\sigma}_{\rho\chi} &= \delta^{\gamma}_{\rho}\delta^{\beta}_{\alpha} - \frac{1}{4}\delta^{\gamma}_{\alpha}\delta^{\beta}_{\rho}
\end{aligned} \tag{D.3}$$

and six $SU(2)$ structures:

$$\begin{aligned}
\text{a.} \quad (R_1)^{z}_{w}(R_1)^{x}_{y} &= \delta^{z}_{w}\delta^{x}_{y} \\
\text{b.} \quad (R_3)^{zq}_{wr}(R_3)^{xr}_{yq} &= \delta^{x}_{w}\delta^{z}_{y} - \frac{1}{2}\delta^{x}_{y}\delta^{z}_{w} \\
\text{c.} \quad \epsilon^{xz}\epsilon_{yw} &= \epsilon^{xz}\epsilon_{yw}
\end{aligned}$$

$$
\begin{aligned}
\text{d.} \quad & \epsilon_{ws}\epsilon^{xt}\,(R_3)^{sq}_{yr}\,(R_3)^{zr}_{tq} &&= \delta^x_w\delta^z_y - \frac{1}{2}\epsilon_{wy}\epsilon^{xz} \\
\text{e.} \quad & (R_1)^z_y\,(R_1)^x_w &&= \delta^z_y\delta^x_w \\
\text{f.} \quad & (R_3)^{zq}_{yr}\,(R_3)^{xr}_{wq} &&= \delta^x_y\delta^z_w - \frac{1}{2}\delta^x_w\delta^z_y
\end{aligned} \tag{D.4}
$$

All possible $n = 1$ operators are then constructed by taking one invariant structure from the list {A-F} above, combining it with one from the list {a-f}, and using it to contract the indices of the operator in eq. (D.1). In this way we can generate a total of 36 operators each labelled by the invariant structure from which it was constructed, e.g. $\mathcal{O}^{Aa}$ comes from contracting indices with the structures listed in A. and a. above.

After the heavy Higgs fields H and $\bar{H}$ acquire their VEV's these operators will contribute Yukawa couplings for each of the standard model fermions with the associated Clebsch-Gordan coefficient. A complete list of the Clebsch-Gordan coefficients can be found in table D.1, where the operators have been grouped such that CLASS I operators have non-zero coefficient for just one fermion, CLASS II-V have non-zero coefficient for two fermions and CLASS VI are non-zero for all fermions. The labels x_u, x_d, x_e, x_ν, correspond to the coefficients of the Yukawa coupling contributions written as,

$$
-\Delta\mathcal{L}_{ij} \propto \left(x_u\, u_i\bar{u}_j\, h^0_u + x_d\, d_i\bar{d}_j\, h^0_d + x_\nu\, \nu_i\bar{\nu}_j\, h^0_u + x_e\, e_i\bar{e}_j\, h^0_d\right). \tag{D.5}
$$

In the case that $n > 1$, there will be more indices to contract, which allows more representations, and hence more Clebsch coefficients. For example for $n = 2$ we already have 400 possible operators. To simplify things we restrict ourselves to the case where the additional factors of $H\bar{H}$ form gauge singlets. This means that the higher powers of $H\bar{H}$ simply contribute extra powers of $\delta = v\bar{v}/M^2$ and leaves the Clebsch-Gordan coefficients unchanged from those of the $n = 1$ operators. This is clearly just a small subset of the possible $n > 1$ operators. Therefore we can simply

write this subset as,

$$\begin{aligned} \mathcal{O}'^{\Pi\pi} &= \mathcal{O}^{\Pi\pi}\delta \\ \mathcal{O}''^{\Pi\pi} &= \mathcal{O}^{\Pi\pi}\delta^2 \\ \mathcal{O}'''^{\Pi\pi} &= \mathcal{O}^{\Pi\pi}\delta^3 \\ &\ldots. \end{aligned} \tag{D.6}$$

Where, $\Pi \in \{\text{A-F}\}$ and $\pi \in \{\text{a-f}\}$.

CLASS	$\mathcal{O}$	x_u	x_d	x_e	x_ν
I	$\mathcal{O}^{Ce}$	2	0	0	0
I	$\mathcal{O}^{Cc}$	0	2	0	0
I	$\mathcal{O}^{Ec}$	0	0	2	0
I	$\mathcal{O}^{Ee}$	0	0	0	2
II	$\mathcal{O}^{Ac}$	0	$\sqrt{2}$	$\sqrt{2}$	0
II	$\mathcal{O}^{Dc}$	0	$\frac{2}{\sqrt{5}}$	$\frac{4}{\sqrt{5}}$	0
II	$\mathcal{O}^{Fc}$	0	$\frac{8}{5}$	$\frac{6}{5}$	0
II	$\mathcal{O}^{Bc}$	0	$\sqrt{\frac{2}{5}}$	$-3\sqrt{\frac{2}{5}}$	0
III	$\mathcal{O}^{Ae}$	$\sqrt{2}$	0	0	$\sqrt{2}$
III	$\mathcal{O}^{De}$	$\frac{2}{\sqrt{5}}$	0	0	$\frac{4}{\sqrt{5}}$
III	$\mathcal{O}^{Fe}$	$\frac{8}{5}$	0	0	$\frac{6}{5}$
III	$\mathcal{O}^{Be}$	$\sqrt{\frac{2}{5}}$	0	0	$-3\sqrt{\frac{2}{5}}$
IV	$\mathcal{O}^{Ef}$	0	0	$\frac{4}{\sqrt{5}}$	$\frac{2}{\sqrt{5}}$
IV	$\mathcal{O}^{Ea}$	0	0	$\sqrt{2}$	$\sqrt{2}$
IV	$\mathcal{O}^{Eb}$	0	0	$-\sqrt{2}$	$\sqrt{2}$
IV	$\mathcal{O}^{Ed}$	0	0	$\frac{2}{\sqrt{5}}$	$\frac{4}{\sqrt{5}}$
V	$\mathcal{O}^{Cb}$	$\sqrt{2}$	$-\sqrt{2}$	0	0
V	$\mathcal{O}^{Ca}$	$\sqrt{2}$	$\sqrt{2}$	0	0
V	$\mathcal{O}^{Cd}$	$\frac{4}{\sqrt{5}}$	$\frac{2}{\sqrt{5}}$	0	0
V	$\mathcal{O}^{Cf}$	$\frac{2}{\sqrt{5}}$	$\frac{4}{\sqrt{5}}$	0	0
VI	$\mathcal{O}^{Dd}$	$\frac{4}{5}$	$\frac{2}{5}$	$\frac{4}{5}$	$\frac{8}{5}$
VI	$\mathcal{O}^{Df}$	$\frac{2}{5}$	$\frac{4}{5}$	$\frac{8}{5}$	$\frac{4}{5}$
VI	$\mathcal{O}^{Ff}$	$\frac{8}{5\sqrt{5}}$	$\frac{16}{5\sqrt{5}}$	$\frac{12}{5\sqrt{5}}$	$\frac{6}{5\sqrt{5}}$
VI	$\mathcal{O}^{Fd}$	$\frac{16}{5\sqrt{5}}$	$\frac{8}{5\sqrt{5}}$	$\frac{6}{5\sqrt{5}}$	$\frac{12}{5\sqrt{5}}$
VI	$\mathcal{O}^{Ad}$	$\frac{2\sqrt{2}}{5}$	$\frac{\sqrt{2}}{5}$	$\frac{\sqrt{2}}{5}$	$\frac{2\sqrt{2}}{5}$
VI	$\mathcal{O}^{Af}$	$\frac{\sqrt{2}}{5}$	$\frac{2\sqrt{2}}{5}$	$\frac{2\sqrt{2}}{5}$	$\frac{\sqrt{2}}{5}$
VI	$\mathcal{O}^{Bd}$	$\frac{2\sqrt{2}}{5}$	$\frac{\sqrt{2}}{5}$	$-\frac{3\sqrt{2}}{5}$	$-\frac{6\sqrt{2}}{5}$
VI	$\mathcal{O}^{Bf}$	$\frac{\sqrt{2}}{5}$	$\frac{2\sqrt{2}}{5}$	$-\frac{6\sqrt{2}}{5}$	$-\frac{3\sqrt{2}}{5}$
VI	$\mathcal{O}^{Bb}$	$\frac{1}{\sqrt{5}}$	$-\frac{1}{\sqrt{5}}$	$\frac{3}{\sqrt{5}}$	$-\frac{3}{\sqrt{5}}$
VI	$\mathcal{O}^{Db}$	$\sqrt{\frac{2}{5}}$	$-\sqrt{\frac{2}{5}}$	$-2\sqrt{\frac{2}{5}}$	$2\sqrt{\frac{2}{5}}$
VI	$\mathcal{O}^{Ab}$	1	-1	-1	1
VI	$\mathcal{O}^{Fb}$	$\frac{4\sqrt{2}}{5}$	$-\frac{4\sqrt{2}}{5}$	$-\frac{3\sqrt{2}}{5}$	$\frac{3\sqrt{2}}{5}$
VI	$\mathcal{O}^{Fa}$	$\frac{4\sqrt{2}}{5}$	$\frac{4\sqrt{2}}{5}$	$\frac{3\sqrt{2}}{5}$	$\frac{3\sqrt{2}}{5}$
VI	$\mathcal{O}^{Aa}$	1	1	1	1
VI	$\mathcal{O}^{Da}$	$\sqrt{\frac{2}{5}}$	$\sqrt{\frac{2}{5}}$	$2\sqrt{\frac{2}{5}}$	$2\sqrt{\frac{2}{5}}$
VI	$\mathcal{O}^{Ba}$	$\frac{1}{\sqrt{5}}$	$\frac{1}{\sqrt{5}}$	$-\frac{3}{\sqrt{5}}$	$-\frac{3}{\sqrt{5}}$

Table D.1: Clebsch-Gordan coefficients for the complete set of $n = 1$ operators. Here the coefficients have been normalised so that the sum of the squares equals 4.

Appendix E

D-terms from the breaking of SU(4) and $SU(2)_R$

In this appendix we outline the origin of the D-term splitting of the soft scalar masses in eq. (3.26). These D-terms contributions arise from the breaking of the Pati-Salam group down to the standard model gauge group.

Firstly we shall summarise the index conventions used on the Pati-Salam fields.

$$\begin{aligned} F_i^{a\alpha} &= (4,2,1), \quad \bar{F}_{i\,x\alpha} = (\bar{4},1,\bar{2}) \\ h_a{}^x &= (1,\bar{2},2) \\ H^{a\alpha} &= (4,1,2), \quad \bar{H}_{x\alpha} = (\bar{4},1,\bar{2}), \end{aligned} \tag{E.1}$$

where $\alpha = 1\ldots4$ is an SU(4) index, $a, x = 1,2$ are $SU(2)_{L,R}$ indices, and $i = 1\ldots3$ is a family index. The first/second gauge index should be read as corresponding to the row/column of the matrix. Furthermore the up/down indices are related to the gauge transformation properties of the multiplet, e.g. the raised a and α signifies that F transforms in the **2** representation of $SU(2)_L$ and the **4** of SU(4), whereas the lower index x and α signifies that $\bar{F}$ transforms in the $\bar{\mathbf{2}}$ of $SU(2)_R$ and $\bar{\mathbf{4}}$ of SU(4) .

Following in the same manner as eq. (2.60-2.63) we may write the $SU(2)_R$ and SU(4) D-term contributions as,

$$V_D \subset \frac{g_{2R}^2}{2}\sum_{a=1}^{3} D_{2R}^a D_{2R}^a + \frac{g_4^2}{2}\sum_{m=1}^{15} D_4^m D_4^m. \tag{E.2}$$

Here the subscripts $2R$ and 4, denote the D-terms corresponding to the groups $SU(2)_R$ and SU(4) respectively. For the contributions to the scalar mass terms it will only be necessary to look at the diagonal generators τ_R^3 of $SU(2)_R$ and T^{15} of SU(4), where,

$$\tau_R^3 = \frac{1}{2}\text{diag}(1,\,-1), \quad T^{15} = \sqrt{\frac{3}{2}}\text{diag}\left(\frac{1}{6},\,\frac{1}{6},\,\frac{1}{6},\,-\frac{1}{2}\right). \tag{E.3}$$

Then it is straight forward to rewrite eq. (E.2) in terms of the fields in eq. (E.2),

$$\begin{aligned} D_{2R}^3 &= \bar{H}^{\dagger x\alpha}\left(-\tau_R^{3*}\right)_x{}^y \bar{H}_{y\alpha} + H_{x\alpha}^{\dagger}\left(\tau_R^3\right)^x{}_y H^{y\alpha} \\ &\quad + \bar{F}^{\dagger x\alpha}\left(-\tau_R^{3*}\right)_x{}^y \bar{F}_{y\alpha} + h^a{}_x\left(\tau_R^3\right)^x{}_y h_a{}^y \\ D_4^{15} &= \bar{H}^{\dagger x\alpha}\left(-T^{15*}\right)_\alpha{}^\beta \bar{H}_{x\beta} + H_{x\alpha}^{\dagger}\left(T^{15}\right)^\alpha{}_\beta H^{x\beta} \\ &\quad + \bar{F}^{\dagger x\alpha}\left(-T^{15*}\right)_\alpha{}^\beta \bar{F}_{x\beta} + F_{x\alpha}^{\dagger}\left(T^{15}\right)^\alpha{}_\beta F^{x\beta}. \end{aligned} \tag{E.4}$$

The factors of, $-\tau_R^{3*}$ and $-T^{15*}$, come from the fact that the complex conjugate representations $\bar{\mathbf{2}}$ and $\bar{\mathbf{4}}$ are generated by the matrices, $-\tau^{a*}$ and $-T^{a*}$. The $SU(2)_R$ and SU(4) groups are broken via the heavy Higgs developing VEV's,

$$\langle H\rangle = H^{14} = H_\nu, \quad \langle \bar{H}\rangle = \bar{H}_{14} = \bar{H}_\nu.. \tag{E.5}$$

Following the above symmetry breaking the D-terms of eq. (E.4) may be expanded as,[1]

$$D_{2R}^3 = \frac{1}{2}\left(-|\bar{H}_\nu|^2 + |H_\nu|^2 + |\tilde{d}^c|^2 + |\tilde{e}^c|^2 - |\tilde{u}^c|^2 - |\tilde{\nu}^c|^2 - |h_d|^2 + |h_u|^2\right), \tag{E.6}$$

[1]Here we have written u^c, etc. instead of $\bar{u}$ as in eq. (3.4) or u_R as in eq. (2.66).

$$D_4^{15} = \sqrt{\frac{3}{2}}\left(-\frac{1}{2}|\bar{H}_\nu|^2 + \frac{1}{2}|H_\nu|^2 + \frac{1}{6}|\tilde{d}^c|^2 + \frac{1}{2}|\tilde{e}^c|^2 - \frac{1}{6}|\tilde{u}^c|^2 - \frac{1}{2}|\tilde{\nu}^c|^2 - \frac{1}{2}|\tilde{Q}|^2 + \frac{1}{2}|\tilde{L}|^2\right). \tag{E.7}$$

These results may be summarised as,

$$-D_{2R}^3 = D_H + \sum_\phi I_\phi |\phi|^2, \quad -D_4^{15} = \sqrt{\frac{3}{2}} D_H + \sqrt{\frac{3}{2}} \sum_\phi \left(\frac{B-L}{2}\right)_\phi |\phi|^2, \tag{E.8}$$

here we have defined, $D_H = \frac{1}{2}\left(|\bar{H}_\nu|^2 - |H_\nu|^2\right)$ and ϕ denotes any of the fields $\tilde{u}^c$, $\tilde{d}^c$, $\tilde{e}^c$, $\tilde{\nu}^c$, $\tilde{Q}$, $\tilde{L}$, h_u, h_d. The factor I_ϕ relates to the charge carried by ϕ with respect to the $SU(2)_R$ group and $(B-L)/2$ to the semi-difference between the baryon and lepton numbers of ϕ. These can easily be read from eq. (E.6) and (E.7).

Finally we can now rewrite eq. (E.2) in terms of eq. (E.6) and (E.7) as,

$$\begin{aligned} V_D &\subset \frac{g_{2R}^2}{2} D_{2R}^3 D_{2R}^3 + \frac{g_4^2}{2} D_4^{15} D_4^{15} \\ &\subset D_H \left(\sum_\phi g_{2R}^2 I_\phi + \frac{3}{2} g_4^2 \frac{(B-L)}{2}\right) |\phi|^2. \end{aligned} \tag{E.9}$$

This leads us to the following contributions to the soft scalar masses,

$$\begin{aligned} m_Q^2 &= m_F^2 + g_4^2\, D^2 \\ m_{u_R}^2 &= m_{\overline{F}}^2 - (g_4^2 - 2g_{2R}^2)\, D^2 \\ m_{d_R}^2 &= m_{\overline{F}}^2 - (g_4^2 + 2g_{2R}^2)\, D^2 \\ m_L^2 &= m_F^2 - 3g_4^2\, D^2 \\ m_{e_R}^2 &= m_{\overline{F}}^2 + (3g_4^2 - 2g_{2R}^2)\, D^2 \\ m_{\nu_R}^2 &= m_{\overline{F}}^2 + (3g_4^2 + 2g_{2R}^2)\, D^2 \\ m_{H_u}^2 &= m_h^2 - 2g_{2R}^2\, D^2 \\ m_{H_d}^2 &= m_h^2 + 2g_{2R}^2\, D^2., \end{aligned} \tag{E.10}$$

where $D^2 = \frac{1}{4} D_H$. The last two lines of eq. (E.10) implies that our model has non-

universal Higgs masses, split by the D-term contributions outlined above.

Bibliography

[1] M. E. Peskin and D. V. Schroeder, *An Introduction To Quantum Field Theory,* Reading, USA: Addison-Wesley (1995) F. Halzen and A. D. Martin, *Quarks And Leptons: An Introductory Course In Modern Particle Physics,* New York, USA: Wiley (1984) M. Kaku, *Quantum Field Theory: A Modern Introduction,* New York, USA: Oxford Univ. Pr. (1993) T. P. Cheng and L. F. Li, *Gauge Theory Of Elementary Particle Physics,* New York, USA: Oxford Univ. Pr. (1984) J. L. Rosner, arXiv:hep-ph/0108195.

[2] M. Kobayashi and T. Maskawa, Prog. Theor. Phys. **49** (1973) 652.

[3] K. Hagiwara *et al.* [Particle Data Group Collaboration], Phys. Rev. D **66** (2002) 010001.

[4] D. P. Roy, Acta Phys. Polon. B **34** (2003) 3417 [arXiv:hep-ph/0303106].

[5] LEP Elctroweak Working Group, http://www.cern.ch/LEPEWWG/.

[6] M. Colless *et al.*, arXiv:astro-ph/0306581.

[7] E. L. Wright, arXiv:astro-ph/0306132.

[8] H. E. Haber and G. L. Kane, Phys. Rept. **117**, 75 (1985). M. Drees, arXiv:hep-ph/9611409. A. Bilal, arXiv:hep-th/0101055. J. D. Lykken, arXiv:hep-th/9612114.

[9] S. Dawson, arXiv:hep-ph/9712464. S. P. Martin, arXiv:hep-ph/9709356. N. Polonsky, Lect. Notes Phys. **M68** (2001) 1 [arXiv:hep-ph/0108236].

[10] L. Girardello and M. T. Grisaru, Nucl. Phys. B **194** (1982) 65.

[11] J. F. Gunion, H. E. Haber, G. L. Kane and S. Dawson, SCIPP-89/13.

[12] ATLAS: Detector and physics performance technical design report. Volume 1, CERN-LHCC-99-14.

[13] M. C. Gonzalez-Garcia and Y. Nir, Rev. Mod. Phys. **75** (2003) 345 [arXiv:hep-ph/0202058]. R. D. Peccei, AIP Conf. Proc. **490** (1999) 80 [arXiv:hep-ph/9906509]. S. M. Bilenky, arXiv:hep-ph/0210128. S. F. King, arXiv:hep-ph/0310204. V. Barger, D. Marfatia and K. Whisnant, Int. J. Mod. Phys. E **12** (2003) 569 [arXiv:hep-ph/0308123]. R. R. Volkas, Prog. Part. Nucl. Phys. **48** (2002) 161 [arXiv:hep-ph/0111326].

[14] K. S. Hirata *et al.* [Kamiokande-II Collaboration], Phys. Lett. B **280** (1992) 146. Y. Fukuda *et al.* [Kamiokande Collaboration], Phys. Lett. B **335** (1994) 237.

[15] Y. Fukuda *et al.*, Super-Kamiokande Collaboration, Phys. Lett. **B433**, 9 (1998); *ibid.* Phys. Lett. **B436**, 33 (1998); *ibid.* Phys. Rev. Lett. **81**, 1562 (1998).

[16] R. Becker-Szendy *et al.*, Nucl. Phys. Proc. Suppl. **38** (1995) 331. E. Kearns, Nucl. Phys. Proc. Suppl. **70** (1999) 315 [arXiv:hep-ex/9803007].

[17] Q. R. Ahmad *et al.* [SNO Collaboration], Phys. Rev. Lett. **89** (2002) 011301 [arXiv:nucl-ex/0204008]; Q. R. Ahmad *et al.* [SNO Collaboration], Phys. Rev. Lett. **89** (2002) 011302 [arXiv:nucl-ex/0204009].

[18] K. Eguchi *et al.* [KamLAND Collaboration], Phys. Rev. Lett. **90** (2003) 021802 [arXiv:hep-ex/0212021].

[19] Z. Maki, M. Nakagawa and S. Sakata, Prog. Theor. Phys. **28** (1962) 870.

[20] M. Apollonio *et al.* [CHOOZ Collaboration], Phys. Lett. B **466** (1999) 415 [arXiv:hep-ex/9907037].

[21] G. L. Fogli, E. Lisi, A. Marrone, D. Montanino, A. Palazzo and A. M. Rotunno, arXiv:hep-ph/0212127; P. C. de Holanda and A. Y. Smirnov, arXiv:hep-ph/0212270; V. Barger and D. Marfatia, Phys. Lett. B **555** (2003) 144 [arXiv:hep-ph/0212126]; A. Bandyopadhyay, S. Choubey, R. Gandhi, S. Goswami and D. P. Roy, arXiv:hep-ph/0212146. M. Maltoni, T. Schwetz and J. W. Valle, arXiv:hep-ph/0212129.

[22] S. F. King, Phys. Lett. B **439** (1998) 350 [arXiv:hep-ph/9806440]; S. F. King, Nucl. Phys. B **562** (1999) 57 [arXiv:hep-ph/9904210]; S. F. King, Nucl. Phys. B **576** (2000) 85 [arXiv:hep-ph/9912492].

[23] T. Blažek, S. F. King and J. K. Parry, J. High Energy Phys. JHEP 05 (2003) 016, arXiv:hep-ph/0303192.

[24] I. Antoniadis and G. K. Leontaris, Phys. Lett. B **216** (1989) 333; I. Antoniadis, G. K. Leontaris and J. Rizos, Phys. Lett. B **245** (1990) 161.

[25] G. Shiu, S. H. H. Tye, Phys. Rev. **D58**, 106007 (1998); L. L. Everett, G. L. Kane, S. F. King, S. Rigolin and L. T. Wang, Phys. Lett. B **531** (2002) 263 [arXiv:hep-ph/0202100].

[26] S. F. King and M. Oliveira, Phys. Rev. D **60** (1999) 035003 [arXiv:hep-ph/9804283].

[27] S. F. King and M. Oliveira, Phys. Rev. D **63** (2001) 095004 [arXiv:hep-ph/0009287].

[28] T. Blažek and S. F. King, Phys. Lett. B **518** (2001) 109 [arXiv:hep-ph/0105005].

[29] S. F. King and M. Oliveira, Phys. Rev. D **63** (2001) 015010 [arXiv:hep-ph/0008183].

[30] M. E. Gomez, G. Lazarides and C. Pallis, Nucl. Phys. B **638** (2002) 165 [arXiv:hep-ph/0203131].

[31] M. E. Gomez, G. Lazarides and C. Pallis, arXiv:hep-ph/0301064.

[32] T. Affolder *et al.* [CDF Collaboration], Phys. Rev. Lett. **86** (2001) 4472 [arXiv:hep-ex/0010052].

[33] J. C. Pati, A. Salam, Phys. Rev. **D10**, 275 (1974).

[34] H. Arason, D. Castano, B. Keszthelyi, S. Mikaelian, E. Piard, P. Ramond and B. Wright, Phys. Rev. Lett. **67** (1991) 2933.

[35] S. F. King, Phys. Lett. B **325** (1994) 129 [Erratum-ibid. B **325** (1994) 538]; B. C. Allanach and S. F. King, Nucl. Phys. B **456** (1995) 57 [arXiv:hep-ph/9502219]; B. C. Allanach and S. F. King, Nucl. Phys. B **459** (1996) 75 [arXiv:hep-ph/9509205]; B. C. Allanach, S. F. King, G. K. Leontaris and S. Lola, Phys. Rev. D **56** (1997) 2632 [arXiv:hep-ph/9610517].

[36] S. F. King, JHEP **0209** (2002) 011 [arXiv:hep-ph/0204360].

[37] T. Blažek and S. F. King, arXiv:hep-ph/0211368.

[38] T. Blažek, M. Carena, S. Raby and C.E.M. Wagner, Phys. Rev. D **56** (1997) 6919 [arXiv:hep-ph/9611217].

[39] M.Carena, J.R. Espinosa, M.Quiros and C. Wagner, Phys. Lett. B**355**, 209 (1995); M.Carena, M.Quiros and C. Wagner, Nucl. Phys. B**461**, 407 (1996); J.A. Casas, J.R. Espinosa, M. Quiros and A. Riotto, Nucl. Phys. B**436**, 3 (1995).

[40] R. Hempfling, Phys. Rev. D**49**, 6168 (1994). L. Hall, R. Ratazzi and U. Sarid, Phys. Rev. D**50**, 7048 (1994). M. Carena, M. Olechowski, S. Pokorski and C. Wagner, Nucl. Phys. B**426**, 269 (1994).

[41] T. Blazek, S. Raby and S. Pokorski, Phys. Rev. D **52**, 4151 (1995) [arXiv:hep-ph/9504364].

[42] A. Dedes, H. K. Dreiner, U. Nierste and P. Richardson, arXiv:hep-ph/0207026; T. Kamon, arXiv:hep-ph/0301019.

[43] K. Hagiwara, A. D. Martin, D. Nomura and T. Teubner, Phys. Lett. B **557** (2003) 69 arXiv:hep-ph/0209187. M. Davier, S. Eidelman, A. Hocker and Z. Zhang, arXiv:hep-ph/0208177. A. Hoefer, J. Gluza and F. Jegerlehner, Eur. Phys. J. C **24**, 51 (2002) [arXiv:hep-ph/0107154]. B.V. Geshkenbein, arXiv:hep-ph/0301265.

[44] M. Davier, S. Eidelman, A. Hocker and Z. Zhang, arXiv:hep-ph/0208177.

[45] C. Brown [BABAR Collaboration], arXiv:hep-ex/0212009.

[46] T. Blažek, R. Dermíšek and S. Raby, Phys. Rev. Lett. **88** (2002) 111804; T. Blažek, R. Dermíšek and S. Raby, Phys. Rev. **D65**:115004 (2002); K. Tobe and J. Wells, arXiv:hep-ph/0301015; D. Auto, H. Baer, C. Balazs, A. Belyaev, J. Ferrandis and X. Tata, arXiv:hep-ph/0302155.

[47] T. Blažek, S. F. King and J. K. Parry, arXiv:hep-ph/0308068.

[48] S. R. Choudhury and N. Gaur, Phys. Lett. B **451** (1999) 86 [arXiv:hep-ph/9810307]. K. S. Babu and C. F. Kolda, Phys. Rev. Lett. **84**, 228 (2000) [arXiv:hep-ph/9909476]. C. S. Huang, W. Liao, Q. S. Yan and S. H. Zhu, Phys. Rev. D **63**, 114021 (2001) [Erratum-ibid. D **64**, 059902 (2001)] [arXiv:hep-ph/0006250]. P. H. Chankowski and L. Slawianowska, Phys. Rev. D **63**, 054012 (2001) [arXiv:hep-ph/0008046]. C. Bobeth, T. Ewerth, F. Kruger and J. Urban, Phys. Rev. D **64**, 074014 (2001) [arXiv:hep-ph/0104284]. A. Dedes, H. K. Dreiner and U. Nierste, Phys. Rev. Lett. **87**, 251804 (2001) [arXiv:hep-ph/0108037]. G. Isidori and A. Retico, JHEP **0111**, 001 (2001) [arXiv:hep-ph/0110121]. R. Arnowitt, B. Dutta, T. Kamon and M. Tanaka, Phys. Lett. B

538, 121 (2002) [arXiv:hep-ph/0203069]. C. Bobeth, T. Ewerth, F. Kruger and J. Urban, Phys. Rev. D **66**, 074021 (2002) [arXiv:hep-ph/0204225]. A. Dedes, H. K. Dreiner, U. Nierste and P. Richardson, arXiv:hep-ph/0207026. A. J. Buras, P. H. Chankowski, J. Rosiek and L. Slawianowska, Phys. Lett. B **546**, 96 (2002) [arXiv:hep-ph/0207241]. J. K. Mizukoshi, X. Tata and Y. Wang, Phys. Rev. D **66**, 115003 (2002) [arXiv:hep-ph/0208078]. S. Baek, P. Ko and W. Y. Song, JHEP **0303**, 054 (2003) [arXiv:hep-ph/0208112]. G. Isidori and A. Retico, JHEP **0209**, 063 (2002) [arXiv:hep-ph/0208159]. A. Dedes and A. Pilaftsis, Phys. Rev. D **67** (2003) 015012 [arXiv:hep-ph/0209306]. A. J. Buras, P. H. Chankowski, J. Rosiek and L. Slawianowska, arXiv:hep-ph/0210145. C. S. Huang and X. H. Wu, Nucl. Phys. B **657**, 304 (2003) [arXiv:hep-ph/0212220]. T. Hurth, arXiv:hep-ph/0212304. T. Kamon [CDF Collaboration], arXiv:hep-ex/0301019. D. A. Demir, arXiv:hep-ph/0303249. A. Brignole and A. Rossi, arXiv:hep-ph/0304081. R. Dermisek, S. Raby, L. Roszkowski and R. Ruiz De Austri, JHEP **0304**, 037 (2003) [arXiv:hep-ph/0304101].

[49] Y. B. Dai, C. S. Huang and H. W. Huang, Phys. Lett. B **390** (1997) 257 [Erratum-ibid. B **513** (2001) 429] [arXiv:hep-ph/9607389]. C. S. Huang and Q. S. Yan, Phys. Lett. B **442** (1998) 209 [arXiv:hep-ph/9803366]. C. S. Huang, W. Liao and Q. S. Yan, Phys. Rev. D **59** (1999) 011701 [arXiv:hep-ph/9803460]. S. R. Choudhury and N. Gaur, Phys. Lett. B **451** (1999) 86 [arXiv:hep-ph/9810307].

[50] C. Hamzaoui, M. Pospelov and M. Toharia, Phys. Rev. D **59**, 095005 (1999) [arXiv:hep-ph/9807350].

[51] A. J. Buras, arXiv:hep-ph/9806471.

[52] T. Blazek and S. Raby, Phys. Rev. D **59** (1999) 095002 [arXiv:hep-ph/9712257].

[53] F. Borzumati and A. Masiero, Phys. Rev. Lett. **57** (1986) 961. J. Hisano and D. Nomura, Phys. Rev. D **59** (1999) 116005 [arXiv:hep-ph/9810479]. J. R. Ellis,

M. E. Gomez, G. K. Leontaris, S. Lola and D. V. Nanopoulos, Eur. Phys. J. C **14** (2000) 319 [arXiv:hep-ph/9911459]. S. Lavignac, I. Masina and C. A. Savoy, Phys. Lett. B **520** (2001) 269 [arXiv:hep-ph/0106245]. J. A. Casas and A. Ibarra, Nucl. Phys. B **618** (2001) 171 [arXiv:hep-ph/0103065].

[54] D. Guetta, J. M. Mira and E. Nardi, Phys. Rev. D **59** (1999) 034019 [arXiv:hep-ph/9806359]. A. Rossi, arXiv:hep-ph/0311320. A. Brignole and A. Rossi, Phys. Lett. B **566** (2003) 217 [arXiv:hep-ph/0304081].

[55] K. S. Babu and C. Kolda, Phys. Rev. Lett. **89** (2002) 241802 [arXiv:hep-ph/0206310].

[56] A. Dedes, J. R. Ellis and M. Raidal, Phys. Lett. B **549** (2002) 159 [arXiv:hep-ph/0209207].

[57] J. Hisano, T. Moroi, K. Tobe and M. Yamaguchi, Phys. Rev. D **53** (1996) 2442 [arXiv:hep-ph/9510309]. J. Hisano, T. Moroi, K. Tobe, M. Yamaguchi and T. Yanagida, Phys. Lett. B **357** (1995) 579 [arXiv:hep-ph/9501407].

[58] M. Sher, Phys. Rev. D **66** (2002) 057301 [arXiv:hep-ph/0207136].